Membrane development for organic solvent nanofiltration: A sustainable solution to chemical separation and purification

by

Sharafat Ali

A thesis

presented to the University of Waterloo

in fulfillment of the

thesis requirement for the degree of

Doctor of Philosophy

in

Civil Engineering

Waterloo, Ontario, Canada, 2026

© Sharafat Ali 2026

Examining Committee Membership

The following served on the Examining Committee for this thesis. The decision of the Examining Committee is by majority vote.

External Examiner:	Professor Raja Ghosh Department of Chemical Engineering, McMaster University
Supervisor:	Professor Xianshe Feng Department of Chemical Engineering University of Waterloo
Internal Member(s):	Professor Giovanni Cascante Department of Civil and Environmental Engineering University of Waterloo
	Associate Professor Rebecca Saari Department of Civil and Environmental Engineering University of Waterloo
Internal-external Member	Professor Eric Croiset Department of Chemical Engineering University of Waterloo

Author's Declaration

This thesis consists of material all of which I authored or co-authored: see Statement of Contributions included in the thesis. This is a true copy of the thesis, including any required final revisions, as accepted by my examiners.

I understand that my thesis may be made electronically available to the public.

Statement of Contributions

This thesis consists of seven chapters: Chapter 1, Introduction, and Chapter 2, Literature Review, which are based on published review papers authored by the candidate (SA) as the first author. Chapter 3 presents experimental results from another published journal article, for which the candidate conducted the experimental work and wrote the manuscript, which was approved by the supervisor. Chapter 4 is based on a separate published research article, where the candidate conducted the experiments, wrote the first draft of the manuscript, and made revisions based on feedback from co-authors, as well as further revisions to the manuscript before publication. Chapter 5 consists of a peer-reviewed published research article, led by the candidate as first author, and incorporated suggestions from the co-authors. Chapter 6 summarizes the research's conclusions and offers recommendations for future work.

Professor Xianshe Feng from the Chemical Engineering Department served as the candidate's supervisor, providing laboratory resources, guiding the research, and reviewing the work.

Chapters 1 and 2

Citations:

1. **Sharafat Ali**, Shah, I.A., Ihsanullah, I., Feng, X., "Nanocomposite membranes for organic solvent nanofiltration: Recent advances, challenges, and prospects", *Chemosphere Journal, 2022*. https://doi.org/10.1016/j.chemosphere.2022.136329
2. **Sharafat Ali**, Wang, R., Shah, I.A., Huang, H., Yin, S., Feng, X., "Per- and polyfluoroalkyl substances separation by membranes: A critical evaluation of advances and future perspectives", *Environmental Science: Water Research and Technology,* 2024. https://doi.org/10.1039/D4EW00066H
3. **Sharafat Ali**, Zhang, J., Karnik, R., Feng, X., "Advances in polybenzimidazole-based membranes for efficient separation and energy delivery", Journal of Membrane Science, 2025. https://doi.org/10.1016/j.memsci.2025.124502

The work presented in chapters 1 and 2 is based on the parts of the review articles listed above, all of which were published during the candidate's PhD studies. Not all sections of the published

papers were used in these two chapters, but only parts of the papers that the candidate deemed necessary were included. The candidate, Sharafat Ali (SA), is the first author of these papers and was primarily responsible for developing the concepts, conducting comprehensive literature reviews, writing the original drafts, and revising the manuscripts based on feedback from co-authors and the journal's anonymous reviewers.

Prof. Xianshe Feng supervised and provided technical guidance for the published papers. The listed co-authors contributed through intellectual discussion, feedback, and revision of the manuscripts before submission.

Chapter 3

Citation:

Sharafat Ali, Feng, X., "Interfacially Crosslinked polydopamine/polybenzimidazole composite membranes for organic solvent nanofiltration", ACS Applied Materials & Interfaces, 2024. https://doi.org/10.1021/acsami.4c14283

The work presented in this chapter is based on the above-mentioned publication. The candidate (SA) conducted the research under the supervision of Prof. Xianshe Feng from the Chemical Engineering Department. The candidate was primarily responsible for designing and executing the experiments, analyzing the data, and preparing the manuscript. The study was designed in consultation with Prof. Feng, who provided technical guidance and offered feedback on the research outcomes. The first draft of the manuscript was prepared by the candidate and subsequently revised based on Prof. Feng's suggestions and the journal's anonymous reviewers.

Chapter 4

Citation:

Sharafat Ali, Zhang, J., Yin, S., Feng, X., "Tailoring pore size and chemical resistance of polybenzimidazole membranes for organic solvent nanofiltration (OSN) via chemical crosslinking and sulfocalix[4]arene impregnation", Chemical Engineering Journal, 2025. https://doi.org/10.1016/j.cej.2025.159244

The work presented in Chapter 4 is based on the experimental work reported in the above-mentioned published article. The candidate (SA) is the first author and was primarily responsible for designing and conducting the experiments, performing data analysis, and preparing the manuscript under the supervision of Prof. Feng. The candidate prepared the initial draft of the manuscript, which all co-authors subsequently reviewed. Revisions were made by the candidate based on feedback from the co-authors and the journal's anonymous reviewers.

Chapter 5

Citation:

Sharafat Ali, Zhang, J., Feng, X., "Triglycidyl isocyanurate crosslinked polybenzimidazole membranes for solvent-resistant and extreme pH nanofiltration", Journal of Membrane Science, 2025. https://doi.org/10.1016/j.memsci.2025.124638

Chapter 5 is based on the experimental work described in the above-cited publication. The candidate is the first author and was primarily responsible for conceptualizing the study, conducting membrane fabrication and characterization experiments, analyzing the data, and preparing the manuscript. The research was supervised by Prof. Feng, who provided funding for lab supplies, technical guidance, and critical feedback throughout the project. The initial manuscript draft was written by the candidate, reviewed by the co-authors, and subsequently revised by the candidate based on their input and the journal reviewers' comments.

Abstract

Chemical separation is an integral part of the pharmaceuticals, food, petrochemicals, and fine chemicals industries for purifying and producing high-value products, extracting catalysts, and recycling organic solvents. These industries depend on conventional distillation processes for chemical separation, which are energy-intensive, costly, and generate millions of tons of CO_2 annually. Membrane-based separation, particularly organic solvent nanofiltration (OSN), has emerged as an alternative low-energy separation process for separating solutes in organic media. However, current OSN membranes face challenges such as limited solvent stability, poor rejection of low molecular-weight solutes, and trade-offs between permeability and selectivity. This research was designed to address these issues through systematic design, fabrication, and modification of polybenzimidazole (PBI)-based membranes, utilizing chemical crosslinking, interfacial engineering, and supramolecular functionalization. PBI was selected as the membrane-fabrication polymer because of its exceptional thermal stability and mechanical strength, making it an ideal candidate for large-scale fabrication and deployment of OSN technology. Pristine PBI membranes could be used for separation in both polar and non-polar solvents, but they are not resistant to polar aprotic solvents, which hinder its large-scale application. Therefore, proper post-treatment modifications are required to make the membrane chemically resistant for a wide range of OSN applications.

A series of PBI membranes was fabricated and crosslinked using covalent and non-covalent techniques to improve their chemical stability and selective transport behavior. In Chapter 3, interfacial oxidative polymerization of polydopamine (PDA) combined with covalent crosslinking using α,α′-dibromo-p-xylene (DBX) yielded composite membranes with excellent solvent stability. The membrane showed excellent rejection efficiency and solute fractionation while maintaining competitive permeance to organic solvents. Following the successful completion of the first study, Chapter 4 investigated the impact of chemical crosslinker chemistry on membrane performance. Two different crosslinkers with aromatic (dichloro-p-xylene (DCX)) and aliphatic (1,4-dibromobutane (DBB)) structures were used to control the interchain spacing of the PBI polymer and enhance its solvent stability. It was revealed that aromatic crosslinkers led to higher degrees of crosslinking and improved chemical resistance to strong aprotic solvents (e.g., NMP

and DMAc), while aliphatic crosslinkers resulted in membranes with larger intersegmental spacing and lower chemical resistance. Subsequently, integrating with sulfocalix[4]arene (SCA4) host molecules created a framework of dual crosslinking and ionic interactions, significantly tightening the polymer network while maintaining a sharp pore size cut-off without compromising the membrane's solvent permeance.

Building upon these insights, in Chapter 5, a chemically stable PBI membrane was reported by covalent crosslinking with a novel crosslinker, triglycidyl isocyanurate (TGIC). The results revealed that the epoxide groups in TGIC underwent nucleophilic ring-opening reactions with the secondary amine groups of PBI, forming a three-dimensional polymer network with exceptional chemical resistance to both organic solvents and extreme pH conditions (pH 1 & pH 14). The membranes showed higher rejection of organic dyes with robust permeance to organic solvents and water, surpassing the available membranes. The reported membrane also demonstrated selective fractionation of mixed solutes, underscoring its potential for industrial separation processes.

Overall, this thesis provides the structure-property-performance relationships of chemically modified PBI membranes involving a combination of covalent crosslinking, supramolecular assembly, and interfacial modification. This approach improves the chemical stability of PBI membranes and finely tunes selectivity and permeability at the molecular level. The findings demonstrate that PBI-based membranes can achieve the stability and performance required for industrial organic solvent separations, enabling their use for solvent recovery and fine chemical purification in large-scale industrial applications.

Acknowledgements

This thesis would not have been possible without the support, guidance, and encouragement of many remarkable people and institutions, to whom I owe a deep sense of gratitude.

I would like to thank Professor Xianshe Feng for his guidance and support during my doctoral studies. I am also grateful to my labmates at the University of Waterloo for the stimulating and supportive environment they provided. I sincerely express my gratitude to Professor Tizazu Mekonnen from the Department of Chemical Engineering, University of Waterloo, for granting me access to his lab.

I had the privilege of spending time as a visiting PhD student in Professor Rohit Karnik's lab at the Massachusetts Institute of Technology (MIT), an experience that significantly broadened my research perspective and enriched my doctoral training. I am deeply thankful to Professor Karnik for his mentorship and financial support during my visit, and to all members of his research group for their warm welcome, friendship, and the many enriching scientific discussions we shared.

This work was generously supported by the Natural Sciences and Engineering Research Council (NSERC) of Canada through the Vanier Canada Graduate Scholarship and the Michael Smith Foreign Study Supplement (MSFSS), the latter of which enabled my research visit to MIT. I am also grateful to the Waterloo Institute for Nanotechnology (WIN) for the Nano-Fellowship, the Ontario Government for the Ontario Graduate Scholarship (OGS), and the University of Waterloo for the President's Graduate Scholarship and the International Experience Award.

During the final year of my PhD, I was blessed with the birth of my son, whose arrival gave me renewed strength to carry this work to completion.

Table of Contents

Examining Committee Membership ii
Author's Declaration iii
Statement of Contributions iv
Abstract vii
Acknowledgements ix
List of Figures xiii
List of Tables xviii
List of Abbreviations and Acronyms xix
List of Symbols xxvi
Chapter 1 Introduction 1
1.1. Background 1
1.2. Fundamentals of the OSN membranes 3
1.3. Advances in OSN 5
1.4. Research Motivation and Objectives 7
1.5. Thesis Outline 9
Chapter 2 Literature Review 11
2.1. Polybenzimidazole (PBI) polymer 11
2.1.1. Background of PBI 11
2.1.2. Synthesis of PBI 11
2.1.3. Properties 13
2.2. Fabrication of PBI-based membranes 16
2.3. Applications of PBI-based membranes 19
2.3.1. PBI-based membranes for gas separation 19
2.3.2. PBI-based membranes for water and wastewater treatment 21
2.3.3. PBI-based membranes for pervaporation 23
2.3.4. PBI-based membranes for OSN 24
2.3.5. PBI-based proton exchange membrane fuel cells 25
2.3.6. PBI-based membranes for redox flow batteries 27
Chapter 3 29
Interfacially crosslinked polydopamine/polybenzimidazole composite membranes for OSN 29
3.1. Experimental Methods 30

3.1.1. Materials and Reagents 30
3.1.2. Membrane fabrication 31
3.1.3. Membrane characterization 32
3.1.4. Pore size distribution and molecular weight cut-off 33
3.1.5. Nanofiltration separation tests 34
3.1.6. Membrane stability/dissolution test 35
3.2. Results and discussion 36
3.2.1. Crosslinking of PDA/DBX on PBI membrane 36
3.2.2. Membrane Characterization 40
3.2.3. Membrane performance 46
3.3. Conclusions 54
Chapter 4 56
Tailoring pore size and chemical resistance of PBI membranes for OSN via chemical crosslinking and sulfocalix[4]arene impregnation 56
4.1. Experimental Methods 57
4.1.1. Materials 57
4.1.2. Fabrication of PBI-based membranes 57
4.1.3. Crosslinking and Modification of PBI Membranes 58
4.1.4. Characterization 60
4.1.5. OSN performance evaluation 61
4.2. Results and discussion 63
4.2.1. Characterization of membranes 63
4.2.2. Molecular weight cut-off and pore size distribution 67
4.2.3. Chemical stability evaluation 68
4.3. OSN performance of membranes 70
4.3.1. Pure solvent permeance 70
4.3.2. Membrane separation performance 73
4.3.3. Mixed solutes separation 74
4.3.4. Membrane durability 75
4.4. Conclusions 76
Chapter 5 78
Triglycidyl isocyanurate crosslinked PBI membranes for solvent-resistant and extreme pH nanofiltration 78

5.1. Experimental Methods 78
5.1.1. Materials 78
5.1.2. Membrane fabrication 79
5.1.3. Characterization 79
5.1.4. Nanofiltration Performance 80
5.2. Results and Discussion 82
5.2.1. Membrane characterization 82
5.2.2. Membrane Performance 92
5.3. Conclusions 104
Chapter 6 Conclusions and future work 105
6.1 Conclusions 105
6.2. Future Work 106
References 109
Appendices 134

List of Figures

Figure 1.1. Schematic illustration of the membrane filtration process and the nominal pore diameter of different membranes. 2

Figure 1.2. Schematic illustration of the fundamentals of OSN processes: (a) pressure-driven and (b) osmosis-driven. 5

Figure 1.3. Development of OSN membranes after the 1960s. 7

Figure 2.1. Synthesis of mPBI by (A) two-stage melt condensation polymerization process using tetraaminobiphenyl (TAB) and diphenyl isophthalate (DPIP), (B) single-stage polymerization process using isophthalic acid catalyzed with organophosphorus and silicon compounds, and (C) homogeneous solution polymerization process using aromatic diamines and dicarboxylic acids in polyphosphoric acid (PPA). 13

Figure 2.2. (A) Ternary phase diagram of a polymer-solvent-nonsolvent system (adopted and modified from [39]). (B) The concept of instantaneous and delayed demixing principles, along with their typical structures (adapted and modified from [65], SEM images reproduced from [66, 67]). (C) The solubility parameters plot of PBI and organic solvents (adapted and modified from [39])..... 17

Figure 2.3. (A) Procedure for fabricating PBI flat-sheet membrane. The dope solution may be prepared by dissolving PBI in an organic solvent (e.g., DMAc). After casting, the nascent membrane is submerged in a coagulation bath (typically water) for phase inversion. (B) Procedure for fabricating PBI hollow fiber membranes, where the dope solution and bore fluid are coextruded through a spinneret into a coagulation bath for phase inversion. (C) Illustration of the ideal morphology of MMMs containing fillers (adapted and modified from [69]). 19

Figure 3.1. Schematic illustration of the dead-end filtration system used in this study. 35

Figure 3.2. Photographs of membranes after 72 hours of agitation in organic solvents..... 37

Figure 3.3. The possible chemical reaction between PDA, DBX, and PBI..... 39

Figure 3.4. Photographs of dopamine solution showing color changes over time and its time-dependent UV-Vis absorbance at 405 nm and 417 nm. Initial concentration: 2 mg/ml. 40

Figure 3.5. ATR-FTIR spectra of the pristine PBI, PBI-PDA (M0), DBX-PBI, and DBX-PDA (M2) membranes. 41

Figure 3.6. Scanning electron microscopy (SEM) images of the membranes. Cross-sectional and surface images of pristine PBI membrane (a & e), PDA-coated PBI membrane (M0, not crosslinked) (b & f), PBI-DBX crosslinked membrane (c & g), and PDA-coated DBX crosslinked membrane (M2) (d & h). 43

Figure 3.7. 3D atomic force microscopy (AFM) images of pristine membrane (a), PDA-coated PBI membrane-M0 (b), PBI-DBX crosslinked membrane (c), and PDA-coated DBX crosslinked membrane-M2 (d). Ra represents the average surface roughness. 45

Figure 3.8. (a) pore size distribution, (b) molecular weight cut-off of the pristine PBI, PBI-DBX, and DBX-PDA (M2) membranes. 45

Figure 3.9. (a) Water contact angle of the pristine PBI, PBI-PDA (M0), DBX-PBI, and DBX-PDA (M2) membranes. (b) Pure solvent permeance of membranes PBI-DBX, M1 (PDA deposition time 10 min), M2 (PDA deposition time 20 min), and M3 (PDA deposition time 40 min). Operating pressure 8 bar and temperature 22 ºC. 46

Figure 3.10. Dye rejection of PBI-DBX, M1, M2, and M3 membranes. (a) Rose Bengal, (b) Remazol brilliant blue, (c) Methyl orange, and (d) N,N-dimethylacetamide. Solvent, ethanol; transmembrane pressure, 8 bar. 48

Figure 3.11. Nanofiltration performance of M2 membrane. (a) Pure solvent permeance, (b) plot of solvent permeance vs combined solvent property (viscosity, molar diameter, and solubility parameter), (c) dye rejection in DMF, and (d) dye rejection in ethanol. The experiments were conducted at 22 ºC under 8 bars. 51

Figure 3.12. M2 membrane separation of mixed dyes (DMNA and RBB) in ethanol (a) and DMF (b). UV-vis absorption spectra of DMNA and RBB in ethanol (c) and in DMF (d). Physical appearance of the permeate samples after filtration in ethanol (e) and DMF (f). The experiments were conducted at 22 ºC and 8 bar. 52

Figure 3.13. M2 membrane rejection of high molecular weight mixed dyes (RBB and MO) in ethanol (a) and DMF (b). 53

Figure 3.14. Comparison of methyl orange (MW=327 g/mol) rejection and ethanol permanence of M2 membrane with the state-of-the-art OSN membranes reported in the literature. References: POSS/PI [171], Kevlar nanofibrous [172], MLD/TFC [173], DBX/SCA4/PBI [1], and PDA/PI [154]. 54

Figure 4.1. (a) The chemical reaction between the PBI monomer and DCX crosslinker is followed by the ionic interaction of the PBI and SCA4 molecule. (b) The chemical reaction between the PBI monomer and DBB crosslinker is followed by the ionic interaction of the PBI and SCA4 molecules. 59

Figure 4.3. Scanning electron microscopy (SEM) and atomic force microscopy (AFM) images of the pristine and crosslinked PBI membranes. Top-view SEM images of (a) P-PBI, (b) DBB-PBI, and (c) DCX-PBI membranes. Cross-sectional view of P-PBI (d&g), DBB-PBI (e&h), and DCX-PBI membranes (f&i). AFM 3D images of P-PBI (j), DBB-PBI (k), and DCX-PBI membranes (l), where Rq represents root-mean-square roughness. 66

Figure 4.4. (a) The water contact angle of P-PBI, crosslinked, and SCA4-modified membranes (The error bars represent the standard deviation of 5 measurements on different spots). (b) PEG rejection and the MWCO values (inserted table) of the fabricated membranes. (c) Pore size distribution of the pristine and modified membranes. (d) The quantity of PBI dissolved in NMP and DMAc (the membrane samples were kept in the solvents for 60 h at a room temperature of 22 ºC, and the concentration of PBI in the solvent was quantified using a UV-Vis spectrophotometer). 68

Figure 4.5. Photographs of the membrane's pieces immersed in different solvents for 20 days. The pristine PBI membrane completely disintegrated in NMP (a). The DCX crosslinked membrane showed resistance to all solvents (b), while the DBB crosslinked membrane dissolved to a certain level in NMP (slightly turbid at the bottom) (c). 70

Figure 4.6. (a) Solvent permeance vs 1/η and (b) solvent permeance vs Mv/η for DBB-SCA4 and DCX-SCA4 membranes. 71

Figure 4.7. Pure solvent permeance of pristine and modified membranes. 72

Figure 4.8. (a) Rejection of Rose Bengal, (b) Remazol brilliant blue, (c) Methyl orange in ethanol (Feed solution = 50 ppm). (d) Mixed dye solution filtered through pristine, crosslinked, and SCA4-

modified membranes (Feed solution each dye = 20 ppm, temperature = 22 ± 1 ºC, pressure = 8 bar). (e) Pictures of the mixed feed and permeate solution. 74

Figure 4.9. The separation performance for dye rejection from ethanol. DCX-SCA4 membrane: (a) Rose Bengal and (b) Remazol brilliant blue. DBB-SCA4 membrane: (c) Rose Bengal and (d) Remazol brilliant blue. Feed solution 50 ppm, temperature 22 ºC, pressure 8 bar. 75

Figure 4.10. Comparison of permeance (solvent ethanol) and rejection (MO, MW 327.33 g/mol) of this work with other membranes reported in the literature. 1. POSS/PI [171]; 2. PDA-DBX-PBI [191]; 3. Kevlar nanofibrous [172]; 4. MLD/TFC [173]; 5. DBX/SCA4/PBI [1]; 6.PDA/PI [154]; 7. PBI–NGDGE [117]; 8. PBI–NGDGE [117]; 9. Crosslinked PI [192]; 10. B-CD/TC [193]. ... 76

Figure 5.1. (a) Illustration of PBI crosslinking with TGIC. (b) Images of P-PBI membrane (the leftover membrane is the polypropylene substrate, and the PBI top layer is completely dissolved except for acetic acid and HCl, which did not dissolve the P-PBI) and (c) X-PBI membrane after 24 h of soaking in strong organic solvents and acids. (d) Images of the X-PBI membrane immersed in NMP and DMAc on day 1 (left) and after 1 month (right)..... 83

Figure 5.2. FTIR spectra of P-PBI and X-PBI, showing characteristic absorption peaks corresponding to functional groups. 84

Figure 5.3. XPS spectra of P-PBI and X-PBI membranes..... 85

Figure 5.4. N1s XPS narrow scans of P-PBI (a) and X-PBI (b) membranes. C1s XPS narrow scans of P-PBI (c) and X-PBI (d) membranes..... 87

Figure 5.5. X-ray diffraction (XRD) patterns of P-PBI and X-PBI membranes. 88

Figure 5.6. Thermogravimetric analysis (TGA) of P-PBI and X-PBI membranes, showing weight loss as a function of temperature. 89

Figure 5.7. Water contact angle of P-PBI and X-PBI membranes, showing surface hydrophilicity. 90

Figure 5.8. SEM images of the cross-sectional and surface morphologies of the P-PBI membrane (a,c & e) and X-PBI membrane (b, d & f). 91

Figure 5.9. AFM 3D images of P-PBI (a) and X-PBI (b) with root-mean-square (RMS) roughness (Rq). 92

Figure 5.10. Pure solvents permeance of P-PBI and X-PBI membranes at 6 bars. 93

Figure 5.11. Solvent permeance through X-PBI membrane vs a lumped parameter for solvent properties (a). Solvent permeance as a function of the applied pressure (b). 94

Figure 5.12. Dye rejection of the P-PBI membrane (a) and the X-PBI membrane (b) from ethanol solvent. 95

Figure 5.13. UV-vis absorption spectra of dye solutions before and after nanofiltration through the X-PBI membrane: (a) RB, (b) RBB, (c) MO, and (d) DMNA. Insets show the visual appearance of dye solutions before (left) and after (right) nanofiltration. 96

Figure 5.14. Dyes rejection of the X-PBI membrane from DMF solvent. 97

Figure 5.16. Performance of X-PBI membrane for mixed dye separation in ethanol (a). UV-vis absorbance spectra of the RB and DMNA in mixed feed and permeate (b). Protocol and appearance of the mixed feed and permeate after filtration (c). X-PBI rejection of RB from ethanol over a filtration period of 10 h (d). 99

Figure 5.17 (a) The pure permeance of the X-PBI membrane to water, DMF, and a DMF/water mixture (30:70 by wt). (b) Rejection of X-PBI membrane to RBB in different solutions. (c) Rejection of X-PBI membrane to RB in different solutions (the rejection of RB was not evaluated due to its low solubility at pH 1). UV-vis absorption spectra of RBB at pH 14 (d), RBB at pH 1 (e), and RB at pH 14 (f). 103

List of Tables

Table 2.1. Main-chain structure derivatives of PBI obtained through the solution polymerization method..... 13

Table 3.1. Membranes fabricated in this study..... 32

Table 3.2. Dissolution (%) of membranes in organic solvents. 35

Table 3.3. Properties of dyes used in this study. 47

Table 3.4. Properties of the solvents used in this study. 49

Table 4.1. Properties of the solvents used in this study. 61

Table 4.2. Properties of dyes used in this study. 62

Table 4.4. Solvent swelling degree of the pristine and modified PBI membranes after 20 days of immersion in the solvents. 69

Table 5.1. Dissolution of P-PBI and X-PBI membranes in harsh solvents..... 82

Table 5.2. XPS atomic composition (At%) carbon (C1s), nitrogen (N1s), and oxygen (O1s) of the pristine and crosslinked membranes. 85

Table 5.3. Comparison of the OSN performance of TGIC X-PBI membrane with other polymeric membranes reported in the literature. 100

List of Abbreviations and Acronyms

4F-PBI	4 fluorinated polybenzimidazole
6F-PBI	6 fluorinated polybenzimidazole
AB-PBI	Poly(2,5-benzimidazole)
AFM	Atomic Force Microscopy
ATR-FTIR	Attenuated Total Reflectance -Fourier Transform Infrared
BIpPBI	Benzimidazole-linked polymers
BrTPA	Bromoterephthalic acid
CH_4	Methane
CO_2	Carbon dioxide
CR-PBI	Crosslinked polybenzimidazole membranes
$CuSO_4$	Copper sulfate
DBB	1,4-dibromobutane1x
DBrTPA	Dibromoterephthalic acid
DBX	α,α'-dibromo-p-xylen
DCX	α,α′-Dichloro-p-xylene
DI	Deionized water
DMAc	N,N-dimethylacetamide
DMF	N,N-dimethylformamide

DMNA	N,N-dimethyl-2-nitroaniline
DMSO	dimethyl sulfoxide
DPIP	diphenyl isophthalate
DVS	divinyl sulfone
EtOH	Ethanol
FO	Forward osmosis
GA	Glutaraldehyde
H_2SO_4	Sulfuric acid
H_3PO_4	Phosphoric acid
HCl	Hydrochloric acid
$HClO_4$	Perchloric acid
HFMs	Hollow fiber membranes
HMT-PMBI	hexamethyl-*p*-terphenyl polybenzimidazolium
HNO_3	Nitric acid
HOOC	Oxalic acid
HPLC	High-performance liquid chromatography
HSO_4	Hydrogen sulfate ion
ICRFB	Iron-chromium redox flow battery
IPA	Isopropanol
IR	Infrared

ISA	Integrally skinned asymmetric
K_2CO_3	Potassium carbonate
$K_2S_2O_8$	Potassium persulfate
$KMnO_4$	Potassium permanganate
KOH	Potassium hydroxide
LiCl	Lithium chloride
LiOH	Lithium hydroxide
MeCN	Acetonitrile
MeOH	Methanol
MF	Microfiltration
MLD	Molecular layer deposition
MMMs	Mixed matrix membranes
MO	Methyl orange
MPa	Mega Pascal
m-PBI	meta-Polybenzimidazole
Mv	Molar volume
MW	Molecular weight
MWCO	Molecular weight cut-off
NaCl	Sodium chloride
NaOH	Sodium hydroxide

NF	Nanofiltration
NGDGE	neopentyl glycol diglycidyl ether
NIPS	nonsolvent-induced phase separation
NMP	N-methyl-2-pyrrolidone
OBA	4,40-Oxybis(benzoic acid)
OH	Hydroxyl group
OHPyPB	PBI containing hydroxyl pyridine groups
OPBI	Poly[2,2′-(p-oxydiphenylene)-5,5′-bibenzimidazole]
OSFO	Organic solvent forward osmosis
OSN	Organic solvent nanofiltration
OSRN	Organic solvent-resistant nanofiltration
P-PBI	Pristine polybenzimidazole
PA	Polyamide
PA-doped	Phosphoric acid-doped
PA-PBI	Phosphoric acid doped Polybenzimidazole
PAN	Polyacrylonitrile
PBI	Polybenzimidazole
PBI-4N	Polybenzimidazole-P oly(2,2′-(*m*-phenylene)-5,5′-bibenzimidazole)
PBI-BRT	Polybenzimidazole- 2-Bromoterephthalic acid
PBI-BTBP	Polybenzimidazole- Bis(trifluoromethyl)benzidine

PBI-Bul	Polybenzimidazole- 5-*tert*-Butylisophthalic acid
PBI-DBRT	Polybenzimidazole- 2,5-Dibromoterephthalic acid
PBI-DBX	Polybenzimidazole membrane crosslinked with DBX
PBI-HPEIs	Polybenzimidazole Hyperbranched polyethyleneimine
PBI-I	Polybenzimidazole Isophthalic acid
PBI-PDA	Polybenzimidazole polydopamine
PBI-T	Polybenzimidazole terephthalic acid
PDA	Polydopamine
PDMS	Polydimethylsiloxane
PEEK	Polyether ether ketone
PEG	Polyethylene glycol
PEI	Polyethylenimine
PEM	Proton exchange membrane
PEMFCs	Proton exchange membrane fuel cells
PI	Polyimide
PIMs	Polymers with intrinsic microporosities
POSS	Polyhedral oligomeric silsesquioxane
PP	Polypropylene
PPA	Polyphosphoric acid
PSf	Polysulfone

PTMSP	poly(1-trimethylsilyl-1-propyne)
PV	Pervaporation
PVA	Polyvinyl alcohol
PVDF	Polyvinylidene fluoride
PVP	Polyvinylpyrrolidone
RB	Rose Bengal
RBB	Ramazol brilliant blue
RFB	Redox flow batteries
RIPS	Reaction-induced phase separation
RMS	Root-mean-square
RO	Reverse osmosis
SCA4	Sulfocalix[4]arene
SEM	Scanning electron microscopy
SIPS	Solvent evaporation-induced phase separation
SPBI	Sulfonated polybenzimidazole
sPPSU-HPEI	Sulfonated polyphenylsulfone
SRNF	Solvent-resistant nanofiltration
TAB	Tetraaminobipheny
TADPS-OBA	Tetraaminodiphenylsulfone-oxybis(benzoic acid) polybenzimidazole
TBB	1,3,5-Tris(bromomethyl)benzene

TCL	Terephthaloyl chloride
TFC	Thin-film composite
TFN	Thin-film-nanocomposite
TGA	Thermogravimetric analysis
TGIC	Triglycidyl isocyanurate
THF	Tetrahydrofuran
TIPS	Thermally induced phase separation
TOC	Total organic carbon
TPA	Terephthalic acid
UF	Ultrafiltration
UV	Ultraviolet
VRFBs	Vanadium redox flow batteries
WCA	Water contact angles
XPS	X-ray Photoelectron Spectroscopy
XRD	X-ray diffraction

List of Symbols

A	Effective membrane area	m^2
Cf	Feed concentration	mol L^{-1} or mg L^{-1} or ppm
Cp	Permeate concentration	mol L^{-1} or mg L^{-1} or ppm
ΔP	Transmembrane pressure	Bar
$\Delta\pi$	Osmotic pressure difference	Pa
D	Diffusion coefficient	$m^2\ s^{-1}$
dp	Pore diameter or solute Stokes diameter	nm
E	Binding energy	eV
P	Solvent permeance	$L/(m^2.h.bar))$
R	Solute rejection	%
Rq	root-mean-square roughness	nm
T	Temperature	°C
t	Time	hours
α	Degree of crosslinking	—
θ	Contact angle	°
η	Solvent viscosity	mPa·s
σp	Geometric standard deviation of pore size	—
ζ	Zeta potential	mV

ϕ	Porosity	%
δ	Hensen solubility parameter	$(MPa)^{1/2}$
δd, ,	Dispersion (London) components of δ	$(MPa)^{1/2}$
δp	Polar (dipole-dipole) components of δ	$(MPa)^{1/2}$
δh	Hydrogen bonding components of δ	$(MPa)^{1/2}$
ρ_s	Solvent density	g/cm^3
Mv	Molar volume of solvent	$cm^3\ mol^{-1}$
μp	Mean effective pore radius	nm
μ	Solvent dynamic viscosity	Pa·s
S	Solvent uptake	cm^3/g
Tg	Glfass transition temperature	°C
ρp	Polymer density	$g\ cm^{-3}$
Vm	Molar volume	$cm^3\ mol^{-1}$
V	Volume of permeate	Liter or ml
W_{wet}	Weigh wet	grams
W_{dry}	Weigh dry	grams
W_0	Weight of pristine PBI	%
W_1	Weight of crosslinker	%

Chapter 1 Introduction

**** This chapter is composed of published review papers as outlined in the statement of contributions.***

1.1. Background

Chemical separation plays a critical role in modern industrial processes, including chemical production, pharmaceutical manufacturing, energy generation, and environmental remediation [1]. Conventional separation technologies, such as distillation, evaporation, adsorption, and extraction, are widely used but require high energy input and result in a large carbon footprint [2, 3]. These processes account for approximately 10-15% of the world's energy consumption and nearly half of the total energy used in the chemical industry [4]. Consequently, the development of energy-efficient separation technologies is essential for achieving sustainable industrial processes [5]. Membrane-based separation technologies have therefore attracted attention as more energy-efficient alternatives [6], and it is estimated that up to 90% of energy can be saved in industries by replacing traditional thermal-based separation processes with membrane-based separation [5].

Membranes are semi-permeable barriers that allow selective transport of specific components in a mixture under a driving force such as pressure, temperature, concentration, or electric potential gradients [7]. The pressure-driven membrane processes are divided based on their filtration process, such as microfiltration (MF), ultrafiltration (UF), nanofiltration (NF), and reverse osmosis (RO) (Fig. 1.1). Each membrane has varying pore sizes and capabilities for filtering out particles and microorganisms. MF membranes have the largest pore size and reject large particles and microorganisms, while UF membranes have smaller pores and can reject bacteria and soluble macromolecules like proteins. RO membranes are non-porous and exclude particles and many low molecular mass species like salt ions and organics. NF membranes are relatively new and have pores smaller than UF membranes but larger than RO membranes, exhibiting performance between the range of UF and RO [8]. A major advancement in this field is organic solvent nanofiltration (OSN), also known as organic solvent-resistant nanofiltration (OSRN). This technique differs from traditional nanofiltration, which operates in aqueous media. OSN enables the separation of solutes with molecular weights typically between 200 and 2000 $gmol^{-1}$ in organic solvents [9-13]. OSN offers several advantages over conventional processes for the separation and recovery of various

organic solvents relevant to petrochemical, pharmaceutical, food, and fine chemical industries [12]. Apart from being energy-intensive, traditional separation processes also create hazardous wastes or degrade heat-sensitive products if operated at high temperatures. In contrast, the OSN works at ambient temperatures to retain large solute molecules while allowing smaller solvent molecules to permeate through the membrane, where energy consumption is usually low, and there is essentially no or little loss of the solvents [13]. Depending on the specific OSN separations, the membranes may be subjected to an extensive range of solvents under harsh operating conditions (e.g., high temperatures and pressures). Therefore, membranes used in OSN must withstand harsh solvents, high temperature and pressures while maintaining high permeability and selectivity [14].

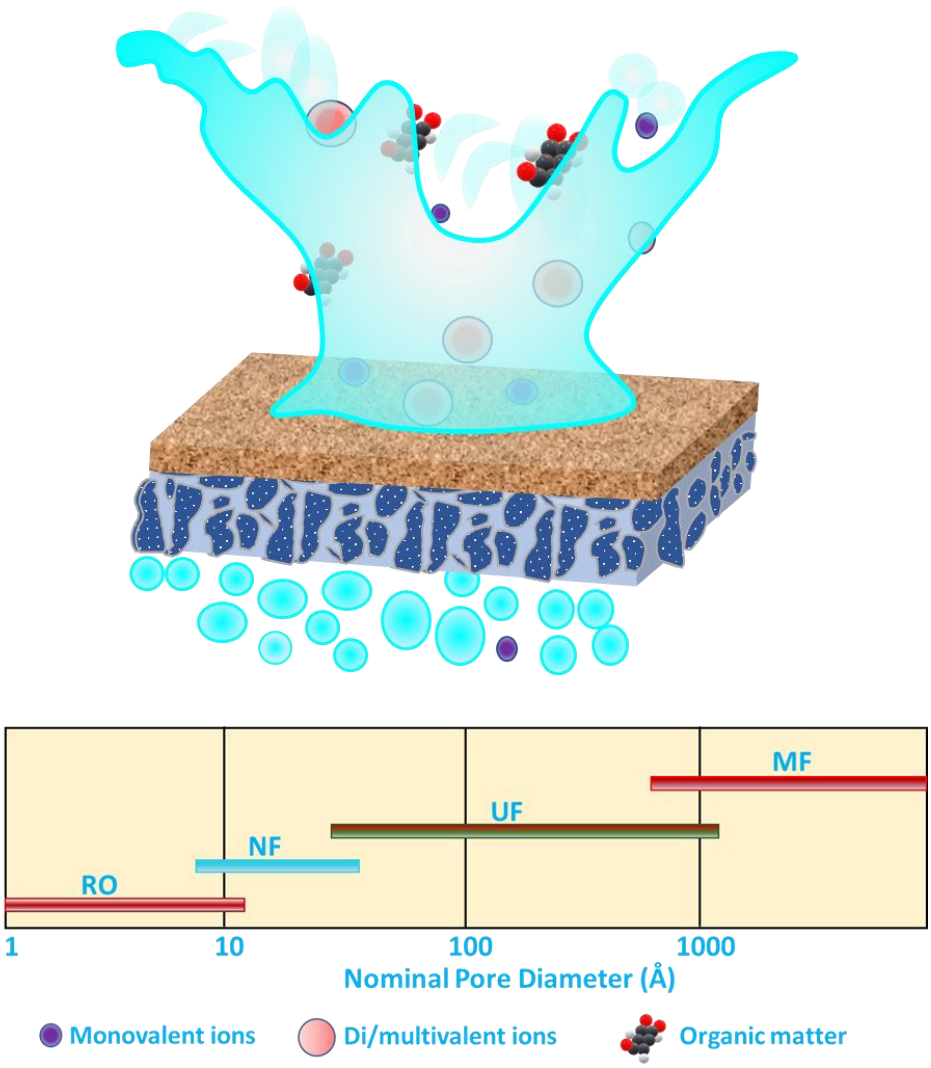


Figure 1.1. Schematic illustration of the membrane filtration process and the nominal pore diameter of different membranes.

Polymeric membranes currently dominate the market for separation. For OSN applications, commonly studied polymers include polyamide (PA) [15], polyimide (PI) [16], polybenzimidazole (PBI) [17], poly [1-(trimethylsilyl)-1-propyne] (PTMSP) [18], polysulfone (PSf) [19], polymers with intrinsic microporosities (PIMs) [20] and silicone rubbers (i.e., polydimethylsiloxane (PDMS)) [21]. With current membrane fabrication technologies, these membranes are not difficult to manufacture, but the trade-off between membrane permeability and selectivity (i.e., solvent permeance vs. solute rejection) and their long-term stabilities to resist organic solvents is still a concern for practical OSN applications [11]. Especially, the OSN membranes often suffer from intense swelling and even solvation when exposed to harsh organic solvents, which significantly compromises their overall performance [9, 22, 23]. For instance, a PTMSP-based thin-film composite (TFC) membrane exhibited a steep decline in permeance due to physical aging [24], while PDMS layers suffered from extensive swelling in non-polar solvents [11, 24, 25]. These challenges emphasize the need for advanced membrane materials capable of maintaining high selectivity while resisting swelling and degradation in aggressive organic solvents.

Among the various polymers investigated for OSN applications, PBI has attracted considerable interest due to its excellent thermal stability, mechanical strength, and chemical resistance. These properties make PBI a promising candidate for developing solvent-resistant membranes suitable for harsh separation environments.

1.2. Fundamentals of the OSN membranes

The OSN membranes for the separation of organic solvents can be classified as pressure-driven and osmosis-driven processes, as shown in Figure 1.2. The pressure-driven membrane process requires an external hydraulic pressure for mass transport, while the osmosis system is driven by the chemical potential gradient across the membrane established under an osmotic pressure difference created by using a draw solution. The pressure-driven process typically allows the smaller solvent molecules to pass the membrane while retaining the larger solute molecules on the feed side (Fig. 1.2a). The osmosis-driven process is not as popular at present, and it concentrates the feed solution by extracting the solvent using a draw solution that has a higher osmotic pressure than the osmotic pressure of the feed solution (Fig. 1.2b) [26, 27], while the diluted draw solution is regenerated appropriately by such means as direct filtration, distillation, and evaporation. The

osmosis-driven process is sometimes also referred to as organic solvent forward osmosis (OSFO), analogous to forward osmosis used in water desalination.

The OSN membrane performance is normally evaluated in terms of solvent flux and solute rejection, which are direct representations of the membrane permeability and selectivity, respectively. Generally, the membrane permeability (or strictly speaking, the permeance) is expressed in volumetric or mass flux normalized by the transmembrane driving force for permeation, while the solute rejection is usually represented by the change in solute concentration between the feed and the permeate relative to the feed solute concentration. For convenience, the membrane permeability and selectivity are often evaluated experimentally under dead-end and cross-flow configurations [28]. While this works well for quick membrane screening or proof-of-concept tests, the long-term performance and durability of the membrane cannot be fully revealed [29].

At present, the majority of OSN membranes are fabricated from polymer solutions via thermally induced phase separation (TIPS), nonsolvent-induced phase separation (NIPS), and reaction-induced phase separation (RIPS). NIPS is the commonly used method to prepare state-of-the-art OSN membranes, which was initially developed for producing asymmetric membranes for water desalination by reverse osmosis in the 1970s. There are two common types of OSN membranes: thin-film composite/nanocomposite (TFC/TFN) membranes and integrally skinned asymmetric (ISA) membranes. The TFC/TFN membranes have the active skin layer deposited on top of a microporous substrate made of different polymer materials, while the ISA membranes have the surface skin layer and the porous support made of the same polymer material. In both cases, the microporous substrates act primarily as mechanical support for the skin layer that is active for the separation. The ISA membranes are typically produced from glassy polymers via phase inversion, while the skin layer of TFC membranes is commonly formed via interfacial polymerization between two monomers dispersed in an aqueous phase and an oil phase, respectively. Thus, both the active and support layers of TFC and TFN membranes can be modified and tailored separately [12]. Presently, there is a growing interest in incorporating or integrating nanomaterials in the polymer matrix of mixed matrix membranes (MMMs) or in the active layer of TFN membranes to yield nanostructured composite OSN membranes with improved performance [30].

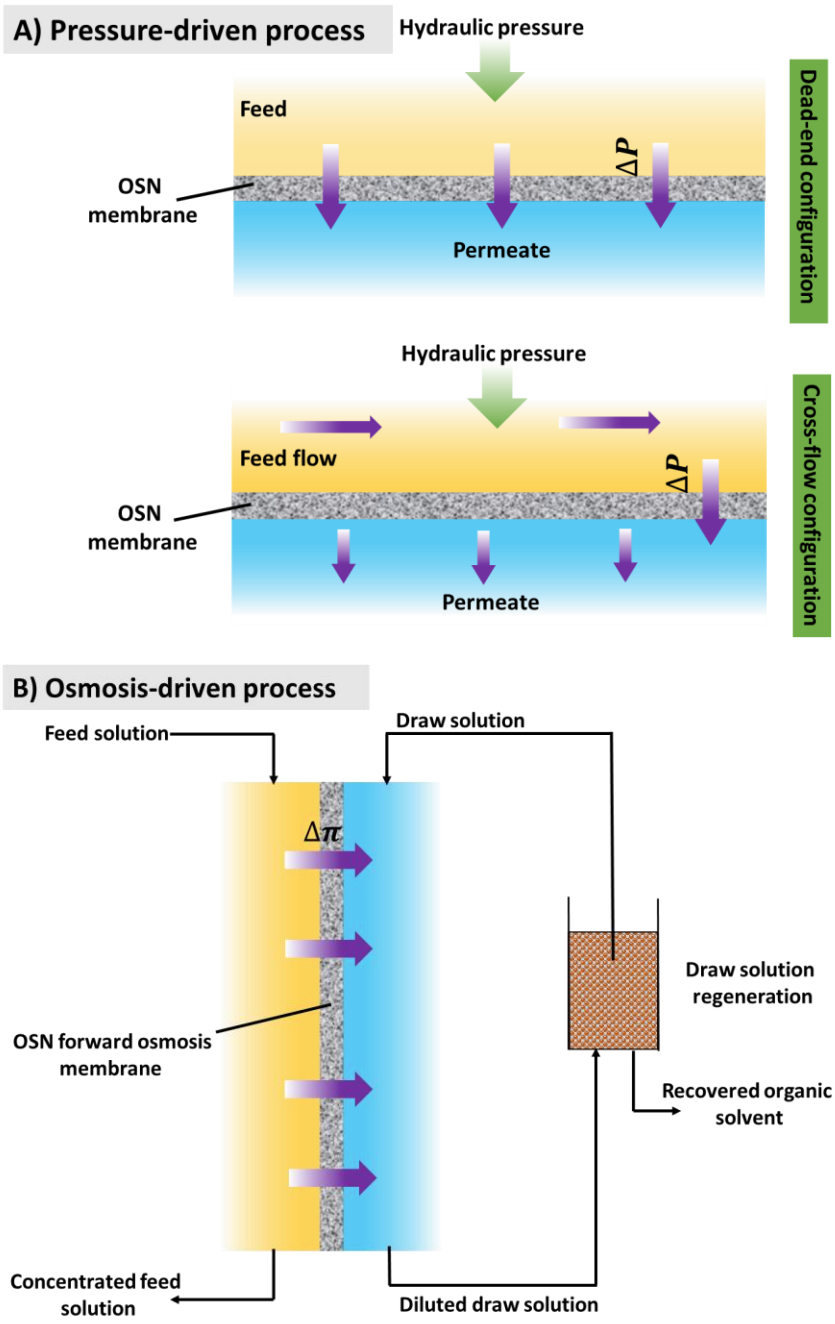


Figure 1.2. Schematic illustration of the fundamentals of OSN processes: (a) pressure-driven and (b) osmosis-driven.

1.3. Advances in OSN

The development of OSN membranes can be traced back to the pioneering work of Loeb and Sourirajan on asymmetric membranes and Cadotte on thin-film composite membranes for RO in

the late 1960s. Subsequently, it was found that by finely tuning the membrane structure, the membranes could reject multivalent ions while allowing monovalent ions to pass through the membrane. As such, nanofiltration is fundamentally no different from reverse osmosis except that a looser membrane structure is appropriate for nanofiltration, which is thus sometimes also called loose reverse osmosis. Nanofiltration was then used for water treatment and desalination [31]. Inspired by the successes of water application, the membranes were expanded to applications involving non-aqueous solutions (Fig. 1.3). In the 1980s, many inventions were disclosed in the form of patents by Exxon, Shell, and Union Carbide for filtration of organic solvents. The term nanofiltration began to be used predominantly over "loose RO" in the mid-1980s, well before the buzzword "nano" we see nowadays. Solvent-resistant nanofiltration membranes based on PDMS were introduced to the market by Koch Membrane Systems in the 1990s. A large commercial OSN plant was commissioned in 1994 by Exxon-Mobil using polyimide-based membranes [31]. By the late 2000s, additional OSN membranes became available commercially from Grace Davison, Koch, Solsep, and GMT (Fig. 1.3).

Meanwhile, on the research front, in 2007, Toh et al. [32] synthesized OSN membranes through chemical crosslinking of PI membranes with aliphatic diamines, and the membranes were shown to be stable in different organic solvents with good separation performance. In the same year, Jeong et al. [33] reported a TFN reverse osmosis polyamide membrane incorporated with zeolite nanoparticles, where the nanoparticle pores were found to play an active role in water permeation and solute rejection. This has motivated the use of various nanomaterials in membranes for OSN applications, and a great deal of work has been done on nano-based OSN membranes over the past decade.

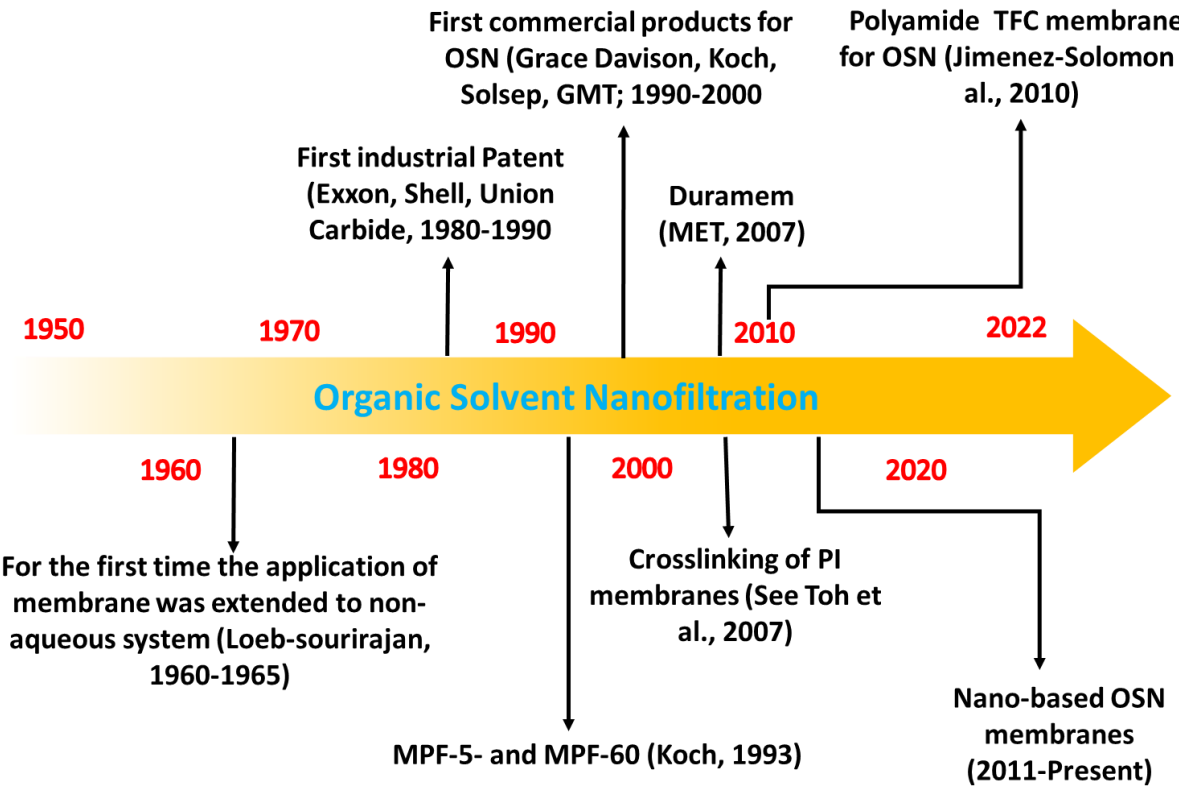


Figure 1.3. Development of OSN membranes after the 1960s.

1.4. Research Motivation and Objectives

Building upon the background, fundamentals, and recent developments in OSN discussed above, the following section outlines the motivation and objectives of this research. Membrane technology has been largely developed for aqueous separations, but its application to non-aqueous separations has gained interest in recent years due to its potential advantages for organic solvents separation. As discussed in Section 1.1, OSN offers a promising membrane-based alternative to traditional thermal separation processes for solvent recovery and solute purification. Despite significant progress in the development of OSN membranes, several challenges remain that limit their broader industrial implementation.

Many polymeric membranes suffer from insufficient chemical stability when exposed to harsh organic solvents, particularly polar aprotic solvents such as dimethylformamide (DMF), dimethylacetamide (DMAc), and N-methyl-2-pyrrolidone (NMP). In addition, OSN membranes often exhibit an inherent trade-off between solvent permeance and solute rejection; increasing

solvent permeance lowers selectivity, while improving rejection reduces permeance. Addressing these limitations requires the development of membrane materials that combine high chemical stability, controlled pore structures, and strong molecular sieving capabilities.

PBI has emerged as a promising polymer for OSN membranes due to its excellent thermal stability, mechanical strength, and chemical resistance. However, pristine PBI membranes may still experience swelling and structural changes in certain aggressive organic solvents. Therefore, structural modification and crosslinking strategies are required to enhance the solvent resistance and separation performance of PBI-based membranes.

Therefore, the objective of this research was to develop chemically stable PBI-based membranes with tailored pore structures for high-performance OSN. To achieve this goal, this thesis explored molecular design, interfacial modification, supramolecular functionalization, and covalent crosslinking strategies to improve membrane stability, permeability, and selectivity under aggressive solvent and extreme pH conditions.

The main objectives are listed below:

1. **To critically review and identify key limitations in existing OSN membranes and the potential of PBI as a base polymer (Chapters 1 & 2).**
   This objective involved a comprehensive review of the state-of-the-art OSN technology, focusing on the chemical, structural, and performance shortcomings of conventional membranes and positioning PBI as a promising candidate due to its intrinsic thermal and mechanical stability.

2. **To engineer interfacially crosslinked composite membranes for enhanced nanofiltration performance (Chapter 3).**
   This objective focused on integrating polydopamine (PDA) layers onto PBI supports and crosslinking with dibromo-p-xylene (DBX) to form a defect-free, solvent-resistant composite membrane with tunable thickness and selectivity. The work sought to understand how interfacial chemistry influences solvent permeance, solute rejection, and long-term operation.

3. **To explore the influence of crosslinker chemistry on the chemical resistance of PBI membrane and to tailor the pore structure through supramolecular functionalization (Chapter 4).**

   Two different crosslinking agents with different chemical structures (aromatic and aliphatic) were used to explore the effects of the crosslinker chemistry on the chemical stability of the PBI membrane. To improve the selectivity of the membrane towards smaller molecular weight solutes, supramolecular functionalization with sulfocalix[4]arene was investigated.

4. **To develop solvent-resistant PBI membranes using multifunctional crosslinker agent (Chapter 5).**

   The aim was to introduce multifunctional crosslinking agent triglycidyl isocyanurate (TGIC) to create chemically stable three-dimensional network structures within PBI, thereby improving its resistance to polar aprotic solvents (e.g., DMF, DMAc, NMP, DMSO) and under extreme pH environments.

Through these strategies, this research aims to establish structure-property-performance relationships in PBI-based OSN membranes and contribute to the development of sustainable membrane technologies for solvent separation and purification.

1.5. Thesis Outline

This thesis is composed of a total of seven chapters listed below. Most of the work mentioned here is from published research papers presented in the statement of contributions section of the thesis. Chapter 1 provides background information on membrane-based separation, introduces OSN technology, and presents fundamental and advancements in OSN technology achieved over time. Additionally, this chapter also outlines the research motivation and objectives of the thesis. Chapter 2 is based on a comprehensive review of the PBI polymer and PBI-based membranes. This chapter presents an overview of PBI synthesis, structure, properties, and fabrication of PBI-based membranes. Finally, the chapter also introduces the application of PBI-based membranes reported in the literature. Chapter 3 provides interfacial crosslinking of the PDA and PBI composite membrane. It discusses the interfacial reaction mechanisms, optimization of coating parameters,

and the resulting improvement in OSN performance and long-term stability. Chapter 4 investigates the effect of crosslinker chemistry and supramolecular modification on the chemical stability, pore structure and molecular sieving behavior of PBI membranes. This chapter compares aromatic and aliphatic crosslinkers to understand how structural rigidity influences membrane stability and performance. Furthermore, the incorporation of sulfocalix[4]arene as a supramolecular modifier is also explored in Chapter 4 to achieve finer pore control and enhanced selectivity without compromising solvent permeance. Chapter 5 focuses on the fabrication and characterization of covalently crosslinked PBI membranes using a multifunctional epoxide crosslinker, triglycidyl isocyanurate (TGIC). This work demonstrates the development of chemically stable PBI membranes capable of operating in harsh organic solvents and extreme pH environments. The chapter discusses the crosslinking mechanism, physicochemical characterization, and the resulting improvements in solvent resistance and membrane performance. Finally, Chapter 6 summarizes the conclusions of the research and offers recommendations for future work.

All references cited in this thesis are listed in the References section at the end of the thesis.

Chapter 2 Literature Review

**** This chapter is composed of a published review paper on polybenzimidazole-based membranes as outlined in the statement of contributions.***

2.1. Polybenzimidazole (PBI) polymer

Chapter 1 introduced the fundamentals of membrane separation and OSN. This chapter focuses specifically on PBI polymers and their applications in membrane technologies.

2.1.1. Background of PBI

Polybenzimidazoles (PBIs) are heterocyclic polymers with benzimidazole groups as the repeating units in the polymer backbones, and they typically belong to the family of engineering plastics [34]. The first fully aromatic polybenzimidazoles were synthesized in 1961 by Vogel and Marvel [35]. At present, PBI is often used as an acronym that refers to the commercially available PBI polymer, which is poly[2,2′-(m-phenylene)-5,5′-bibenzimidazole]. It has been produced by Celanese Corporation since 1983 and is sometimes also called meta-PBI (m-PBI). These polymers are synthesized through the condensation of tetraamines and diacids, having a great number of combinations of these building blocks [36, 37]. PBIs can be partly or fully aromatic and are typically characterized by their excellent thermo-mechanical properties, such as high glass transition temperatures (425-436 ºC) and oxidation resistance [34]. They can maintain stability with a minimal weight loss (<5%) up to 570 ºC [38]. Such remarkable properties make them particularly suitable for a wide range of applications in challenging chemical environments (e.g., membranes, chemical sensors, fire-resistant materials, and electro-optical applications) [39, 40].

2.1.2. Synthesis of PBI

PBI can be synthesized by two main routes: melt/solid phase polymerization (first reported in 1961) [35] and solution polymerization (first reported in 1964 using polyphosphoric acid (PPA)) [41]. During the initial stage of the two-step melt/solid polycondensation reaction of tetraaminobiphenyl (TAB) and diphenyl isophthalate (DPIP) at 260 °C, low molecular weight PBI prepolymer was produced (Fig. 2.1a). The pre-polymer was then ground into fine powders and

subjected to thermal treatment at 400 °C, thereby increasing its molecular weight [35, 42]. One of the drawbacks of the two-stage polymerization process was the formation of a large volume of foam due to the production of phenol and water as by-products of the polymerization reaction, resulting in a viscous solution. The foaming effect restricted the degree of polymerization, and thus a second-stage reaction was required to increase the molecular weight of PBI [43]. Replacing DPIP with isophthalic acid and using organophosphorus and silicon compounds as catalysts, Choe [44] proposed a single-step reaction route (Fig. 2.1b), which not only minimized foam production but also reduced the costs of the raw materials, as isophthalic acid was much more cost-effective than DPIP. The synthesis of PBI could also be achieved through solution polymerization using monomers of aromatic diamines and dicarboxylic acids in PPA, as shown in Figure 2.1(c). Other conventional solvents (e.g., N,N-dimethylacetamide (DMAc) and N-methylpyrrolidone (NMP)) could be used as well. However, PPA is the most used solvent for PBI production via solution polymerization.

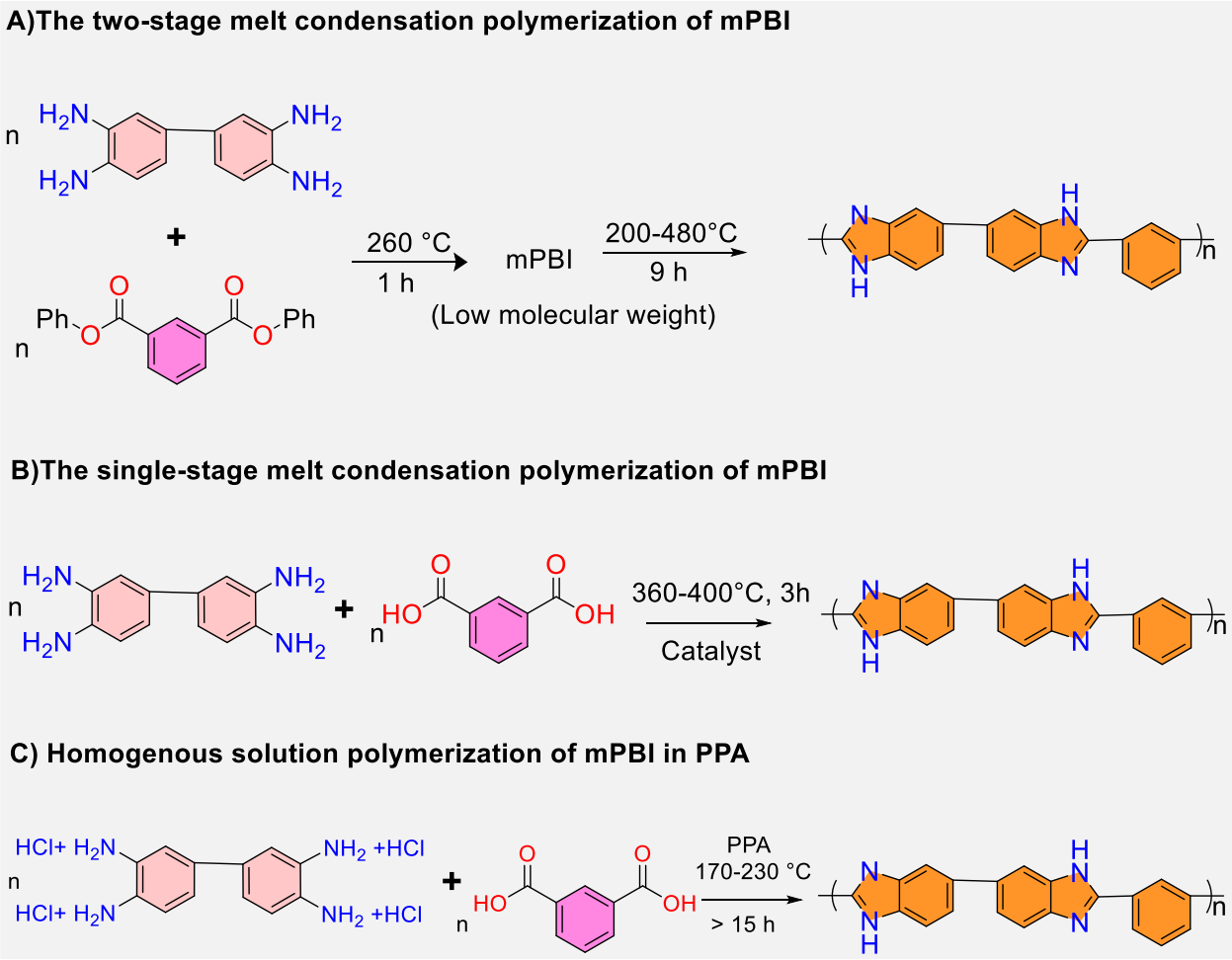
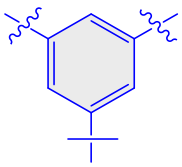


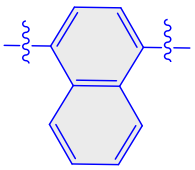
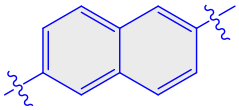
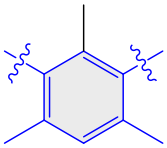
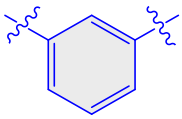
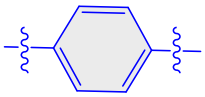
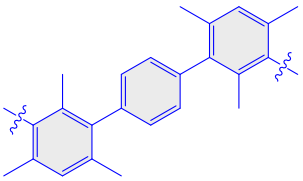
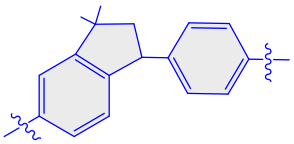
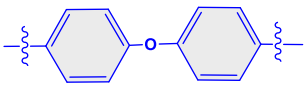
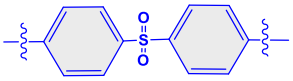
Figure 2.1. Synthesis of mPBI by (A) two-stage melt condensation polymerization process using tetraaminobiphenyl (TAB) and diphenyl isophthalate (DPIP), (B) single-stage polymerization process using isophthalic acid catalyzed with organophosphorus and silicon compounds, and (C) homogeneous solution polymerization process using aromatic diamines and dicarboxylic acids in polyphosphoric acid (PPA).

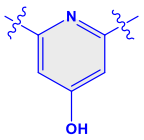
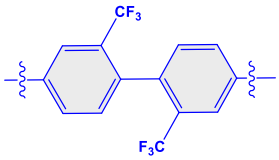
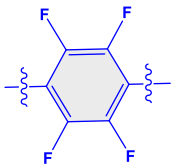
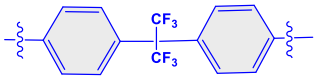
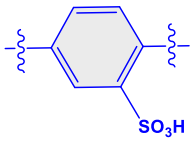
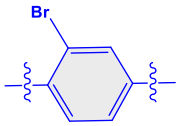
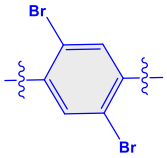
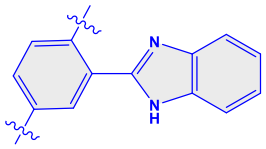
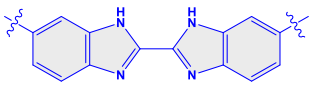
2.1.3. Properties

PBI was originally exploited for use as a non-flammable textile fiber to replace asbestos and was later used as a high-temperature resin for aerospace and defense applications [39]. It has a glass transition temperature (Tg) of 425-436 °C, making it one of the highest Tg polymers available. However, the use of PBI as a thermoplastic material is limited due to its high processing temperature and low solubility in organic solvents [45]. To overcome this drawback, different chemical structures of PBIs have been synthesized and reported. For example, the incorporation of one ether group per repeating unit in poly[2,2′-(p-oxydiphenylene)-5,5′-bibenzimidazole] (OPBI) has significantly improved its processability and solubility for extended applications as compared to unmodified PBI [46]. In addition to strong resistance to a wide range of chemicals, PBI is also resistant to oxidation and hydrolysis. The degree of polymerization of PBI polymers can also be adjusted by manipulating the reaction conditions (e.g., monomers and monomer concentrations, reaction temperature, and duration) [47, 48]. To produce mechanically robust membranes, PBI with a high molecular weight is preferred. In a search for a similar paradigm, various chemical structures and derivatives of PBI have been synthesized and reported in the literature (Table 2.1).

Table 2.1. Main-chain structure derivatives of PBI obtained through the solution polymerization method.

PBI type	R	Dicarboxylic acid, HOOC–R–COOH	Polymerization solvent, T (ºC)	References
PBI-Bul		5-tert-Butylisophthalic (Bul)	PPA, 200 ºC	[49]

N-PBI		1,4-Naphthalenedicarboxylic acid	Eaton's reagent, 14 ºC	[50]
PBI-4N		Poly(2,6-(2,6-naphtyliden)	PPA, 200 ºC	[51]
Mes-PBI		2,4,6-Trimethylisophthalic acid	PPA, 220 ºC	[52]
PBI-I		Isophthalic acid	PPA, 200 ºC	[53]
PBI-T		Terephthalic acid (TPA)	PPA, 200 ºC	[49]
HMT-PMBI		Methylation of hexamethyl-*p*-terphenyl polybenzimidazolium	Eaton's reagent, 120 - 140 ºC	[54]
PBI-phenylindane		1,1,3-Trimethyl-3-phenylindan-40,5-dicarboxylic acid	PPA, 195 ºC	[55]
TADPS-OBA		4,40-Oxybis(benzoic acid) (OBA)	Eaton's reagent, 140 ºC	[56]
SO_2PBI		4,4′-Sulfonyldibenzoic acid	PPA, 200 ºC	[57]

OHPyPB		4-Hydroxy-2,6-pyridinedicarboxylic acid	PPA, 200 ºC	[58]
PBI-BTBP		2,20-Bis(trifuoromethyl)benzidine	Eaton's reagent, 140 ºC	[55]
4F-PBI		Perfluoroterephthalic acid	PPA, P4O10, 140–230 ºC	[59]
6F-PBI		2,2-Bis(4-carboxyphenyl)-hexafuoropropane	PPAc, 220 ºC	[55]
Sulfonated *para-PBI*		2-sulfoterephthalic acid	PPA, 200 ºC	[60]
PBI-BRT		2-Bromoterephthalic acid (BrTPA)	PPAc, 200 ºC	[49]
PBI-DBRT		2,5-Dibromoterephthalic acid (DBrTPA)	PPAc, 200 ºC	[49]
BIpPBI		2-Benzimidazole terephthalic acid	PPA, 240 ºC	[61]
i-AB-PBI		3,4-Diaminobenzoic acid	PPA, 220 ºC	[62]

2.2. Fabrication of PBI-based membranes

PBI-based membranes can be fabricated in various ways appropriate for different applications. Typically, PBI-based proton exchange membranes (PEMs) or redox flow batteries (RFB) membranes are prepared using the solution casting method, followed by solvent evaporation at a specific temperature. Afterward, the membrane is subjected to acid-doping, usually with phosphoric acid, to enhance its proton conductivity. For gas separation, both dense and asymmetric composite membranes have been used, while integrally skinned asymmetric (ISA) membranes are usually preferred for water purification, OSN, and pervaporation. These membranes are usually fabricated from a dope solution of PBI through the phase separation method. Various approaches can be used to induce phase separation, including nonsolvent-induced phase separation (NIPS), thermally induced phase separation (TIPS), and solvent evaporation-induced phase separation (SIPS).

The NIPS technique is the most widely used method for fabricating state-of-the-art PBI membranes for liquid separation, and water is usually used as the non-solvent [63]. The mass transfer during the NIPS process may be illustrated in a ternary phase diagram (Fig. 2.2a). Where the binodal curve separates the triangle into a single-phase region, including polymer and solvent, and a two-phase region where the homogeneous solution separates into a polymer-rich and a polymer-lean phase. During phase inversion, the nascent membranes undergo composition changes that result in two phases in equilibrium (as shown by the tie line). The polymer-rich phase becomes the polymer matrix, while the polymer-lean phase becomes the pores. The final morphology of the membrane depends on the initial casting dope composition, the position of the binodal curve (as determined by the solution thermodynamics of the polymer-solvent-nonsolvent system), and the composition of the precipitation path [64]. The phase inversion kinetics are governed by two mechanisms during NIPS: instantaneous demixing and delayed demixing, which are determined primarily by the exchange rate between the solvent and nonsolvent (Fig. 2.2b). Instantaneous demixing occurs when there is a rapid exchange between the solvent and nonsolvent, causing the solution composition to quickly pass through the binodal curve. This produces a finger-like structure with a dense skin layer, macrovoids in the interior, and a relatively dense bottom layer (Fig. 2.2b). If the solvent-nonsolvent exchange is delayed and the composition path does not cross the binodal curve, a spongy structure may form (Fig. 2.2b) [65]. Therefore, fabricating

membranes with desirable morphologies during the phase inversion process requires careful selection of the solvent and nonsolvent, as well as the system temperature.

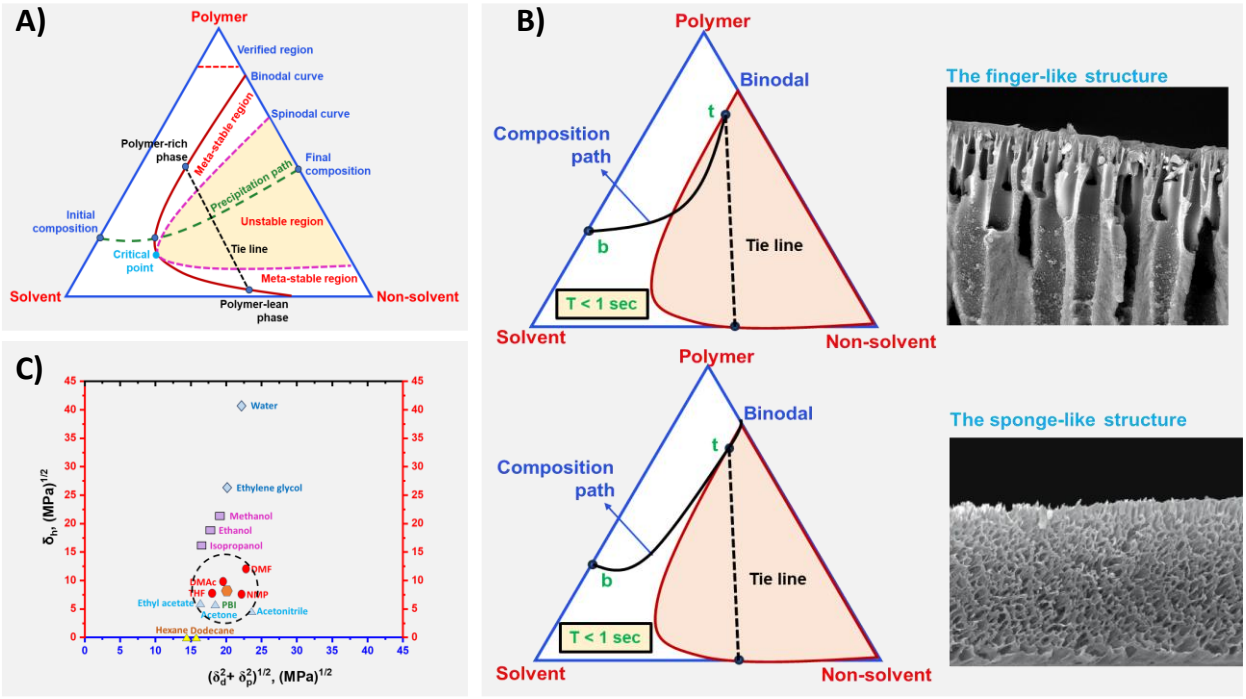


Figure 2.2. (A) Ternary phase diagram of a polymer-solvent-nonsolvent system (adopted and modified from [39]). (B) The concept of instantaneous and delayed demixing principles, along with their typical structures (adapted and modified from [65], SEM images reproduced from [66, 67]). (C) The solubility parameters plot of PBI and organic solvents (adapted and modified from [39]).

The solubility parameter plot of PBI-solvent systems aids in the selection of proper solvents based on PBI solubility in the solvents (Fig. 2.2c). The relationship between PBI and organic solvents is based on three Hansen parameters (δ_d, δ_p, and δ_h), which represent the contribution of dispersive force, polar force, and hydrogen bonding, respectively. The black circle on the plot indicates a solubility parameter difference of less than 5 between PBI and the solvents [39, 68]. According to this plot, DMAc, NMP, THF, DMF, ethyl acetate, and acetone are potential good solvents for PBI. However, it is important to note that PBI is found to be soluble only in high-boiling-point aprotic solvents like DMAc, NMP, and DMF [68].

At present, most PBI-based membranes are available in the form of flat sheets or, to a lesser extent, hollow fibers. Fabricating flat-sheet ISA membranes involves casting the dope solution at

a predetermined thickness onto a microporous substrate, followed by immersion in a nonsolvent (usually water) to initiate the phase inversion (Fig. 2.3a). Typically, the ISA membranes consist of a thin, dense skin layer and a porous support layer, which are formed from the same polymer. The top layer selectively rejects solutes, while the porous layer provides mechanical support to the membrane [63]. Hollow fiber membranes can be fabricated by co-extruding the dope solution and a bore fluid through a spinneret into a nonsolvent bath. The composition of the bore fluid may be the same as or different from that of the nonsolvent bath. The fiber spinning can be further classified as a wet-spinning or dry-wet spinning process, depending on whether the nascent fiber from the spinneret undergoes partial solvent evaporation in an air gap before entering the nonsolvent coagulation bath (Fig. 2.3b) [13]. PBI mixed matrix membranes (MMMs) can be prepared by directly incorporating nanofillers into the dope solution (Fig. 2.3c). In preparing MMMs, it is important to establish a strong connection between the fillers and the polymer phase (e.g., van der Waals forces, hydrogen bonds, or covalent bonds) to prevent agglomeration of the nanofillers during dope preparation and to minimize the potential leaching of the nanomaterials during filtration uses [63].

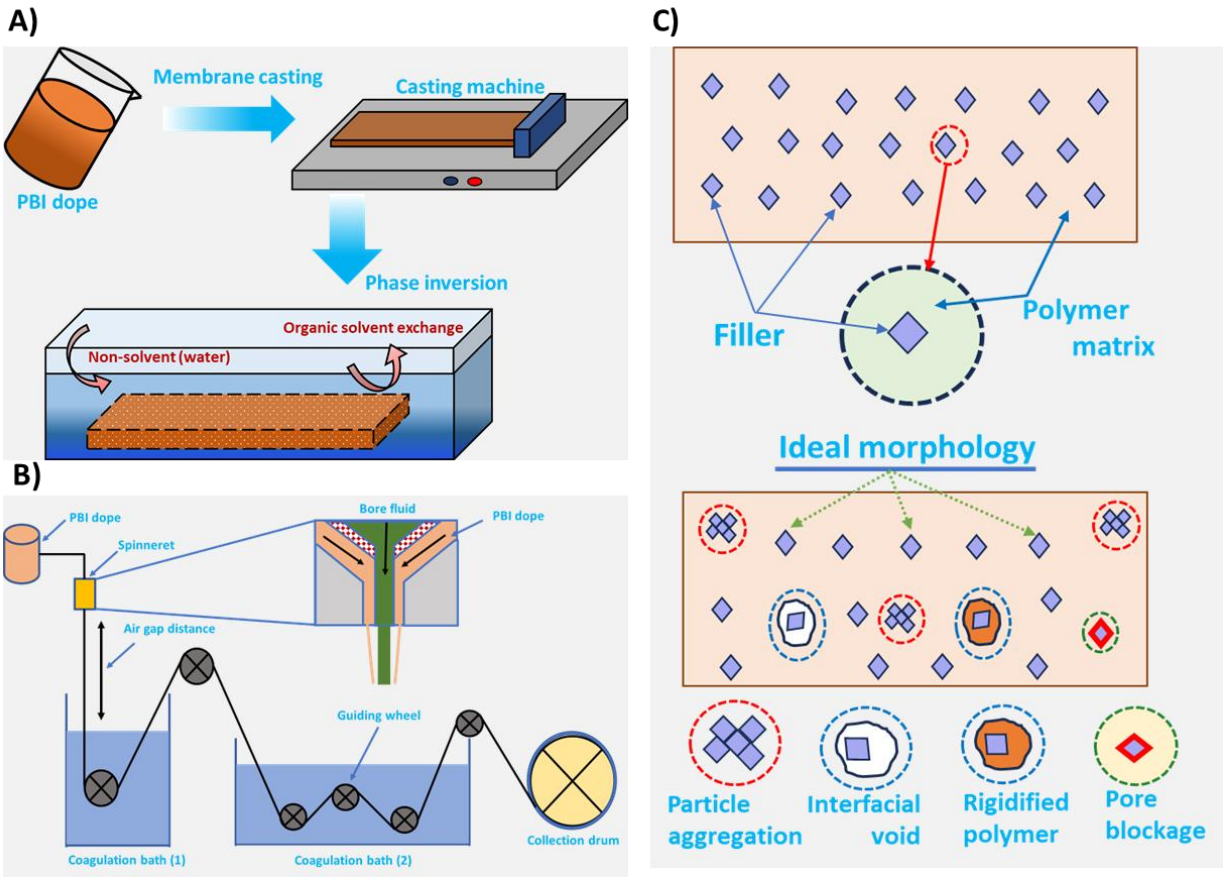


Figure 2.3. (A) Procedure for fabricating PBI flat-sheet membrane. The dope solution may be prepared by dissolving PBI in an organic solvent (e.g., DMAc). After casting, the nascent membrane is submerged in a coagulation bath (typically water) for phase inversion. (B) Procedure for fabricating PBI hollow fiber membranes, where the dope solution and bore fluid are coextruded through a spinneret into a coagulation bath for phase inversion. (C) Illustration of the ideal morphology of MMMs containing fillers (adapted and modified from [69]).

2.3. Applications of PBI-based membranes

2.3.1. PBI-based membranes for gas separation

Gas separation is an important unit operation in energy and chemical production. Gas separation with membranes relies on the permselectivity of gas molecules in the membrane. It is affected by the properties of the gas molecules (e.g., molecular size, condensability, and polarity) and the properties of the membranes (e.g., surface chemistry, morphology, and structure). Generally, dense polymeric membranes dominate, and the separation is based primarily on the solution-diffusion

mechanism [70]. Following this mechanism, gas molecules first dissolve into the membrane and then diffuse through the membrane to reach the other side. The permeability and selectivity of the membranes are directly related to the size of the free volume of the membrane and the interactions between the polymer and the penetrant species. Any defects in the selective layer of the membrane will severely compromise the selectivity of the membrane.

PBI-based membranes can be used for the separation of hydrogen from nitrogen (H_2/N_2), hydrogen from carbon dioxide (H_2/CO_2), oxygen and nitrogen (O_2/N_2), and carbon dioxide and methane (CO_2/CH_4), typically at ambient or high temperatures [71-77]. Membrane-based gas separation offers a range of advantages over traditional gas separation techniques (e.g., cryogenic distillation, solvent scrubbing, and pressure swing adsorption), including high energy efficiency and thus low carbon emissions, a small footprint, and cost-effectiveness [39]. The need for H_2 as a source of clean energy for power generation has seen a significant increase due to increasing concerns about global warming and climate change [78]. Precombustion CO_2 capture combined with H_2 production has been identified as a potential solution to reduce CO_2 emissions from power plants, to make the utilization of fossil fuels more sustainable [79]. To make H_2 production more environmentally friendly, CO_2 must be captured and either used or stored. Membrane technology is a popular choice for bulk H_2/CO_2 separation due to its energy-efficient nature, small size, ease of scale-up, and low maintenance requirements [80]. Due to the smaller kinetic diameter of H_2 (2.89 Å) than CO_2 (3.3Å), hydrogen diffuses through the membrane more rapidly than CO_2. However, CO_2 is more condensable and tends to have a higher solubility in the membrane. That is, the diffusivity and solubility aspects will affect the membrane permselectivity for H_2/CO_2 separation oppositely. Thus, achieving a high permselectivity to H_2 over CO_2 requires selecting appropriate membrane polymer and operating conditions that augment the diffusivity selectivity (which favors H_2 permeation via size sieving) while minimizing the solubility selectivity, which favors permeation of condensable CO_2 [55, 81].

PBI is a unique material with relatively rigid polymer chains, a small free volume, and high Tg, making it an excellent choice for H_2/CO_2 separation at high temperatures [39]. Recent research has demonstrated that PBI membranes can achieve remarkable H_2/CO_2 selectivity through size-exclusion mechanisms that favor H_2 permeation, especially at elevated temperatures above 150 °C. To enhance the performance of the PBI membranes in gas separation, several techniques can

be used, including crosslinking [80, 82, 83], co-polymerization [84], and polymer-blending [85]. Commercial m-PBI has H_2 permeability of 27 Barrers and H_2/CO_2 selectivity of 16 at 150 °C. To improve its size-sieving ability toward H_2/CO_2, PBI has been crosslinked with Terephthaloyl chloride (TCL), 1,3,5-Tris(bromomethyl)benzene (TBB), and dibromo-p-xylene (DBX). For instance, crosslinking with TCL led to a 100% increase in H_2/CO_2 selectivity while retaining 78% of H_2 permeability at 150 °C. For best performance, the crosslinkers should have high reactivity with PBI, preferably multi-functional groups, and small molecular sizes to maintain the structure of PBI [80].

In recent years, MMMs have also emerged as an approach to improving the selectivity and/or permeability of polymeric membranes by minimizing the permeability-selectivity trade-offs. For example, Zhu et al. [86] fabricated PBI MMMs comprising palladium nanoparticles as the sorption fillers for H_2/CO_2 separation. They reported both high H_2 permeability and H_2/CO_2 selectivity that surpassed the 2008 Robeson's upper bound and current state-of-the-art membranes. However, the self-crystallization tendency and low solubility of commonly used nanofillers (e.g., inorganic nanoparticles, metal-organic frameworks) hinder the wide-scale use of MMMs. Recently, Wu et al. [50] proposed a new method for fabricating molecularly mixed composite membranes by adding sulfocalixarenes to a PBI dope solution, and the membranes demonstrated remarkable molecular-sieving abilities for separating H_2/CO_2 with excellent mechanochemical properties that outperform the current state-of-the-art membranes. Therefore, through the proper selection of nanofillers, PBI membranes with desired morphologies and properties can be produced to effectively improve separation efficiency. The significance of filler types, filler content, and the filler-matrix interfacial interactions requires further studies due to their potentially significant impacts on the efficacy of gas separation performance.

2.3.2. PBI-based membranes for water and wastewater treatment

Water scarcity is a major problem facing the world today that affects nearly 2 billion people, and is predicted to get worse soon [87]. To meet the growing water demand, advanced water treatment processes are necessary to augment the supply from such sources as seawater, brackish water, and wastewater. Membrane-based separation technology has gained attention for such applications because of its high efficiency, low energy consumption, and large-scale processing capacities

compared to other technologies [88]. PBI-based membranes have been fabricated for nanofiltration (NF), reverse osmosis (RO), and forward osmosis (FO) processes for water treatment [89-96]. PBI can absorb up to 15% moisture compared to natural materials, suggesting that PBI is a good hydrophilic candidate for the fabrication of NF/RO membranes [39]. The PBI macromolecules contain an imidazole ring, which has a high basicity, resulting in a positive charge on the polymer backbone when protonated in an aqueous environment [97]. Therefore, protonated PBI membranes can have strong hydrophilicity and antifouling properties [98].

NF membranes have a loose structure that yields high water permeability and requires low operating pressure, leading to a more energy-efficient process for certain uses where moderately low salt rejection is needed. NF membranes are widely used for various applications, including water softening, water and wastewater treatment, and biomedical product purification [39]. In addition, PBI is a weak basic polymer (pKa 5.5) [99] because its heterocyclic imidazole group contains two nitrogen atoms, one that can act as a hydrogen bond donor and the other with a lone pair of electrons as a proton acceptor [100]. In aqueous solutions, PBI has the potential to become self-charged due to the delocalization of the protons of the imidazole groups through the adjacent benzene ring. Therefore, Wang et al. [94] used the self-charge characteristics of the PBI membrane to concentrate cephalexin by varying the solution pH.

Compared to NF, RO membranes feature a compact, dense structure that enhances the rejection of low molecular weight solutes, including salts and smaller organic compounds. Wang et al. [95] developed PBI RO hollow fiber membranes with no finger-like macrovoids in the membrane structure from a PBI/DMAc/PVP/IPA dope solution using MeOH/IPA mixtures as the coagulant. The membranes demonstrated potential for desalination, with a NaCl rejection of 99.0% at a feed solution concentration of 1000 ppm NaCl and a water permeability of 0.07 L/(m^2.h.bar). These results are comparable to those of commercial cellulose triacetate RO hollow fiber membranes produced by Toyobo Co. Similarly, Wales et al. [101] fabricated PBI HFMs for wastewater treatment generated in flue gas desulfurization from a coal-fired power plant. The membrane showed stable performance in a single-stage RO operation with a salt rejection of 97%.

PBI is also an ideal candidate for FO applications operating under harsh conditions such as high temperature environments, highly saline brine, and chemically aggressive feed. Chung and

his team are among the pioneers in exploring PBI FO membranes. They fabricated PBI FO membranes with exceptional permeance (11.2 L/(m^2.h.bar)) and high salt rejection rate (98.7%) by utilizing a non-solvent-induced phase inversion method followed by modification via chemical crosslinking [102].

However, despite the generally favorable performance of PBI-based membranes, they can hardly compete with commercial polyamide-based TFC membranes, which are based on in-situ interfacial polymerization and have dominated the current desalination market. The lab-scale studies of PBI membranes show excellent salt rejection and fouling resistance. Still, their long-term performance under realistic conditions (e.g., high salinity, mixed foulants, different pH) is yet to be explored. Additionally, there is limited research evaluating the economic viability and scalability of PBI membrane fabrication for water treatment. This is particularly important given their relatively lower water flux than the current state-of-the-art membranes, which impedes their widespread adoption. However, PBI membranes hold great promise to compete well for the treatment of water with harsh process conditions that require thermal, mechanical, and chemical stabilities.

2.3.3. PBI-based membranes for pervaporation

Pervaporation (PV) is a technique for liquid separation based on the permeability difference of different penetrants under a chemical potential gradient across the membrane by maintaining a low vapor pressure on the permeate side [103]. In PV, the feed solution meets the upstream side of the membrane, while the downstream side is either subjected to an inert gas sweep or placed under a vacuum. The separation occurs due to differing solubilities and diffusivities of the permeating components across the membrane. Compared to traditional separation methods (e.g., liquid-liquid extraction, distillation), pervaporation has several advantages, including low energy consumption, high separation efficiency, low capital costs, and no secondary pollution [104]. It has been widely used for the dehydration of organic solvents, removal of volatile organic compounds from wastewater, and separation of organic mixtures with similar boiling points, which are relevant to such industries as biorefining, petrochemicals, and pharmaceuticals [105]. For optimal performance, the ideal membrane should have strong chemical and thermal stabilities to withstand harsh chemical conditions [39].

The Chung group has carried out some pioneering work on PBI-based pervaporation membranes in flat-sheet and hollow fiber configurations for the pervaporation of organic compounds (e.g., acetone, alcohols, ethyl acetate, ethylene glycol, phenol) from water and organic-organic separations [106-109]. Due to the amphoteric nature of PBI to accept protons (e.g., -N=) or donate protons (e.g., N-H) [110], PBI-based blended membranes have also been developed for PV. For example, the hydrogen bonding interactions in PBI-based blends have been found to involve the N-H stretching of PBI and the carbonyl stretching of imide groups in Matrimid and Torlon [109, 111]. Chung et al. [109] reported that adding a small amount of PBI to Matrimid significantly strengthened the polymer chains of Matrimid and enhanced its performance in high-temperature pervaporation. It was found that blending PBI improved the permeation flux and separation factor for the dehydration of water/tert-butanol (15/85 wt%) mixtures. In addition, poly-benzoxazine crosslinked PBI membranes (CR-PBI-30) showed excellent stability and a high separation factor (>89,900) for THF dehydration [112]. Wang et al. [113] fabricated membranes made of sulfonated polybenzimidazole (SPBI) and investigated their performance in dehydrating acetic acid via pervaporation. At 60 °C, a permeation flux of 207 g m^{-2} h^{-1} and a separation factor of 5461 were obtained for a feed comprising (50/50 wt%) acetic acid and water. Later, Wang et al. [114] fabricated polybenzimidazole/polyetherimide (PBI/PEI) double-layer HFMs for the dehydration of ethyl acetate, and the as-prepared HFMs were reported to be superior to other polymeric membranes due to a synergistic combination of the PBI selective layer and the anti-swelling properties of the PEI support layer. The rigid structure, strong water affinity, and high thermal stability make PBI an attractive candidate for pervaporation applications. Despite the great efforts, there are still some difficulties with these PBI-based membranes, and membrane swelling, low flux, and issues related to process scale-up remain a challenge yet to be addressed.

2.3.4. PBI-based membranes for OSN

As discussed in Chapter 1, OSN offers several advantages over traditional methods and is widely applicable to such industries as petrochemicals, pharmaceuticals, food, and fine chemicals [115]. However, OSN membranes are known to have problems with swelling and solvation when exposed to harsh organic solvents, resulting in deterioration in the membrane performance over time. To overcome this challenge and make the OSN technique applicable to industrial applications, it is

important to develop OSN membranes that are chemically stable, highly permselective, cost-effective, and simple to use and maintain for practical purposes [116].

Although PBI membranes have been investigated for many applications, their use in OSN has attracted particular attention due to their excellent chemical stability. As a membrane material, PBI has the merits of high strength, high glass transition temperature, and broad chemical resistance. Both the Livingston and Chung groups have investigated PBI-based membranes for OSN and have achieved excellent organic solvent resistance and separation. Both flat sheet and hollow fiber PBI membranes for OSN have been developed. For instance, Zhao et al. [9] fabricated braid-reinforced PBI HFMs, and the membranes showed increased mechanical strength and durability for OSN. In developing reinforced HFMs, it is important to consider the interfacial bonding between the PBI coating layer and the reinforcing elements (i.e., braids). Crosslinking is also adopted to further improve the solvent resistance of PBI membranes. Various chemicals can be used as crosslinking agents. Recently, Lee et al. [117] fabricated PBI membranes crosslinked with epoxy-containing agents, and the membrane crosslinking was achieved by the reaction between the imidazole group of PBI and the epoxy group of the crosslinker at a relatively high temperature of 80 ºC. The membranes were stable at a high pH of 13 and displayed a high ethanol permeance of 23.4 L/(m^2.h.bar). Moreover, PBI membranes were also crosslinked by acid-doping (e.g., sulfuric acid) to establish an integrated structure through hydrogen bonds [118]. The acid doping process not only enhanced the membrane rejection capacity but also improved the mechanical and chemical stability. Nevertheless, the development of PBI membranes for large-scale OSN remains a significant challenge that has yet to be overcome.

2.3.5. PBI-based proton exchange membrane fuel cells

Proton exchange membrane fuel cells (PEMFCs) are considered a promising alternative to conventional energy sources because only H_2 and O_2 are required as reactants, and water is released as a byproduct [119, 120]. The main component of PEMFCs is a proton exchange membrane (PEM), sometimes also called a polymer electrolyte membrane. A polymer electrolyte membrane is a thin film that facilitates proton conductivity [121]. PEMs can be roughly classified into three types based on their operating temperatures: (i) low-temperature PEMFCs (LT-PEMFCs), operating at 50-80 °C [122]; (ii) intermediate temperature PEMFCs (IT-PEMFCs), operating at

80-120 °C [123]; and (iii) high-temperature PEMFCs (HT-PEMFCs), operating at 140-200°C [122], generally under anhydrous conditions [124].

PEMFCs operating at temperatures above 100 ºC have several advantages, including increased tolerance to carbon monoxide (CO), improved electrode reaction kinetics, and simplified hydrothermal management, making HT-PEMFCs particularly suitable for low-cost energy conversion devices [125]. The operating temperature of PBI PEMFCs can be much higher than that of those using Nafion or other polymeric PEM fuel cells. PBI is a highly stable heterocyclic polymer with excellent chemical and thermal stabilities, but PBI does not conduct protons itself. It is usually doped with phosphoric acid (PA) or sulfonic acid moieties to enhance its proton conductivity [126-128]. In the mid-1990s, Savinell and co-workers [65] carried out the pioneering work on PEMs based on doped PBI. Their work highlighted the exceptional potential of PA-doped PBI membranes, including low electro-osmotic drag, high proton conductivity at high temperatures, and much lower methanol crossover compared to Nafion membranes. Since then, PBI-based PEMFCs have attracted significant attention as an alternative to Nafion [129]. Compared to other perfluorosulfonic acid membranes and sulfonated hydrocarbon polymers, PBI-based membranes are preferred for HT-PEMFC applications due to their high thermal stabilities (up to 250 ºC) with no humidification [120, 130].

Various acids, alkalis, and salts (including sulfuric acid (H_2SO_4), perchloric acid ($HClO_4$), nitric acid (HNO_3), lithium hydroxide (LiOH), sodium hydroxide (NaOH), potassium hydroxide (KOH), and potassium carbonate (K_2CO_3)) have been used to dope PBI membranes [36, 131-133]. Among them, phosphoric acid has proved to be a superior dopant, and PA-doped benzimidazole membranes are widely studied. The PBI-based membranes doped with PA and its derivatives have shown high proton conductivity, excellent thermal stability up to 250 ºC, low gas crossover, and good tolerance to fuel impurities [134, 135]. PA-doped PBI membranes are a promising candidate material for HT-PEMFCs, and they are appropriate for fuel cells using hydrogen, methanol, ethanol, and propane. These membranes have also been used in sensors, supercapacitors, and electrochromic devices [36].

However, one of the main challenges of PA-doped PBI membranes is the poisoning of catalysts caused by acid leaching, as well as membrane degradation due to harsh operating conditions [136].

Acid leaching occurs primarily due to weak physical interactions between the dopant acid (e.g., phosphoric acid) and the PBI matrix. Under high temperature and humidity gradients, especially during start-up/shut-down cycles or fuel starvation, the loosely bound acid molecules tend to migrate out of the membrane, resulting in a gradual decline in proton conductivity and membrane swelling. Additionally, acid doping at a high level can also lead to membrane plasticization, adversely affecting the mechanical properties and gas tightness of PBI fuel cells. For instance, hyperbranched PBI acid doped at 331% showed poor gas permeability with a low open-circuit voltage of 0.822 V [137]. Therefore, efforts need to address these issues. Two strategies can be followed to overcome these drawbacks: (1) modification of the PBI backbone chains and/or (2) fabrication of composite membranes.

2.3.6. PBI-based membranes for redox flow batteries

Redox flow batteries (RFBs) are another important area for PBI-based membranes, which is gaining increasing research attention to design large-scale stationary energy storage systems. Among the different components used in RFBs, the membrane placed between the negative and positive electrodes plays a crucial role as an ion-conductive membrane or separator that selectively allows ion transport while preventing active species crossover [138, 139]. Additionally, the long-term operation of the RFBs depends on the lifetime of the membrane, which requires excellent mechanical and chemical stability [139, 140]. As a result, PBI membranes have emerged as a promising alternative to conventional membranes for RFBs (e.g., vanadium redox flow batteries (VRFBs) [141-144] or iron-chromium redox flow battery (ICRFB) [145, 146], due to their improved chemical, thermal, and mechanical properties. However, as mentioned in section 2.3.5, a pristine PBI membrane suffers from poor conductivity. To improve the conductivity, doping the membranes with acids is necessary [142]. This process significantly enhances the proton conduction of the PBI membranes; however, it also compromises other properties of the membrane, such as mechanical strength and ion selectivity.

Like PBI PEMFCs, PBI-based RFBs also experience long-term acid leaching and oxidative degradation, particularly under prolonged high-voltage operations. As mentioned above, acid leaching occurs due to the weak interactions of dopant acid and PBI matrix, and the oxidative degradation arises from the generation of reactive O_2 species (e.g., hydrogen peroxide or hydroxyl

radicals) at the electrode-membrane interface during high-voltage. Exposure to strong oxidizing redox species (e.g., vanadium (V)) can further accelerate the degradation. Therefore, both acid loss and oxidative instability are critical issues that need to be addressed. While challenges such as dopant retention or conductivity selectivity trade-offs remain, ongoing innovations in membrane design and functionalization are likely to enhance the prospects of PBI-based membranes in scalable energy storage technologies.

Chapter 3

Interfacially crosslinked polydopamine/polybenzimidazole composite membranes for OSN

**** This chapter is based on the results of a published paper as outlined in the statement of contributions.***

As discussed in Chapters 1 and 2, the development of OSN membranes remains challenging because membrane performance in organic media depends strongly on solvent-membrane interactions, pore structure, and chemical stability under harsh conditions. In particular, effective rejection of low-molecular-weight solutes requires a selective layer with controlled pore size while maintaining adequate solvent permeance and resistance to aggressive solvents. Interfacial polymerization [15], layer-by-layer assembly [147, 148], self-assembly [149] and surface coating [150] have been explored to improve the separation performance of different membranes. These methods allow for better control over the membrane structure and properties, including pore size and surface charge.

Among the available surface-modification strategies, polydopamine (PDA) has recently emerged as a versatile material for modifying the surfaces of various substrates, including nanofiltration membranes [151, 152]. The deposition of PDA on the membrane surface can effectively alter and control the surface properties of the membranes (e.g., hydrophilicity and adhesion), making it a promising approach to enhancing the membrane performance [153]. However, the use of PDA in OSN membranes is not well studied, and there are only a few studies dealing with PDA as a coating material for OSN applications. Xu et al. [154] coated a PDA layer over a polyimide (PI) membrane, and both layers were crosslinked with 1,6-hexanediamine, and the membrane showed excellent OSN performance in challenging organic solvents such as polar aprotic solvents. Recently, Li et al. [155] used PDA as an interlayer between the substrate and a polyamide layer to design high-throughput OSN membranes, and both high permeability and rejection were reported. In another study, Zhao et al. [156] developed an interpenetrating polymer network of PDA/PBI via in situ polymerization, where dopamine was mixed with a PBI solution to encapsulate the dopamine monomers in the PBI backbone. After casting, the membrane was

polymerized in situ to enhance its solvent resistance, and a high DMF permeance of up to 12 L/(m^2.h.bar) was reported.

In this chapter, we fabricated highly selective OSN membranes accomplished through interfacial crosslinking of PDA and DBX on a PBI substrate. An asymmetric PBI substrate membrane was prepared via the nonsolvent-induced phase separation, and then a PDA layer was deposited onto the PBI substrate by exposing the substrate surface to a dopamine solution, followed by crosslinking with DBX. The crosslinking served several purposes: 1) it crosslinked the PBI substrate and PDA active layer to enhance their chemical stabilities, 2) the PDA layer was firmly attached to the PBI substrate, resulting in increased structural integrity, and 3) the highly crosslinked network structure resulted in high selectivity for OSN. The separation performance of the membranes was tested for OSN with a range of organic solvents, and dyes of a broad array of molecular weights were used as model solutes. The membranes demonstrated effective sieving-based separation, providing controllable and tunable OSN membranes for target applications.

3.1. Experimental Methods

3.1.1. Materials and Reagents

Dopamine hydrochloride, tris(hydroxymethyl) aminomethane (Tris, 99.8%), copper sulfate ($CuSO_4$), hydrogen peroxide (H_2O_2, 30 wt%), HPLC grade acetonitrile (MeCN), ethanol (EtOH), methanol (MeOH), acetone, isopropanol (IPA), toluene, N,N-dimethylacetamide (DMAc), N-methyl-2-pyrrolidone (NMP), n-hexane, heptane, N,N-dimethylformamide (DMF), dimethyl sulfoxide (DMSO), tetrahydrofuran (THF), hydrochloric acid (HCl, 37 wt%) and sodium hydroxide (NaOH) were all purchased from Sigma Aldrich. Poly(ethylene glycols) (PEGs) of different molecular weights, Rose bengal (RB, MW 1020 g/mol), Remazol brilliant blue (RBB, MW 626.5 g/mol), methyl orange (MO, MW 327 g/mol), N, N-dimethyl-4-nitroaniline (DMNA, MW 166.2 g/mol) and α,α′-dibromo-p-xylene (DBX) were acquired from Thermo Scientific Chemicals. Polybenzimidazole 26 wt% and 1.5 wt% LiCl in DMAc was supplied by PBI Performance Products Inc. (Charlotte, NC). Polypropylene (PP) nonwoven backing (Novatexx 2471) was kindly provided by Freudenberg Filtration Technologies Inc. (Canada).

3.1.2. Membrane fabrication

The asymmetric PBI substrate membrane was prepared by the phase inversion method described in Chapter 2, followed by PDA deposition and DBX crosslinking specific to this study. The PBI solution (Celazole S26 (26 wt%)) from the supplier was diluted with DMAc to 17 wt%, and the solution was stirred mechanically overnight at room temperature. The homogeneous solution was allowed to stand still for 24 h to remove air bubbles before casting onto the PP nonwoven backing to a thickness of ca. 200 μm. The nascent cast membrane was quickly immersed in water to induce phase separation, and the membrane was allowed to stay in water for 24 h to ensure complete phase inversion. During this course, the water of the coagulation bath was changed several times to remove residual solvent and LiCl released to the water bath. The resulting membrane was then rinsed with isopropanol 3 times to remove any residual solvent DMAc and water and stored in IPA for further use (see Appendix) in subsequent polydopamine deposition and crosslinking.

To deposit PDA onto the PBI substrate, the PBI substrate membrane was mounted between two Teflon plates using rubber gaskets and metal clamps, and then the membrane holder was filled with freshly prepared dopamine solution such that the active surface layer of the PBI membrane would be exposed to the dopamine solution for a predetermined time (10, 20, and 40 min). The dopamine coating solution was prepared by dissolving dopamine hydrochloride (2 mg/mL) in a Tris buffer solution (pH = 8.5, 50 mM) prepared prior to that contained $CuSO_4$ (5 mM) and H_2O_2 (20 mM) to trigger the rapid deposition of dopamine [153, 157]. Afterward, the membrane was rinsed with deionized water to remove unreacted dopamine and PDA aggregates not adhered to the PBI surface, followed by crosslinking with 3 wt% of DBX in acetonitrile at 80 ºC under continuous stirring and reflux for 24 h. The crosslinked membrane was then rinsed with IPA and preserved in IPA for further studies; depending on dopamine deposition time, the membranes so obtained were named M1 (10 min), M2 (20 min), and M3 (40 min) (Table 3.1). For comparison, a control membrane (M0, PDA deposition time 20 min but not crosslinked) and a PBI membrane crosslinked with DBX (PBI-DBX) without a PDA surface layer were also prepared.

The degree of crosslinking in membranes was characterized by using a previously reported method and estimated using eq (1) [82].

$$M_c = \frac{M_{PBI}}{\chi} \quad (1)$$

Where M_c is the average molecular weight (Da) of the polymer chains between the crosslinks, M_{PBI} is the molecular weight of the PBI repeating unit (308 g/mol) and x is the fractional conversion of amine groups in PBI repeating units. The x parameter can be calculated by eq (2).

$$\chi = \frac{m_1 - m_0}{m_0} \frac{M_{PBI}}{M_{DBX}} = \frac{\Delta_m}{m_0} \frac{M_{PBI}}{M_{DBX}} \quad (2)$$

Where Δ_m is the weight increase after crosslinking and M_{DBX} (104.14 g/mol) is the molecular weight of the crosslinks. Higher x values or lower Mc values (<1000 Da) indicate a higher degree of cross-linking.

Table 3.1. Membranes fabricated in this study.

Membrane types	PDA deposition time	Crosslinked
PBI	−	No
PBI-DBX	−	Yes
M0	20 min	No
M1	10 min	Yes
M2	20 min	Yes
M3	40 min	Yes

3.1.3. Membrane characterization

The membrane samples were subjected to characterization with Fourier-transform infrared spectroscopy (FTIR) (Nicolet 6700 ATR-FTIR spectrometer) under attenuated total reflection (ATR) mode. Scanning electron microscopy (SEM) (Tescan VEGA TS-5130) was used to determine the surface and cross-sectional microstructure of the membranes. Samples for SEM were freeze-fractured in liquid nitrogen and sputter-coated with gold using a Polaron (E5100) SEM coater. The surface roughness of membranes was determined from topographic images using atomic force microscopy (AFM) in tapping mode (AC) at room temperature. The water contact angle of the membrane was measured using a contact angle goniometer (Tantec Inc.). A UV–Vis

spectrophotometer (Shimadzu UV-1900i) was used to monitor the absorbance of the dopamine solution during PDA deposition at different time intervals to determine the kinetics of the PDA polymerization.

3.1.4. Pore size distribution and molecular weight cut-off

The molecular probe method was used to determine the pore size distribution and MWCO of the membrane. To carry out the solute rejections, aqueous solutions of PEGs with different molecular weights (200-4,000 g/mol) at a PEG concentration of 0.2 g/L were used in the filtration experiments, where a feed pressure of 6 bar gauge was used to filter the PEG probe solutions in a sequence of increasing molecular weight of PEGs. The rejection (R) of PEGs was evaluated from eq (3):

$$R\ (\%) = \left(1 - \frac{C_p}{C_f}\right) \times 100 \tag{3}$$

where C_p and C_f are the PEG concentrations in the permeate and feed solution, respectively, and they were determined using a total organic carbon analyzer (TOC Shimadzu, Japan).

The Stokes diameters (d_p) of the PEG solute molecules and their molecular weights can be correlated by eq (4) [158-160]:

$$d_p = 33.46 \times 10^{-12} \times MW^{0.557} \tag{4}$$

Regardless of the steric and hydrodynamic interactions between the solute and membrane pores, the pore size distribution of the membrane can be described by eq (5):

$$\frac{dR(d_p)}{dd_p} = \frac{1}{\sqrt{2\pi} d_p \ln \sigma_p} exp\left[-\frac{(\ln d_p - \ln \mu_p)^2}{2(\ln \sigma_p)^2}\right] \tag{5}$$

where μ_p is the mean effective pore diameter obtained at a solute rejection of R = 50%, and σ_p is the geometric standard deviation, which is defined as the ratio of the PEG radius at R = 84.13% over that at R = 50%. The MWCO of the membranes was then calculated with the Stokes diameter of the solute at R = 90%.

3.1.5. Nanofiltration separation tests

The separation performance of the membranes was evaluated with a range of organic solvents using a lab-scale dead-end filtration setup with an effective membrane area of 12.5 cm^2 (Fig. 3.1). Dye compounds with different molecular weights (e.g., RB, RBB, MO, and DMNA) were used as model solutes for the OSN tests at room temperature (22 °C) and an operating pressure of 8 bar. Before each experiment, the membrane was pre-conditioned with deionized water and then with the organic solvent under the same operating pressure. The solvent permeance and solute rejection reported were the average measurements with at least two membrane samples (see Appendix).

The permeance of the membrane to the organic solvent was determined using eq (6):

$$P = \frac{V}{A \times t \times \Delta P} \quad (6)$$

where P is permeance [L/(m^2.h.bar)], V is the volume of the solvent permeate through the membrane over a period of time t (h) at an applied transmembrane pressure of ΔP (bar), and A is the effective area of the membrane for permeation (m^2).

The solute rejection (R) of the membrane was calculated using the same equation (3) that was used for the rejection of PEGs. The dye concentration was measured using a UV–Vis spectrophotometer (Shimadzu UV-1900i). The permeate samples were recycled back to the filtration cell to maintain a constant concentration throughout the experiment.

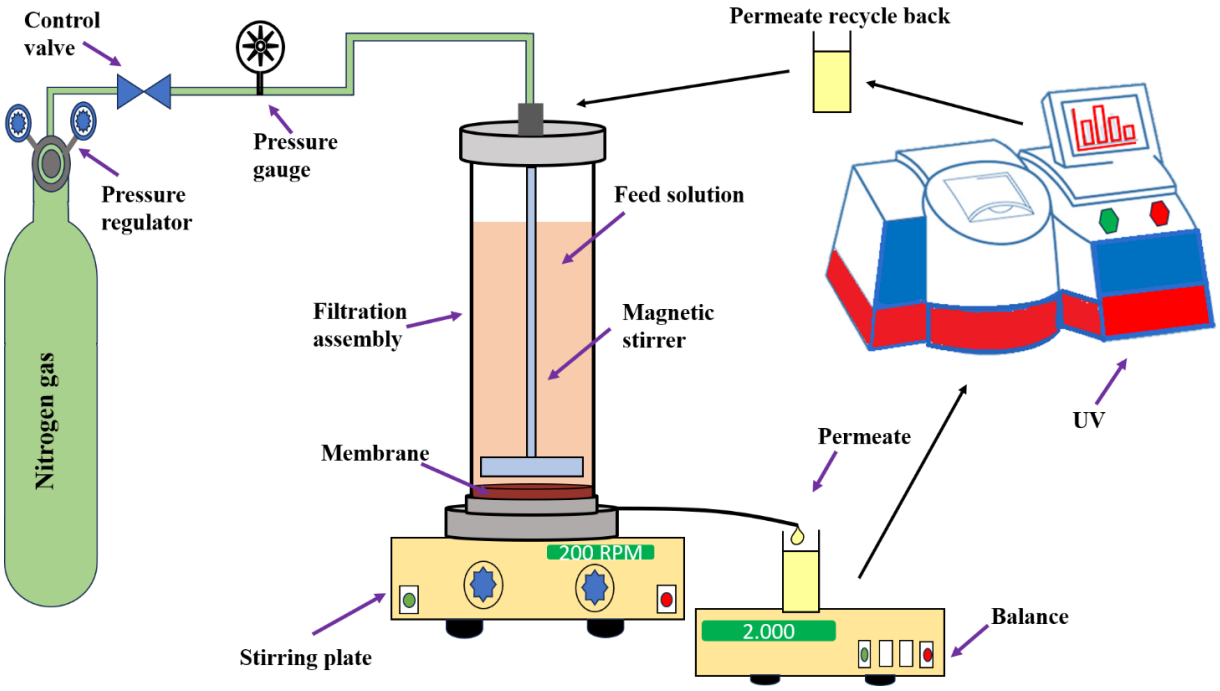


Figure 3.1. Schematic illustration of the dead-end filtration system used in this study.

3.1.6. Membrane stability/dissolution test

After drying in a fume hood until reaching a constant weight, the membrane samples were weighed and then immersed in 15 mL of organic solvent (Table 3.2). The membrane samples submerged in the solvents were agitated in an incubator shaker at 22 °C for 72 h, and then the membrane samples were taken out of the solvent and dried again. The percentage weight loss of the membrane samples was determined from the weight change before and after the dissolution test [156].

Table 3.2. Dissolution (%) of membranes in organic solvents.

Solvents	PBI	PBI-DBX	M0	M2
DMSO	100 ± 0.0	0.6 ± 0.8	98.4 ± 2.8	1.1 ± 0.7
NMP	99.2 ± 1.8	0.7 ± 1.7	98.9 ± 1.3	1.9 ± 0.2
DMAc	100 ± 0.0	1.5 ± 0.4	100 ± 0.0	2.4 ± 1.5
DMF	98.7 ± 2.1	0.2 ± 0.1	97.8 ± 1.4	0.7 ± 0.8
THF	0	0	0	0

Acetone	0	0	0	0

3.2. Results and discussion

3.2.1. Crosslinking of PDA/DBX on PBI membrane

To evaluate whether interfacial PDA/DBX crosslinking could improve the chemical stability of PBI membranes, solvent resistance was first examined using a series of polar aprotic solvents. The membrane stability against the solvents was measured with polar aprotic solvents (DMSO, NMP, DMAc, DMF, THF, and acetone) (Table 3.2). As expected, the pristine PBI membrane was dissolved in all these solvents except THF and acetone, consistent with the results reported in a separate study [1]. PBI membrane (PBI-DBX) modified with DBX showed excellent stability in all solvents. When PDA was deposited on PBI membranes and crosslinked with DBX, the resulting membrane (i.e., membrane M2) exhibited similar stability as the PBI-DBX membrane. On the other hand, like the pristine PBI membrane, the PBI-PDA controlled membrane (M0) without DBX crosslinking completely disintegrated in harsh organic solvents (Table 3.2). Figure 3.2 shows a clear solution of PBI-DBX and M2 membranes, while the pristine PBI membrane was completely dissolved after 72 h of agitation at room temperature. The solutions of the M2 membrane were a little more turbid than the PBI-DBX membrane, presumably due to the partial removal of PDA nanoaggregates. However, disintegration or delamination of the PDA layer was not observed in all cases. These results suggest that the crosslinking of PDA/DBX on the PBI support was the key to achieving a robust solvent-stable selective OSN membrane.

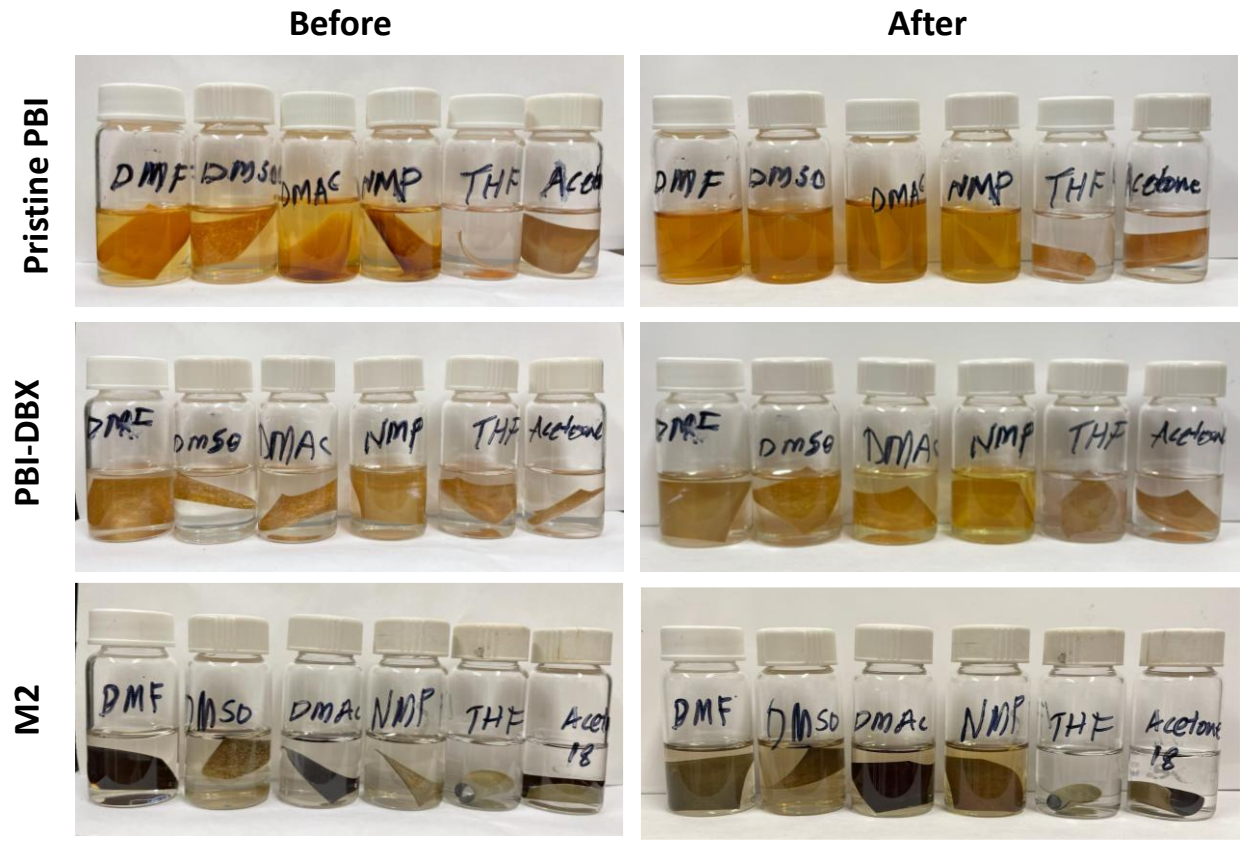


Figure 3.2. Photographs of membranes after 72 hours of agitation in organic solvents.

The following reaction mechanism may be hypothesized to explain the formation of a highly crosslinked membrane of PDA/DBX and PBI (Fig. 3.3). When dopamine solution was poured onto the PBI substrate in the presence of $CuSO_4/H_2O_2$, a rapid dopamine polymerization occurred, and the resulting PDA was deposited on the PBI substrate. Figure 3.4 illustrates the evolution of color change and UV-vis spectra of the dopamine solutions with $CuSO_4/H_2O_2$. Within a few minutes, the solution turned black, indicating rapid polymerization of PDA. The PDA layer was firmly attached to the PBI support due to H-bonding and the strong adhesion characteristics of PDA (Fig. 3.3, step 1). However, the formation of the crosslinked network between PDA and PBI is not strong enough to make the membrane chemically stable, as demonstrated by the dissolution of M0 membranes in the organic solvents (Table 3.2). Therefore, crosslinking of PDA-deposited PBI membranes with DBX was required to make the membrane chemically stable. A previously reported crosslinking strategy was used to crosslink the membranes [161-163]. In the case of the PBI-DBX membrane, the bifunctional DBX crosslinker covalently joined the two adjacent PBI

chains by reacting with the benzimidazole rings [163]. By crosslinking the PDA-deposited PBI membrane, the DBX molecules not only crosslinked the adjacent PBI chains but also generated interchain covalent bonds of PDA and PBI (Fig. 3.3, step 2). The degree of crosslinking for the DBX-PBI was measured to be M_c = 1470 Da, while for the M2 membrane, it was M_c = 1397 Da. This indicates that the M2 membrane had a higher degree of crosslinking compared to the DBX-PBI membrane due to its lower M_c values. Additionally, the x values, calculated from $\Delta m/m_0$ (eq 2) of the M2 membrane (0.221), are also higher than the DBX-PBI membrane (x = 0.209). The higher M_c values and lower x values of the DBX-PBI membrane than the M2 membrane are attributed to the presence of some partially reacted DBX sites [164]. On the other hand, in the case of the M2 membrane, the partially reacted DBX sites attach PDA to PBI as well as crosslinking the PDA molecules. As a result, most of the DBX molecules have been consumed in the reaction, leading to a higher degree of crosslinking of the M2 membrane. Therefore, a highly crosslinked PDA/DBX/PBI network was constructed, which was responsible for the excellent chemical stability and separation performance of the PDA-modified membranes, as discussed in section 3.2.3.

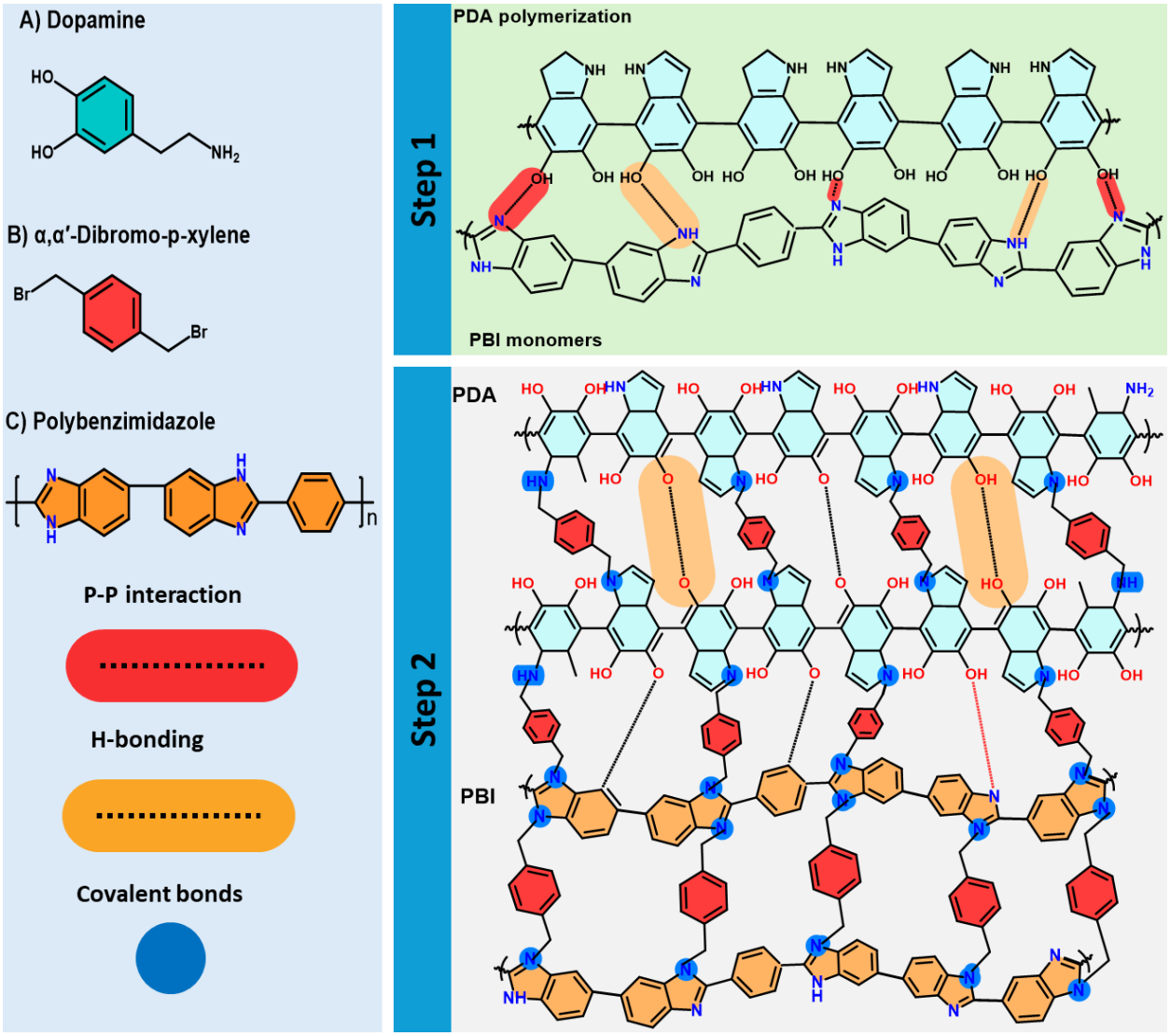


Figure 3.3. The possible chemical reaction between PDA, DBX, and PBI.

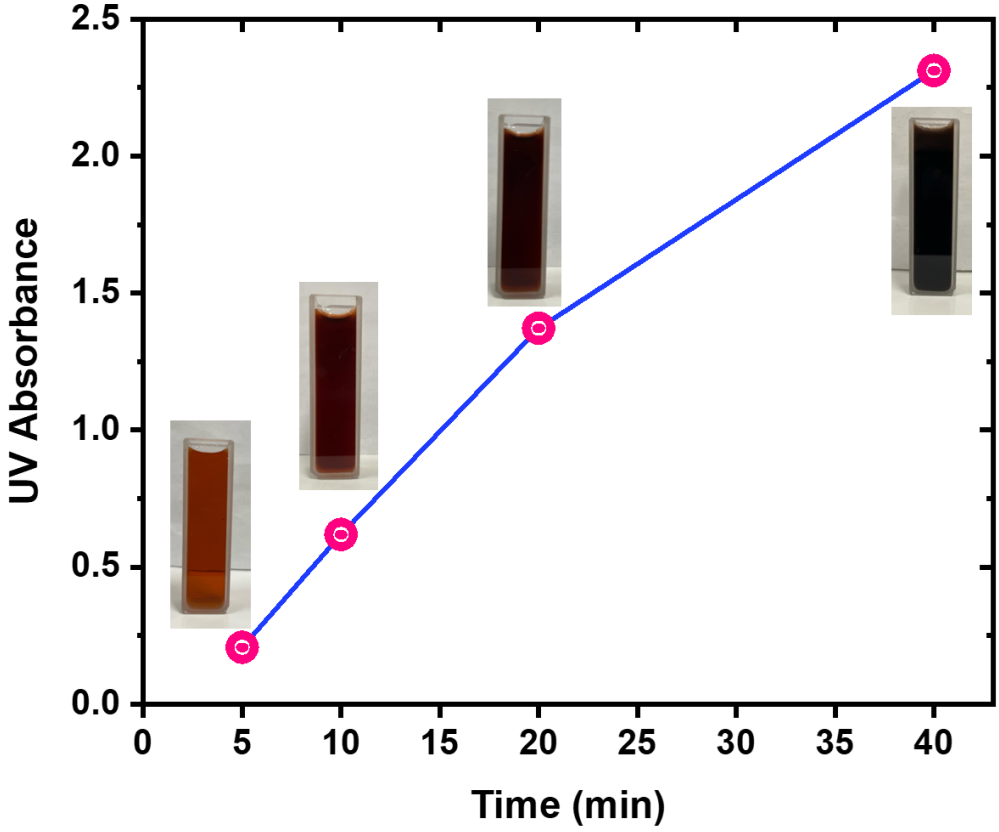


Figure 3.4. Photographs of dopamine solution showing color changes over time and its time-dependent UV-Vis absorbance at 405 nm and 417 nm. Initial concentration: 2 mg/ml.

3.2.2. Membrane Characterization

ATR-FTIR was used to examine the chemical changes, crosslinking, and PDA modification of the membranes. Figure 3.5 illustrates the FTIR spectra of pristine PBI, PBI-PDA coated (M0), PBI-DBX, and PDA/DBX/PBI (M2) membranes. The characteristic peaks of the PBI membrane from 3500 to 3200 cm^{-1} correspond to the non-hydrogen bonded/hydrogen bonded N–H groups and the stretching of aromatic =C–H groups of the imidazole rings [165]. The peaks at 1632, 1590, 1442, 1285, and 790 cm^{-1} are associated with the imidazole and benzene ring and their conjugation in PBI membranes [115]. Similar peaks were observed for the crosslinked and PDA-coated membranes; however, the intensity and location of some peaks were altered due to secondary interactions among PDA, DBX, and PBI. In the PBI-PDA-coated (M0) membrane, the intensity

of the peak at 3301 cm^{-1} increased with PDA coating, possibly due to the –NH– and –OH groups in PDA [154]. However, after crosslinking of pristine and M0 membranes with DBX, the peak intensities significantly decreased, indicating that a secondary amine had been involved in a chemical reaction and transformed into a tertiary amine, evidence of the reaction between the imidazole ring in PBI and the crosslinking agent [1]. Two additional distinct peaks at 2920 and 2850 cm^{-1} appeared in the crosslinked membranes, which may be attributed to the C–H and C–N stretch vibration, possibly due to the terminal C from DBX and chemical crosslinking of PBI backbone and DBX [115, 161].

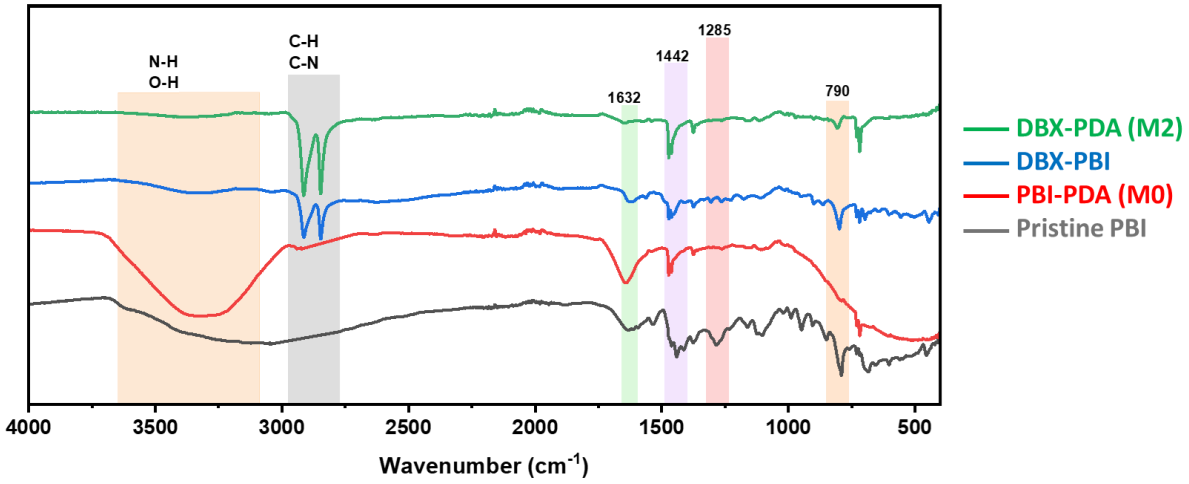


Figure 3.5. ATR-FTIR spectra of the pristine PBI, PBI-PDA (M0), DBX-PBI, and DBX-PDA (M2) membranes.

The cross-sectional and surface morphologies of pristine PBI, PBI-DBX, M0, and M2 membranes were examined under SEM (Fig. 3.6). The cross-sections of the membranes exhibited finger-like structures, which are typical of non-solvent-induced phase-inversion membranes. All membranes showed a porous sublayer and a dense top layer formed as a result of liquid-liquid demixing during the phase inversion process [163]. It was interesting to note that the pristine PBI membrane had a thin dense skin layer (1.09 μm) (Fig. 3.6a), but once modified with DBX, the membrane appears to be more porous and thicker (Fig. 3.6c), which may be attributed to the swelling of the PBI substrate in acetonitrile during crosslinking. The crosslinking also increased the overall thickness of the membrane, while the top dense layer was expanded after crosslinking

(1.14 μm). Similar findings have also been reported elsewhere [166]. Figure 3.5(b) shows that the deposition of PDA on top of the pristine PBI membrane induced penetration of the PDA polymers, closing the large micropores and forming a thicker, dense layer (1.24 μm) on top of the membrane. However, after crosslinking of the PDA-coated PBI membrane (M0) with DBX (Fig. 3.6d), the thickness of the active layer of the membrane was substantially reduced (1.19 μm), possibly due to the removal of unreacted dopamine monomers and PDA nanoaggregates during crosslinking. Since the crosslinking was carried out in a highly concentrated DBX/acetonitrile solution at 80 ºC for 24 h, the PBI-DBX and M2 membranes experienced volumetric expansion. The top surface SEM images of the pristine PBI and PBI-DBX membranes show a smooth and homogenous surface (Fig. 3.6e&g). In contrast, the M0 membrane surface shows PDA aggregates (Fig. 3.6f), resulting from the non-covalent interaction between PDA oligomers after deposition [157].

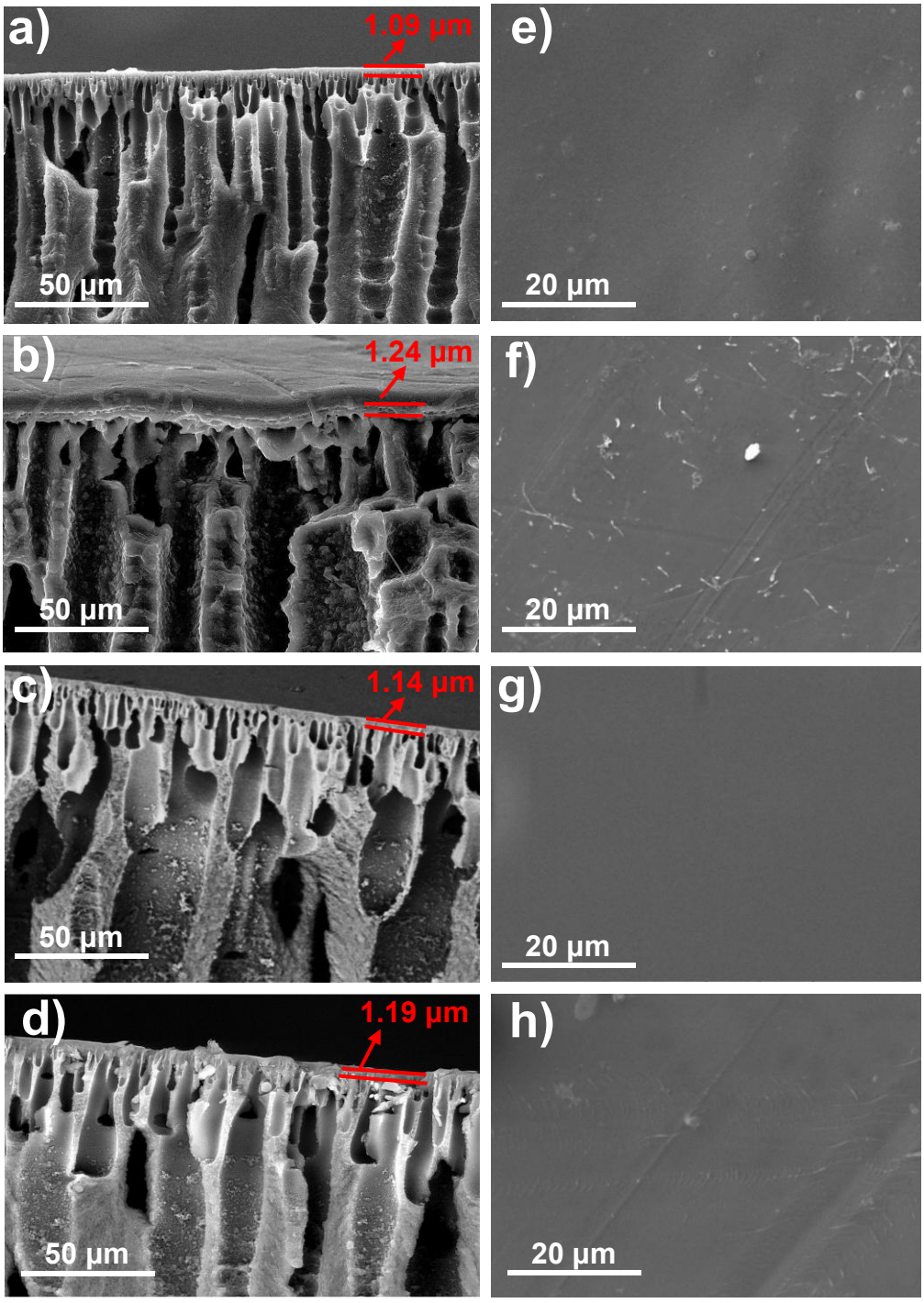


Figure 3.6. Scanning electron microscopy (SEM) images of the membranes. Cross-sectional and surface images of pristine PBI membrane (a & e), PDA-coated PBI membrane (M0, not crosslinked) (b & f), PBI-DBX crosslinked membrane (c & g), and PDA-coated DBX crosslinked membrane (M2) (d & h).

The surface morphology of the membranes was further subjected to AFM analysis. Like the SEM results, the pristine PBI membrane showed a smooth top surface with an average roughness of 5.95 nm (Fig. 3.7a), and crosslinking the PBI membrane with DBX decreased the surface roughness significantly to 1.68 nm (Fig. 3.7c), indicating a dense crosslinked network between DBX and PBI monomers was successfully formed. The pristine PBI membrane coated with PDA (M0) showed the highest surface roughness of 10.78 nm (Fig. 3.7b). The surface roughness of the M0 membrane without DBX crosslinking was higher than that of pristine PBI membranes, which could be attributed to the deposition of PDA aggregates on the membrane surface, as also demonstrated by the SEM images. However, after crosslinking of the M0 membrane with DBX in acetonitrile for 24 h, the surface roughness of the membrane decreased to 7.17 nm (M2 membrane) (Fig. 3.7d). This could be due to the reconfiguration of the polymer chains and removal of the lingering PDA aggregates during the crosslinking reaction [167]. Both the SEM and AFM analyses showed that the interfacial crosslinking of PDA/DBX on PBI membranes (M2) resulted in a rougher surface than pristine PBI and PBI-DBX membranes, but remained smoother than the M0 membrane.

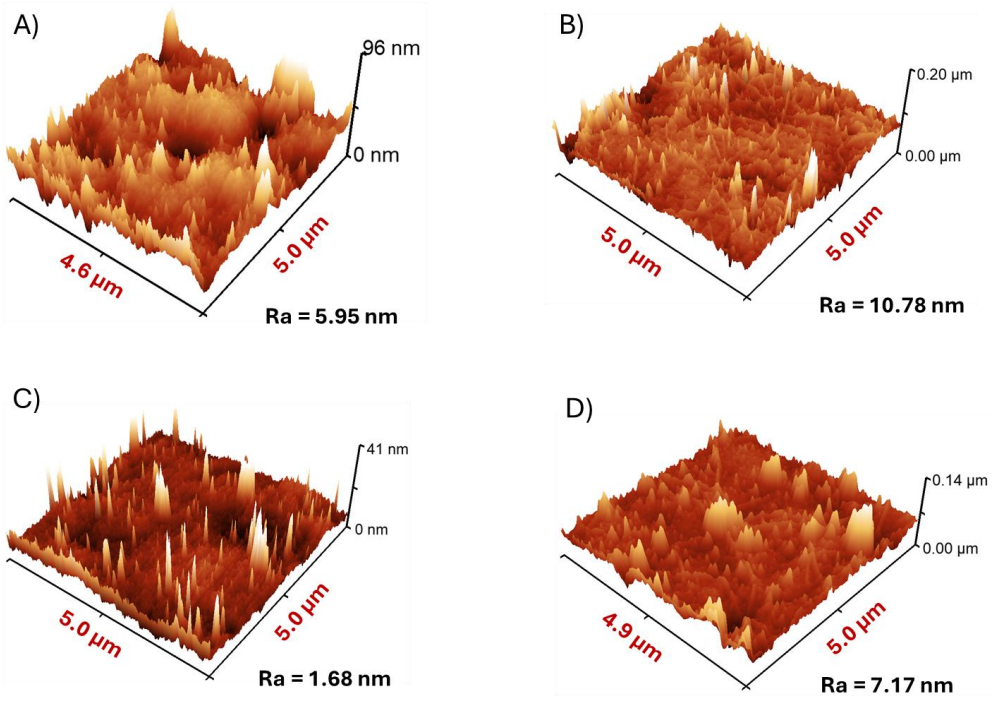


Figure 3.7. 3D atomic force microscopy (AFM) images of pristine membrane (a), PDA-coated PBI membrane-M0 (b), PBI-DBX crosslinked membrane (c), and PDA-coated DBX crosslinked membrane-M2 (d). Ra represents the average surface roughness.

In addition to affecting the surface roughness of the membrane, the PDA coating can also reduce defects and pore size by filling larger, unselective pores and pinholes. The pore size distribution of the membranes was analyzed based on the rejections of neutral PEG molecules with varying molecular weights, and the results are presented in Figure 3.8(a). Membrane M2, which had a PDA deposition time of 20 min, displayed a narrow pore size distribution as compared to the unmodified membranes. The same trend was also observed with the crosslinked PBI-DBX membrane, though the change was not pronounced enough to match the M2 membrane. In keeping with the trend of pore size change, interfacial crosslinking of PDA on PBI substrate greatly reduced the molecular weight cut-off (MWCO) of the membrane. Notably, the M2 membrane showed the lowest MWCO of 286 Da, followed by the PBI-DBX membrane (1001 Da) and the pristine PBI membrane (2710 Da) (Fig. 3.8b). The small pore size and low MWCO of the M2 membrane may be attributed to the crosslinked network of PDA/DBX/PBI that helped cover the pinholes and defects on the PBI substrate; as a result, steeper size-selective rejection was achieved.

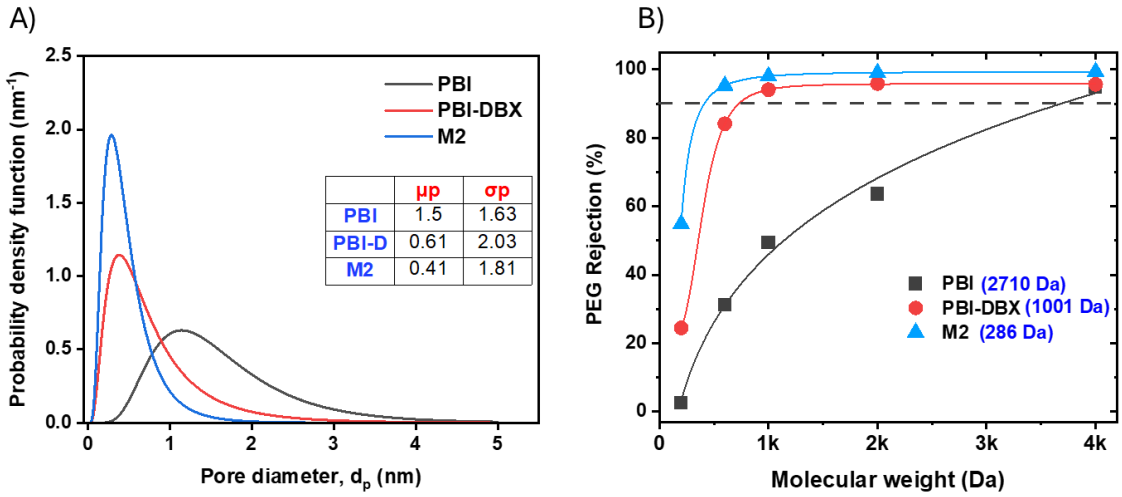


Figure 3.8. (a) pore size distribution, (b) molecular weight cut-off of the pristine PBI, PBI-DBX, and DBX-PDA (M2) membranes.

The surface hydrophilicities of the membranes were measured in terms of water contact angle, as shown in Figure 3.9(a). The pristine PBI substrate membrane displayed the highest water contact

angle of 68.2º, while deposition of PDA on the PBI substrate significantly decreased the water contact angle (48.8º for M0 membrane) due to the hydroxyl functional groups on the PDA surface. After crosslinking of the PDA-deposited membrane, the contact angle increased to 60.6º (M2 membrane). This was understandable in view of the integration of the hydrophobic aromatic linkers and the formation of tertiary amine groups, which was also evidenced by the FTIR analysis. The PBI-DBX membrane displayed a contact angle of 55.8º, lower than the contact angle of the pristine PBI membrane, which is possibly due to the ionic N^+ and unreacted Br^- groups.

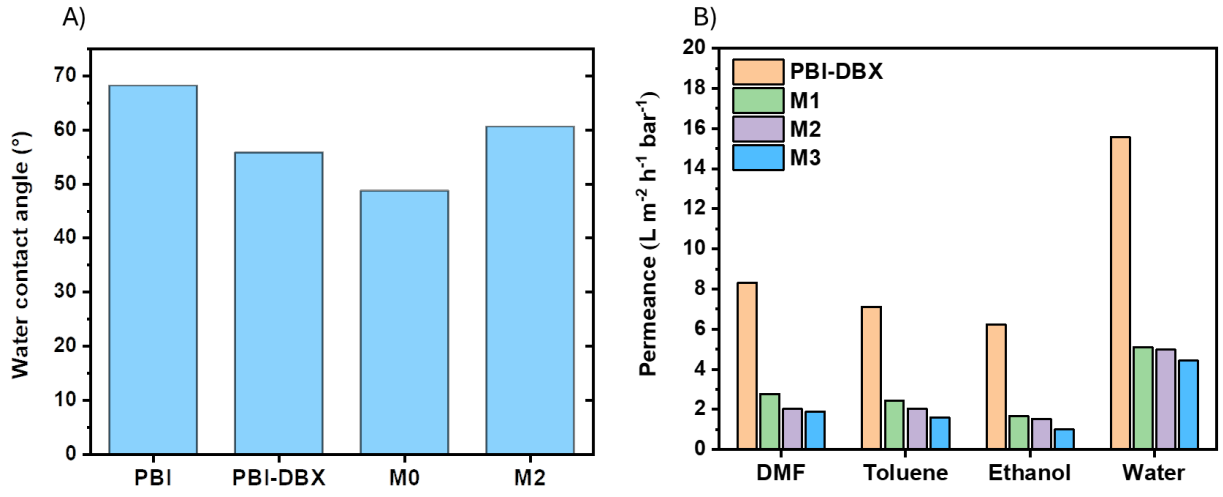


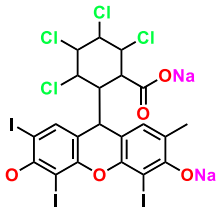
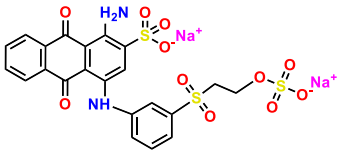
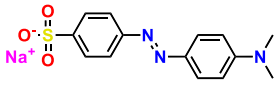
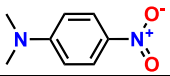
Figure 3.9. (a) Water contact angle of the pristine PBI, PBI-PDA (M0), DBX-PBI, and DBX-PDA (M2) membranes. (b) Pure solvent permeance of membranes PBI-DBX, M1 (PDA deposition time 10 min), M2 (PDA deposition time 20 min), and M3 (PDA deposition time 40 min). Operating pressure 8 bar and temperature 22 ºC.

3.2.3. Membrane performance

The OSN performance of the membranes was evaluated in terms of solvent permeance and solute rejection. It was postulated that different PDA coating times would affect the active layer thickness and pore structure of the membrane, thereby influencing the membrane performance. Hence, we decided to investigate the permeation of solvents and the rejection of model solute dyes with different molecular weights (RB, RBB, MO, and DMNA) through the membranes. The properties of these dyes are given in Table 3.3. It may be noted that the pristine PBI and M0 membranes were not resistant to aprotic solvents and, therefore, they were excluded from further OSN evaluations.

Crosslinked PBI membrane (PBI-DBX) without the PDA layer was included for comparisons, and this membrane had a higher permeance due to its larger pore size and looser structure, as shown in Figure 3.9(b). Comparing the permeance of M1, M2, and M3 membranes showed that the membrane permeance to the solvents was correlated to the PDA deposition time (which ultimately affected the thickness of the PDA layer on the membrane) (Fig. 3.9b). As expected, a longer PDA deposition time would yield a thicker active layer, which would slow down the solvent permeation rate through the membrane.

Table 3.3. Properties of dyes used in this study.

Dyes	Molar weight (g/mol)	Chemical structure
Rose Bengal	1019.64	
Remazol brilliant blue	626.54	
Methyl orange	327.33	
N,N-Dimethylacetamide	166.21	

The membrane performance for solute rejection from solvent ethanol is shown in Figure 3.10. The interfacially crosslinked membranes PDA/DBX on PBI (M1, M2, M3) showed almost 99% rejection to RB (MW=1020 g/mol), RBB (MW=626.5 g/mol) and MO (MW=327.3 g/mol), while the rejection to DMNA (which are smaller molecules, MW=166 g/mol) was lower than 40% in all membranes. The PBI-DBX membrane was able to reject over 90% of RB and RBB but less than 60% of MO, whereas it displayed almost no rejection to DMNA. The benchmarked M2 membrane had a lower MWCO (286 Da) than that of the PBI-DBX membrane (about 1000 Da), which may explain the high solute rejection of the PDA-coated membranes. In view of the MWCO, it was understandable that the M2 membrane had a higher rejection to MO (MW=327 g/mol) than DMNA

(MW=166 g/mol). The M1 membrane showed a little higher permeance than the M2 and M3 membranes, which was easy to understand in consideration of the PDA layer thickness being affected by the PDA deposition time. However, M2 and M3 membranes were not significantly different in their solute rejection and permeance, indicating that a PDA deposition time of 20 min was appropriate to form an active layer that would yield a high rejection with decent solvent permeance (e.g., M2 membrane) (Fig. 3.10).

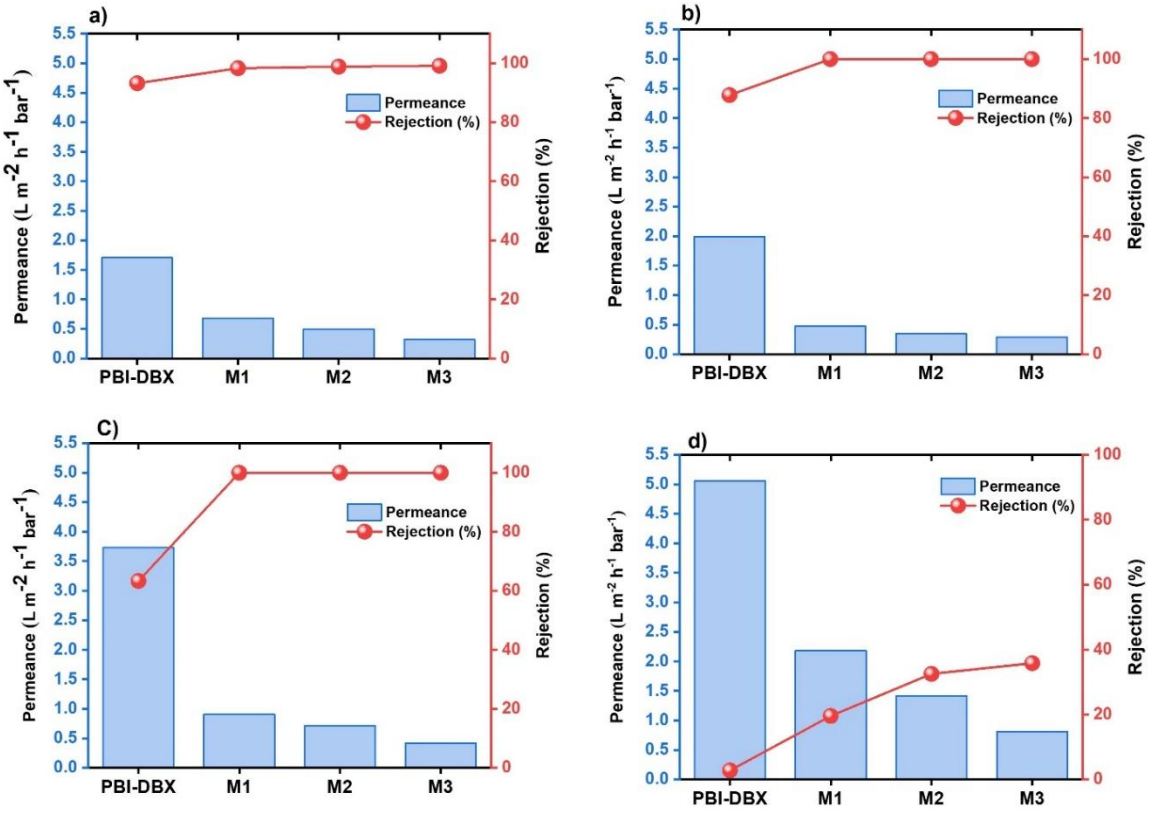


Figure 3.10. Dye rejection of PBI-DBX, M1, M2, and M3 membranes. (a) Rose Bengal, (b) Remazol brilliant blue, (c) Methyl orange, and (d) N,N-dimethylacetamide. Solvent, ethanol; transmembrane pressure, 8 bar.

To better understand solvent permeation in the interfacially crosslinked PDA/PBI membrane, the M2 membrane was further tested with a series of solvents (e.g., non-polar, polar protic, and polar aprotic solvents), and the results are shown in Figure 3.11(a). Acetonitrile (MeCN), displayed the highest permeance [10.8 L/(m^2.h.bar)], followed by methanol (MeOH) [8.4 L/(m^2.h.bar)] and

acetone [4.9 L/(m^2.h.bar)], whereas a low permeance was observed for THF [1.1 L/(m^2.h.bar)] and IPA [1.2 L/(m^2.h.bar)]. In general, the solvent permeance appears to be correlated with the viscosity of the solvent. Among the solvents tested, IPA was a solvent of high viscosity and exhibited low permeance, consistent with some other OSN membranes reported in the literature [168-170]. Note that solvent viscosity is not a dominating factor affecting its permeance; its molecular size and affinity to the membrane are also expected to play a role. For instance, THF had a rather low permeance in the membrane in spite of its low viscosity. There appeared to be a clearer trend when the solvent permeance was plotted against the combined solvent properties (viscosity, solubility parameter, and molecular diameter), as shown in Figure 3.11(b). These properties are given in Table 3.4. Figure 3.11(b) shows that for a given membrane, solvents with lower viscosities, smaller sizes, and stronger affinities/polarities to the membrane tended to have a higher permeance.

Table 3.4. Properties of the solvents used in this study.

Solvents	η^a	d_m [b]	M_V [c]	Hansen solubility parameter ($Mpa^{1/2}$)			
	(mPa s)	(nm)	(cm^3/mol)	d_d	d_p	d_h	$\delta = \sqrt{\delta_d^2 + \delta_P^2 + \delta_h^2}$
Isopropanol	2.06	0.62	58.7	15.8	6.1	16.4	23.5
Tetrahydrofuran	0.55	0.62	81.1	16.8	5.7	8	19.4
Toluene	0.59	0.7	106.9	18	1.4	2	18.2
Ethanol	1.08	0.57	52.9	15.8	8.8	19.4	26.6
Acetone	0.33	0.62	76.4	15.5	10.4	7	20.1
Methanol	0.6	0.51	40.7	15.1	12.3	22.3	29.7
Acetonitrile	0.38	0.55	52.9	15.3	18	6.1	24.6
Heptane	0.41	0.78	147.5	15.3	0	0	15.3
DMF	0.8	0.63	77	17.4	13.7	11.3	24.8

[a] Viscosity (at 25 °C mPa.s), [b] Molar diameter, [c] Molar volume. Viscosity and molar volume data were taken from [115] and the Hansen solubility parameters and the molar diameter data were taken from references [15].

The performance of the M2 membrane to reject RB, RBB, MO, and DMNA in ethanol and DMF is shown in Figure 3.11(c&d), respectively. The M2 membrane showed a rejection of over 99% to RB and RBB in both DMF and ethanol owing to the higher solute molecular weights than the MWCO of the membrane, whereas the membrane permeance to DMF was 2 – 3 times higher than the membrane permeance to ethanol, which is due to the difference in the physical properties of the solvents e.g. lower viscosity of DMF than ethanol (Table 3.4). The rejection of MO (MW=327 g/mol) in DMF was about 95%, which was lower than that in ethanol (~99%), indicating that the solute rejection by OSN was also affected by the solvent involved. Note that in general, the membrane rejection to DMNA in both ethanol and DMF was low (< 35%), which was not unexpected due to the small molecular size of DMNA compared to the MWCO of the membrane (286 Da). These results demonstrated the competitive nanofiltration performance of the M2 membrane for nanofiltrating such solvents as DMF and ethanol while rejecting solutes with molecular weights above 286 Da.

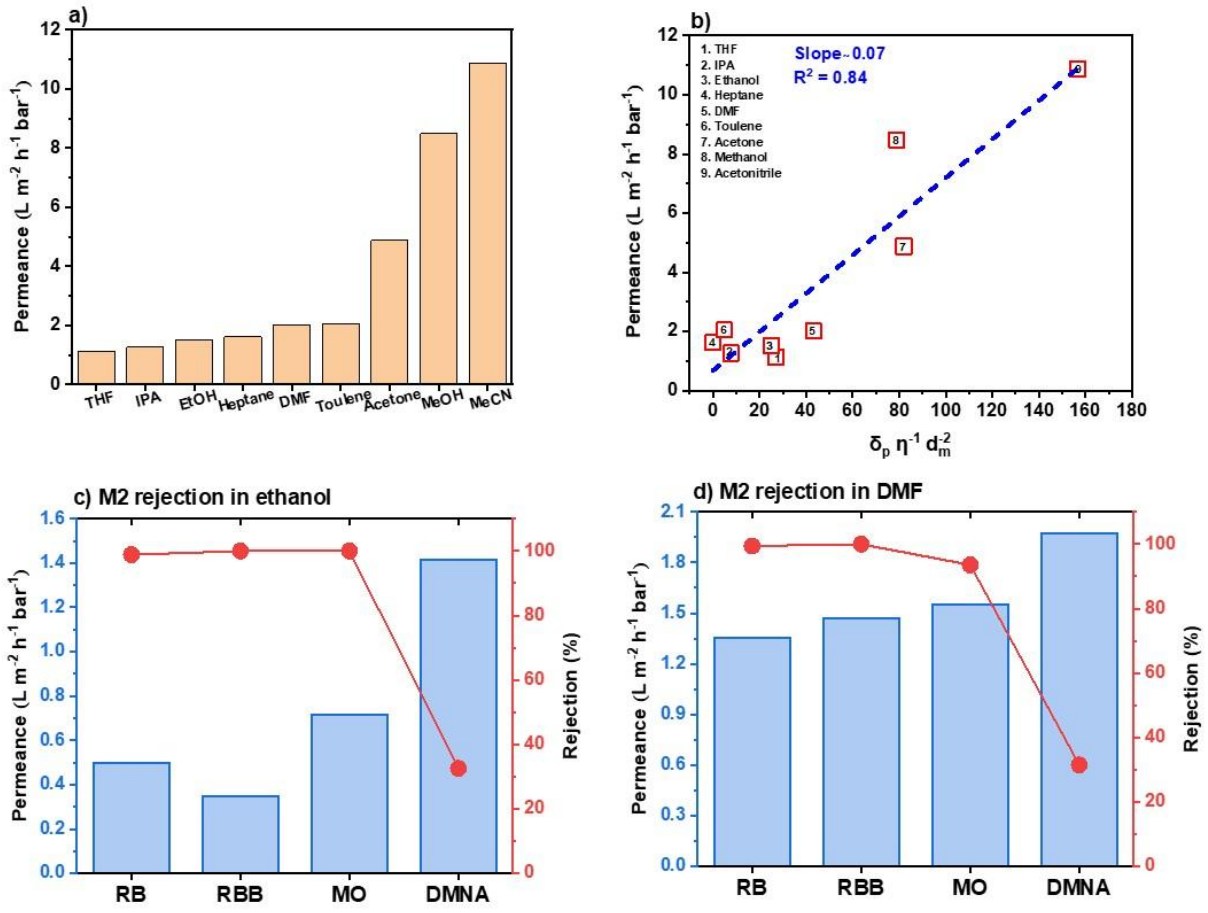


Figure 3.11. Nanofiltration performance of M2 membrane. (a) Pure solvent permeance, (b) plot of solvent permeance vs combined solvent property (viscosity, molar diameter, and solubility parameter), (c) dye rejection in DMF, and (d) dye rejection in ethanol. The experiments were conducted at 22 ºC under 8 bars.

The molecular sieving performance of the M2 membrane for rejecting mixed dyes in a solution was further investigated to determine fractionation and partial separation of the solutes while nanofiltrating the solvents. RBB and DMNA were chosen to segregate from each other due to the difference in their molecular weights and colors, as well as their characteristic absorbance at different wavelengths from an experimental standpoint. Figure 3.12 (a-d) shows that the M2 membrane was able to reject RBB almost completely in both ethanol and DMF solutions while allowing DMNA to permeate through the membrane, as shown in the UV-vis absorption spectra of the feed and permeate (Fig. 3.12 c&d). There was a considerably large amount of DMNA in the permeate, with essentially no RBB. The DMNA rejection rate was about 25% in both solvents,

ethanol and DMF. As shown in Figure 3.12(e&f), after filtration through the membrane, the color of the retentate solution closely resembled the color of the DMNA solution (light yellow). In addition, the membrane showed a permeance of about 0.4 and 0.6 L/(m^2.h.bar) to ethanol and DMF in the mixed solutes rejection test, respectively.

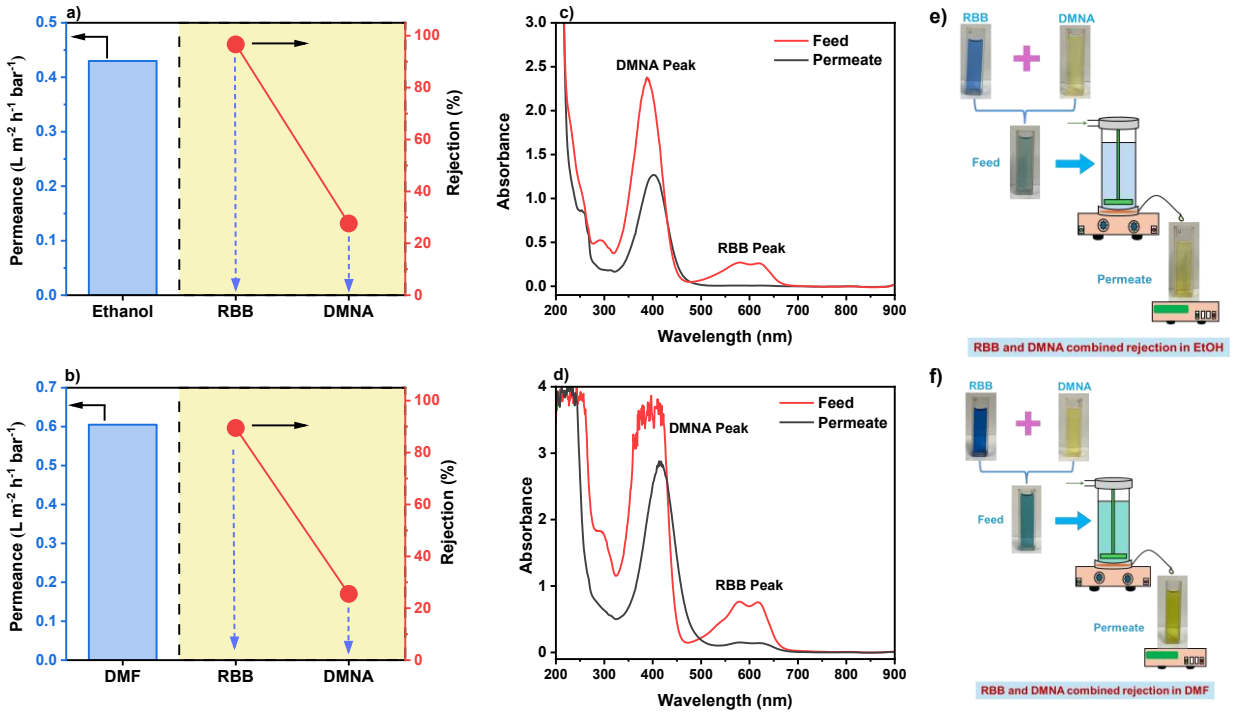


Figure 3.12. M2 membrane separation of mixed dyes (DMNA and RBB) in ethanol (a) and DMF (b). UV-vis absorption spectra of DMNA and RBB in ethanol (c) and in DMF (d). Physical appearance of the permeate samples after filtration in ethanol (e) and DMF (f). The experiments were conducted at 22 ºC and 8 bar.

To further confirm the size-based selectivity of the M2 membrane toward different molecular weight solute species, the membrane was further investigated for nanofiltration of ethanol and DMF with mixed dyes (RBB and MO) that had much higher molecular weights than the MWCO of the membrane (286 Da) (Fig. 3.13). It was shown that both dyes were completely rejected by the membrane, demonstrating the selectivity of the membrane based on molecular sieving for higher-dimension molecules from mixtures. Compared to other state-of-the-art OSN membranes reported in the literature, the M2 membrane showed a good solute rejection to low molecular weight dyes (e.g., MO) (Fig. 3.14), while additional effort to improve the solvent permeance was

needed. This could be achieved by reducing the thickness of the top active layer of the membrane, a subject for further studies.

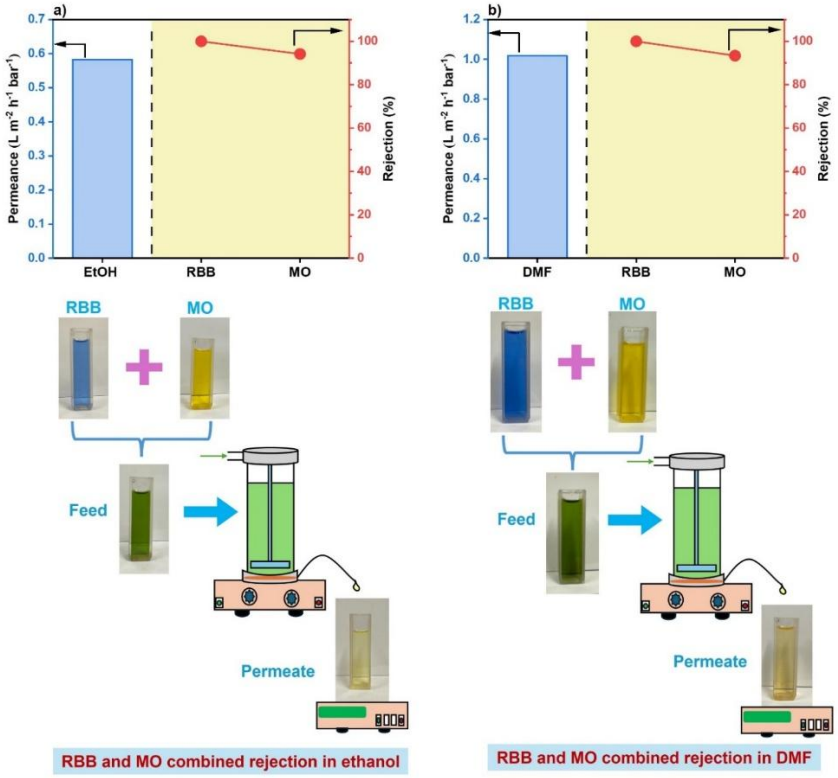


Figure 3.13. M2 membrane rejection of high molecular weight mixed dyes (RBB and MO) in ethanol (a) and DMF (b).

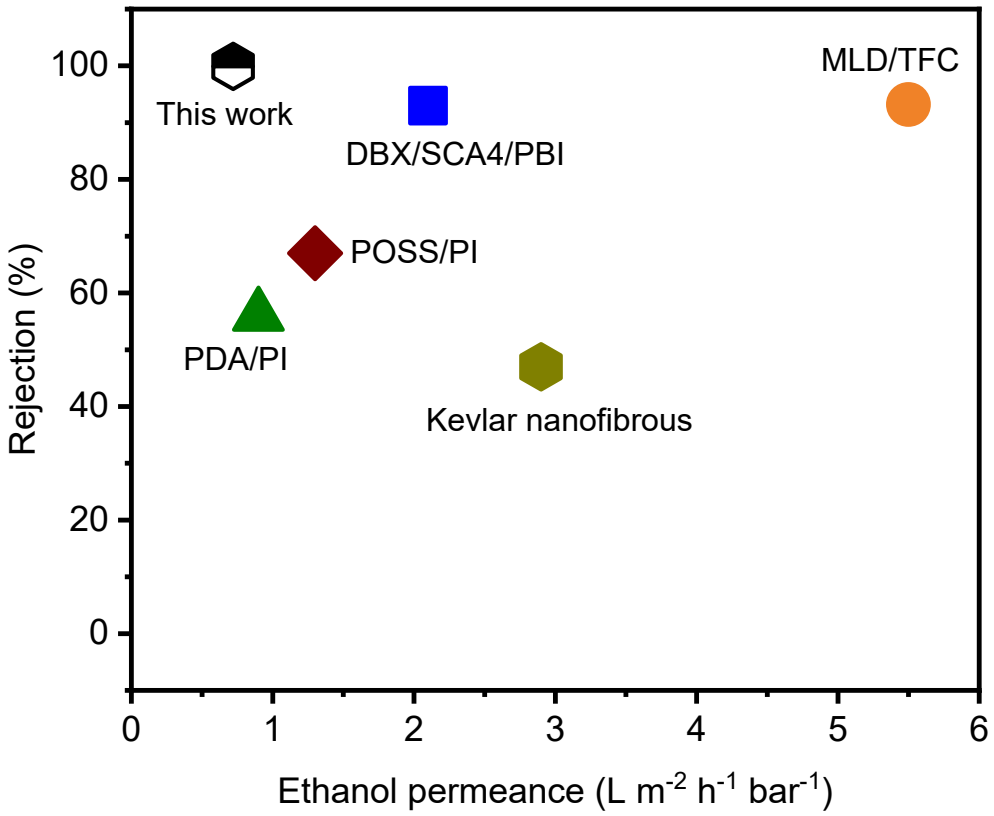


Figure 3.14. Comparison of methyl orange (MW=327 g/mol) rejection and ethanol permanence of M2 membrane with the state-of-the-art OSN membranes reported in the literature. References: POSS/PI [171], Kevlar nanofibrous [172], MLD/TFC [173], DBX/SCA4/PBI [1], and PDA/PI [154].

3.3. Conclusions

In this chapter, interfacial crosslinking was used to fabricate a composite OSN membrane comprising a PDA active layer formed on a PBI substrate. PDA deposition alone was insufficient to produce membranes that were chemically stable in harsh polar aprotic solvents. Therefore, the composite membrane was chemically cross-linked with DBX to improve its chemical stability. The PDA coating allowed for finely tuning the MWCO of the membrane. The morphology and surface properties of the membranes were characterized, and a membrane with a MWCO of 286 Da was investigated for OSN of a series of solvents. The solvent permeance followed the order MeCN > MeOH > acetone > toluene > DMF > heptane > EtOH > IPA > THF. Rejections greater

than 99% were achieved for RB and RBB in both DMF and ethanol, while MO rejection reached about 99% in ethanol and 95% in DMF, demonstrating a relatively sharp pore-size distribution. The membrane also showed effective fractionation of mixed solutes. Overall, the results demonstrate that interfacial PDA/DBX crosslinking is an effective strategy for improving the chemical stability and molecular sieving performance of PBI-based OSN membranes, although further work is needed to increase solvent permeance, for example, by reducing the thickness of the active layer.

While the PDA/DBX interfacial crosslinking strategy improved solvent stability and molecular sieving performance, further control over pore size and polymer chain packing was still needed. Therefore, Chapter 4 investigates how crosslinker structure and supramolecular modification influence the chemical resistance and separation behavior of PBI membranes.

Chapter 4

Tailoring pore size and chemical resistance of PBI membranes for OSN via chemical crosslinking and sulfocalix[4]arene impregnation

**** This chapter is based on the results of a published paper as outlined in the statement of contributions.***

Post-chemical crosslinking is an effective strategy for improving the chemical stability of PBI membranes. This can be achieved through the reaction between the –NH– functional groups of the imidazole ring present in PBI and the reactive functional groups of crosslinking agents [174]. Additionally, the nitrogen groups in PBI allow for chemical crosslinking without altering the polymer backbone structure [166, 175, 176]. This exceptional feature enhances PBI's resistance to harsh organic solvents and improves its chemical durability [1]. Several crosslinkers have been studied to crosslink PBI through its nitrogen groups. For instance, Valtcheva et al. (2014) introduced α,α'-dibromo-p-xylene (DBX) as a crosslinking agent for PBI, and crosslinking of PBI with DBX resulted in the formation of a highly stable membrane that exhibited excellent stability across a wide pH range (0-14) and in both polar and non-polar solvents [161]. Potassium persulfate was also used as a radical initiator to crosslink PBI membranes through its imidazole nitrogen atoms [17]. However, tailoring the selectivity of the membranes was found to be difficult [162]. These studies suggest that the selection of appropriate crosslinkers and reaction conditions is critical to optimizing the membrane performance and chemical stability for OSN use.

As shown in Chapter 3, chemical crosslinking improves the solvent resistance of PBI membranes. Understanding the influence of the crosslinker's structure on PBI is therefore necessary for assessing chemical stability, selecting the appropriate crosslinker, and optimizing membrane performance. This chapter investigates how crosslinker chemistry and supramolecular modification influence the pore structure and chemical stability of PBI membranes. We employed two different crosslinkers: α,α′-dichloro-p-xylene (DCX), which has an aromatic structure, and 1,4-dibromobutane (DBB), which features an aliphatic structure, to modify the PBI membrane. The aim was to investigate how the crosslinking agent structure affects the PBI membrane's chain packing density and chemical stability through covalent bonding. To improve the separation

performance, the crosslinked PBI membranes were impregnated with sulfocalix[4]arene (SCA4), a macrocycle with four phenolic groups in a closed loop ring, enabling size-based rejections of solutes and the removal of molecules larger than their intrinsic cavities [177-179]. Incorporated into the selective layer of the PBI membrane, SCA4 would act as a gatekeeper, imparting better pore size control and improved molecular separation performance [115]. In addition, SCA4 can potentially establish extensive hydrogen bonding interactions with the polymer chains, which help suppress solvation effects and self-aggregation propensities. These properties facilitate homogeneous dispersion of SCA4 and strong integration within membranes [180]. This study is expected to further help expand the knowledge of chemical crosslinking of PBI OSN membranes.

4.1. Experimental Methods

4.1.1. Materials

A solution containing 26 wt% PBI (Celazole S26) (MW 27,000 g/mol) and 1.5 wt% LiCl in N,N-dimethylacetamide (DMAc) was purchased from PBI Performance Products Inc. (USA). Non-woven polypropylene (PP) support (Novatexx 2471) was kindly provided by Freudenberg Filtration Technologies Inc. (Canada). α,α′-Dichloro-p-xylene (DCX, 98%) and 1,4-dibromobutane (DBB) crosslinkers were acquired from Sigma Aldrich. All solvents used in this work, including acetonitrile (MeCN), ethanol (EtOH), methanol (MeOH), acetone, isopropanol (IPA), toluene, N,N-dimethylacetamide (DMAc), N-methyl-2-pyrrolidone (NMP), n-hexane, and tetrahydrofuran (THF), were purchased from Sigma Aldrich. 4-Sulfocalix[4]arene hydrate (SCA4 > 98.0%), poly(ethylene glycols) (PEGs, MW 200, 600, 1000, 2000, 4000 g/mol) and dyes (methyl orange (MO, MW 327.33 g/mol), Ramazol brilliant blue (RBB, MW 626.54 g/mol), and Rose Bengal (RB, MW 1019.64 g/mol) were acquired from Thermo Scientific and used as received.

4.1.2. Fabrication of PBI-based membranes

Asymmetric PBI substrate membranes were prepared by the phase inversion method described in Chapter 3.

4.1.3. Crosslinking and Modification of PBI Membranes

The crosslinking of the membranes was carried out following the parameters described by Valtcheva et al. [161]. A 3 wt% solution of DCX and a 10 wt% DBB solution in acetonitrile were separately prepared. The pristine PBI (P-PBI) membranes were immersed in the solutions at 80 ºC for 24 h under continuous stirring and reflux to crosslink the membranes with DCX or DBB, and the crosslinked membranes were named DCX-PBI and DBB-PBI, respectively. After removal from the solutions and rinsing with IPA to remove any lingering chemicals, the membranes were stored in IPA for further use (see Appendix).

Some DCX-PBI and DBB-PBI membranes were subjected to modification with SCA4. This was done by submerging the membranes into a 0.03 wt% solution of SCA4 in water/methanol (50:50 wt%) at 22 ºC for 5 h. To determine the amount of SCA4 loaded onto the membranes, the pH of the SCA4 solutions was measured before and after membrane immersion. By quantifying the change in H^+ within the solution before and after membrane immersion, the SCA4 concentration can be back-calculated [1, 177, 181, 182]. For example, the initial pH of our 0.03 wt% SCA4 solution was 2.98, and after immersion of the DBB crosslinked membrane, the pH of the solution increased to 3.17. The volume of the solution was 47 ml (0.047L), and H^+ absorbed by the membrane can be calculated by $(= (10^{-2.98} - 10^{-3.17}) \times 0.047 = 17.44\ \mu mol)$. As we know, each SCA4 can dissociate 4 $H^+ = 17.44/4 = 4.36$, therefore, the total SCA4 molecules attached to the DBB membrane were 4.36 μmol. The molecular weight of SCA4 is 744.74 g/mol, and the weight of the DBB membrane sample was 0.781 g; therefore, the actual loading of 0.03wt% SCA4 can be calculated by $= \frac{744.74 \times 10^{-6} \times 4.36}{0.781} \times 100 = 0.42\%$. Based on this calculation, the actual SCA4 loadings were 0.42% and 0.45% for DBB membranes and DCX crosslinked membranes, respectively. The SCA4-modified membranes were named DCX-SCA4 and DBB-SCA4, respectively. The chemical interactions involved in the modification are illustrated in Figure 4.1, including the covalent crosslinking reaction between the crosslinkers and PBI and the ionic interactions between PBI and SCA4 molecules.

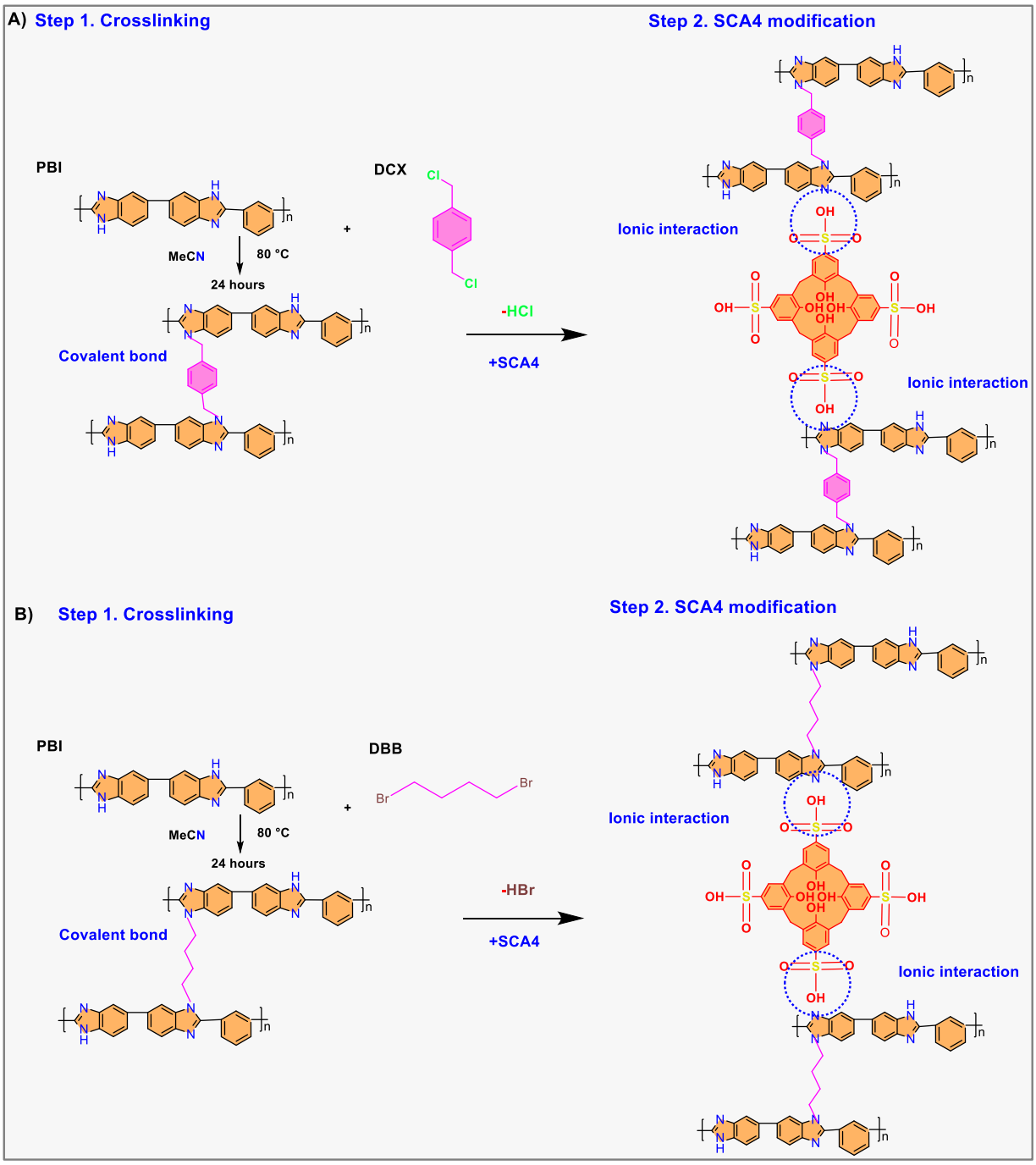


Figure 4.1. (a) The chemical reaction between the PBI monomer and DCX crosslinker is followed by the ionic interaction of the PBI and SCA4 molecule. (b) The chemical reaction between the PBI monomer and DBB crosslinker is followed by the ionic interaction of the PBI and SCA4 molecules.

4.1.4. Characterization

4.1.4.1. Surface characterization

Scanning electron microscopy (SEM) (Tescan VEGA TS-5130) was employed to scrutinize the surface and cross-sectional morphologies of the membranes. The membrane samples were freeze-fractured in liquid nitrogen and then sputter-coated with gold using a Polaron SEM coater (E5100). The hydrophilicities of the membranes were evaluated with water contact angle measured using a contact angle goniometer (Tantec Inc.). Atomic force microscopy (AFM) operated in tapping mode was performed to examine the surface roughness and topography of the membrane. Fourier transform infrared (FTIR) spectroscopy (Thermo Nicolet 6700 ATR-FTIR spectrometer) in ATR mode was used in the wavelength range 400-4000 cm^{-1} to elucidate the chemical structure of the membranes. X-ray diffraction (XRD) patterns of the membranes were obtained in the scanning range of 5-45° using a Rigaku Miniflex II X-ray diffractometer to study the structural changes induced by the crosslinkers. For XRD analysis, dense membranes were prepared and crosslinked under the same conditions to observe the crosslinking of PBI without interference from the substrate membrane. Thermogravimetric analysis (TGA) of the membranes was performed with simultaneous DSC-TGA at a heating rate of 10 °C/min under a nitrogen atmosphere using a TA Instrument thermogravimetric analyzer (Q600). The degree of crosslinking was calculated from the weight loss of the membranes between 200 to 500 °C from [183].

4.1.4.2. Chemical stability test

The chemical stability and swelling degree of the membranes were evaluated by immersing a 3×3 cm^2 sheet of each membrane in polar protic, polar aprotic, and nonpolar organic solvents (Table 4.1) for 20 days. Afterward, the membrane samples were taken from the solvents, blotted dry with tissue paper to remove the excess solvent from the membrane surface, and weighed (weight W_{wet}). Then the membrane samples were dried in a vacuum oven at 50 ºC for 2 h, and the dried sample weight (W_{dry}) was recorded. The swelling degree (%) was calculated based on equation (1) from [184]:

$$Swelling\ degree\ (\%) = \frac{W_{wet} - W_{dry}}{W_{dry}} \times 100 \quad (1)$$

To further assess the stability of the membranes in such harsh organic solvents as NMP and DMAc, a 1.5×1.5 cm^2 piece of each membrane was soaked in 10 ml of NMP and DMAc for 60 h, respectively. Subsequently, the samples were removed from the solvents, and the quantity of PBI dissolved in the solvents was quantified using a UV-Vis spectrophotometer (UV-1900i Shimadzu, Japan).

Table 4.1. Properties of the solvents used in this study.

Solvents	Viscosity (25°C) (mPa.s)	Hansen solubility parameter ($MPa^{1/2}$)				Diameter (nm)	Molar volume (cm^3/mol)
		δ_d	δ_p	δ_h	$\delta = \sqrt{\delta_d^2 + \delta_P^2 + \delta_h^2}$		
Isopropanol	2.06	15.8	6.1	16.4	23.5	0.62	58.7
Tetrahydrofuran	0.48	16.8	5.7	8.0	19.4	0.62	81.1
Toluene	0.59	18.0	1.4	2.0	18.2	0.70	106.9
Hexane	0.33	15.0	0.0	0.0	15	0.72	130.5
Ethanol	1.08	15.8	8.8	19.4	26.6	0.57	52.9
Acetone	0.33	15.5	10.4	7.0	20.1	0.62	76.4

Viscosity and molar volume data were taken from [115], and the Hansen solubility parameter and the molar diameter data were taken from references [15].

4.1.4.3. Molecular weight cut-off and pore size distribution

The pore size distribution and MWCO of the membranes were determined by the molecular probe method described in Chapter 3.

4.1.5. OSN performance evaluation

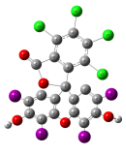
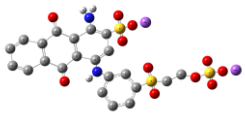
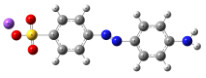
The OSN performance of the pristine and modified membranes was evaluated using the dead-end filtration setup described in Chapter 3 (Fig. 3.1). All experiments were conducted at 22 °C with constant stirring and at a transmembrane pressure of 8 bar. The separation performance of the membranes was determined based on membrane permeance to pure solvents (IPA, EtOH, hexane, toluene, THF, and acetone), the rate of rejection of the dyes (RB, RBB, and MO) in EtOH, and

long-term performance of the membrane. The properties of these solvents and dyes are given in Table 4.1 and Table 4.2. EtOH was chosen for the dye rejection tests in this study because it is one of the most common solvents in industrial processes. Before each experiment, the membrane was preconditioned with deionized water. Afterward, the feed solution was charged to the stainless-steel membrane unit, and the permeate samples were collected to determine the solvent permeance and dye rejection after the steady-state permeation was achieved. The solvent permeance and solute rejection reported were the average measurements with at least two membrane samples (see Appendix).

The dye rejection of the membrane was calculated using equation (3) from Chapter 3.

The solvent permeance of the membrane was calculated by equation (6) from Chapter 3, where P is the solvent permeance expressed in units L/(m^2.h.bar), V is the volume of permeate collected over permeation time *t* (h), A is the membrane area (m^2), and ΔP is the applied transmembrane pressure (bar). where C_p and C_f are the dye concentrations in the permeate and feed solution, respectively, and were measured using a UV–Vis spectrophotometer (Shimadzu UV-1900i). The permeate samples were recycled back to the filtration cell to maintain a constant concentration throughout the experiment (Fig. 3.1, Chapter 3).

Table 4.2. Properties of dyes used in this study.

Dyes	Molar weight (g/mol)	Chemical structure
Rose Bengal	1019.64	
Remazol brilliant blue	626.54	
Methyl orange	327.33	

4.2. Results and discussion

4.2.1. Characterization of membranes

Figure 4.1 illustrates a two-stage chemical reaction of PBI, crosslinkers (DCX and DBB), and SCA4. The first stage of the reaction involves the release of chlorine or bromine and electrophilic alkylation of the PBI polymer chains with the crosslinkers. In the second stage, ionic bonds form between PBI and SCA4, resulting in a tight membrane structure. ATR-FTIR spectroscopy was used to verify the chemical crosslinking and membrane modification with SCA4 (Fig. 4.2a). In the pristine PBI membrane, the broad peak ranging from 3700 to 3100 cm^{-1} corresponds to non-hydrogen bonded/hydrogen bonded N–H groups and the stretching of aromatic =C–H groups of the imidazole rings [115, 161]. Peaks at approximately 1630, 1540, and 1442 cm^{-1} are associated with the stretching of the C=N and C=C of the benzimidazole ring [1, 163]. Moreover, peaks at 1285 and 790 cm^{-1} are linked to the breathing of the imidazole rings and the bending of the C–H groups. The peaks in the fingerprint area are all associated with the imidazole and benzene ring and their conjugation in PBI membranes [1]. However, in chemically crosslinked membranes, the vibration intensity of N–H peaks decreased, suggesting that a secondary amine was involved in a chemical reaction and was transformed into a tertiary amine. Therefore, the crosslinked membranes displayed two additional peaks at 2920 and 2850 cm^{-1}, which corresponded to the C–H and C–N stretch vibrations associated with the terminal C of the crosslinker and the crosslinking between the DCX or DBB molecules and the polymer backbone [1, 161]. This provided further evidence of the crosslinking of the membranes. Additionally, the membranes modified with SCA4 displayed a peak at about 1043 cm^{-1}, indicating the presence of S=O bonds [115, 181].

The alterations in the polymer structure due to crosslinking were further verified through XRD analysis (Fig. 4.2b). In the pristine PBI membrane, the diffraction peak at 23.3º is associated with the π–π stacking of the aromatic rings. This peak shifted to 23.8º for the DBB crosslinked membrane and 25.1º for the DCX crosslinked membrane. Additionally, the *d*-spacing of the polymer chains was reduced from 3.82 Å for the pristine membrane to 3.73 Å for the DBB crosslinked membrane and 3.54 Å for the DCX crosslinked membrane (Fig. 4.2b). This indicated a decrease in the average distance between adjacent polymer chains, resulting in a more tightly packed membrane structure [10, 82]. TGA was used to further validate the crosslinking and

determine the degree of crosslinking in the membranes (Fig. 4.2c). The results show that DCX-PBI exhibited slightly greater weight loss compared to P-PBI and DBB-PBI, likely due to the release of residual crosslinking byproducts. The weight loss attributed to the DBB and DCX crosslinkers was 8.04% and 15.25% (Table 4.3). The findings indicate that the DCX crosslinked membrane achieved a higher degree of crosslinking (calculated as 0.49) compared to the DBB crosslinked membrane (0.46) (Table 4.3). Note that between the two crosslinked membranes, the DCX membrane exhibited a smaller interchain spacing than the DBB membrane, which was the primary factor contributing to the superior chemical resistance of the DCX membrane compared to the pristine or DBB crosslinked membranes (Fig. 4.2d).

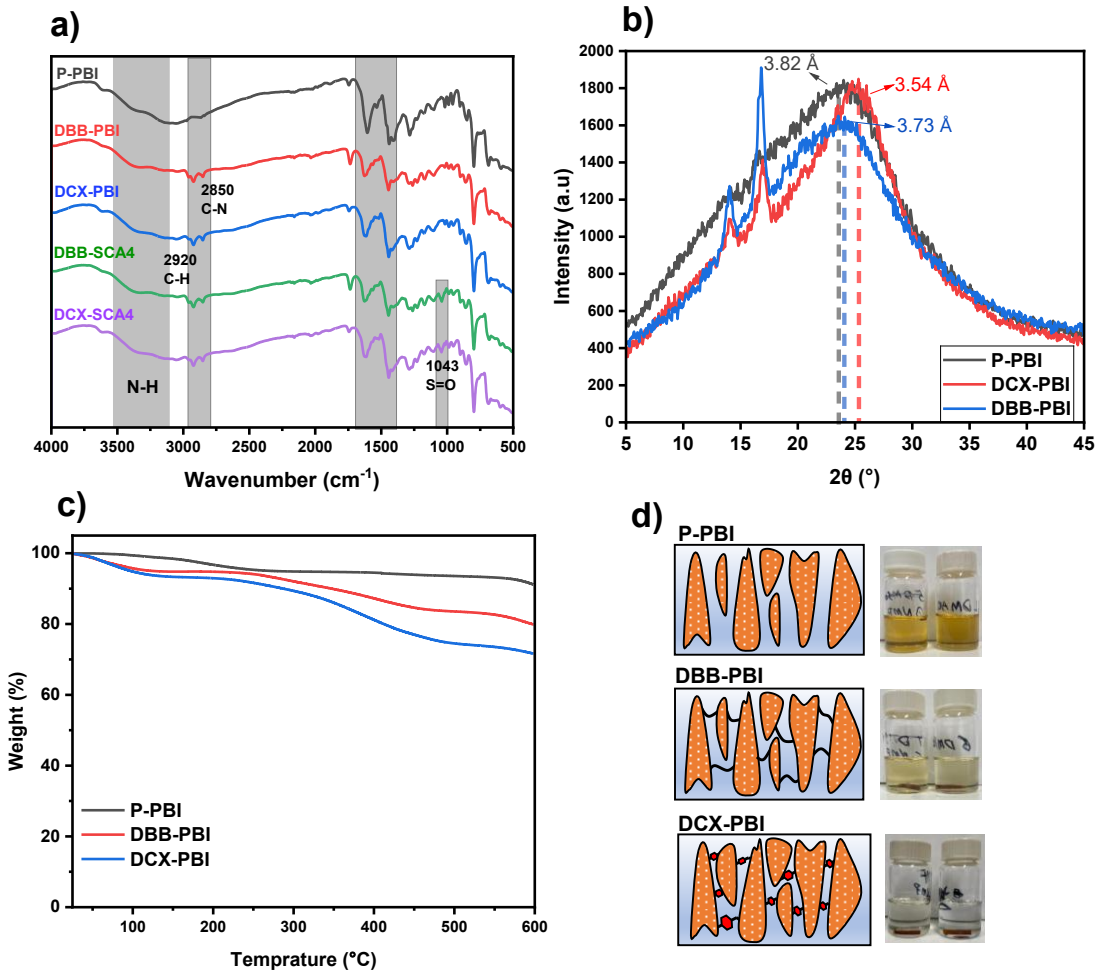


Figure 4.2. Chemical and structural analysis of pristine and crosslinked PBI membranes. (a) FTIR spectra of pristine PBI (P-PBI), crosslinked PBI, and SCA4-modified membranes. (b) XRD pattern of pristine and crosslinked PBI membranes. (c) TGA analysis results of the P-PBI, DBB-PBI, and

DCX-PBI membranes. (d) Schematic of the P-PBI, DBB crosslinked, and DCX crosslinked membrane structures and their dissolution in NMP and DMAc solvents. After soaking for 8 days, it was observed that the pristine PBI membrane was completely dissolved in NMP and DMAc solvents, whereas the DBB crosslinked membrane was dissolved to a certain level but did not completely disappear. The DCX crosslinked membrane was found to be very stable in both strong solvents, attributed to the higher degree of crosslinking and aromatic structure of the crosslinker, which created a tight membrane structure by squeezing the polymer chains.

The membrane morphologies were examined using SEM and AFM (Fig. 4.3). The SEM surface images of the membranes all displayed a smooth top surface with no visible defects (Fig. 4.3a-c). The cross sections of the membranes showed finger-like structures underneath the dense selective surface layer at the top, which was typical of asymmetric membranes formed in the non-solvent-induced phase inversion process (Fig. 4.3d-f). In comparison, the crosslinked membranes exhibited a thicker top surface layer than the pristine membrane (Fig. 4.3g-i), which could be attributed to the expansion of the top layer during membrane crosslinking in acetonitrile. The AFM 3-dimensional images also revealed that the surfaces of the crosslinked membranes were smoother than those of the pristine membrane (Fig. 4.3j-l). The root-mean-square (RMS) roughness (R_q) decreased after crosslinking from 12.1 nm (P-PBI) to 6.3 nm (DBB-PBI) and 7.7 nm (DCX-PBI), which could be attributed to the formation of a dense active layer resulting from the crosslinker-induced network of the PBI chains.

Table 4.3**.** Weight loss and degree of crosslinking of DBB and DCX crosslinked membranes.

Membranes	Weight loss (%)[a]	Degree of crosslinking	Molecular weight (g/mol)[b]
DBB	8.04	0.46	56.104
DCX	15.25	0.49	104.15

[a] The weight loss due to the crosslinker from 200-500°C. [b] The calculated molecular weight after the crosslinking reaction.

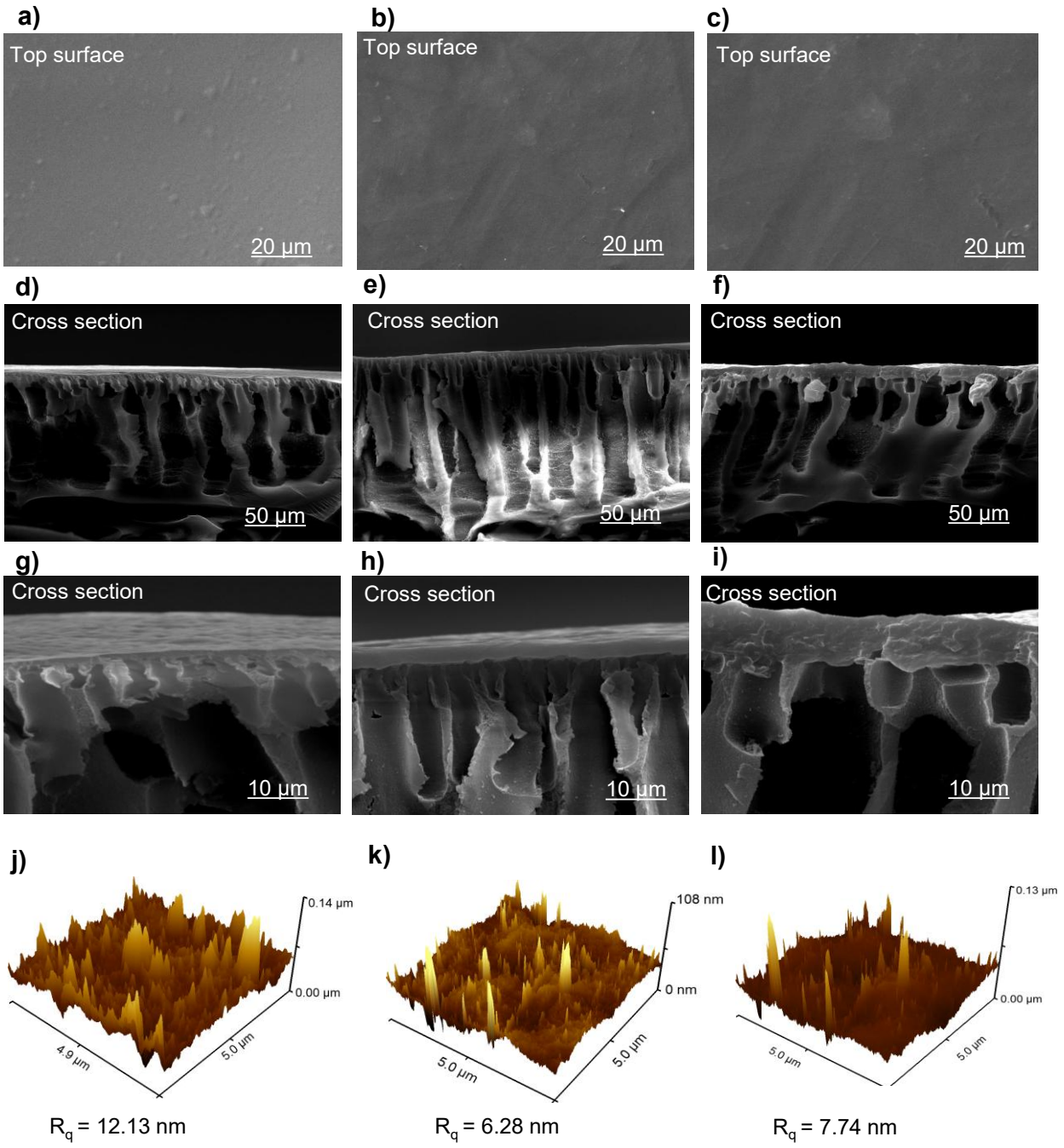


Figure 4.3. Scanning electron microscopy (SEM) and atomic force microscopy (AFM) images of the pristine and crosslinked PBI membranes. Top-view SEM images of (a) P-PBI, (b) DBB-PBI, and (c) DCX-PBI membranes. Cross-sectional view of P-PBI (d&g), DBB-PBI (e&h), and DCX-PBI membranes (f&i). AFM 3D images of P-PBI (j), DBB-PBI (k), and DCX-PBI membranes (l), where Rq represents root-mean-square roughness.

The hydrophilicities of the membranes are presented in Figure 4.4(a). The water contact angle of the pristine PBI membrane decreased substantially from about 75º to 61º and 56º after crosslinking with DCX and DBB, respectively. This hydrophilicity of the crosslinked membranes was affected by the existence of -Br, -COCL, or -Cl groups as well as the formation of quaternary ammonium during chemical crosslinking. The DBB crosslinked membrane showed the lowest water contact angle, which agreed with its high pure solvent permeance. Similar results were also reported in the literature [1, 161, 162]. After modification of crosslinked membranes with SCA4, the water contact angles of DCX-PBI and DBB-PBI membranes further decreased to about 54º and 48º, respectively, which can be attributed to the -HSO_4 and -OH functional groups in the SCA4. In all studied membranes, the DBB-SCA4 membrane showed the lowest water contact angle. The increased hydrophilicity of the modified membrane suggests that the membrane will have a strong affinity for the hydrophilic organic solvents that would favor solvent transport across the membranes.

4.2.2. Molecular weight cut-off and pore size distribution

The PEG rejection of the pristine and modified membranes is shown in Figure 4.4(b). As expected, the PEG rejection of the membranes increased with an increase in the molecular weight of PEGs. The P-PBI membrane was found to have the lowest rejection to PEG and therefore the largest MWCO. However, the MWCO of the membranes was significantly reduced after chemical crosslinking and modification with SCA4. The pore size distribution was plotted in Figure 4.4(c) using the exponential probability density function for the PEG rejection and the PEG Stokes diameter, and the average pore size and geometric standard deviation of the membranes are shown in the figure as well. The P-PBI membrane has the largest mean pore size and the broadest pore size distribution. However, after chemical crosslinking with DCX and DBB, the membrane structure was tightened, yielding a smaller pore size and narrower distribution. The average pore size of the DCX crosslinked membrane was 0.63 nm, which is smaller than that of the DBB crosslinked membrane (0.87 nm). DBB is a long-chain aliphatic crosslinker that does not decrease the *d*-spacing of the PBI polymer sufficiently, compared with DCX, which has an aromatic structure. Therefore, the DBB membrane has shown a larger pore size than the DCX membrane. These are consistent with the results revealed by the XRD analysis of the *d*-spacing of the polymer chains. Ionic modification of the crosslinked membranes with SCA4 appeared to have further

narrowed the pore size distribution and the effective mean pore size of the membranes (Fig. 4.4c). Among the fabricated membranes, the DCX-SCA4 modified membrane was found to have the smallest MWCO (262 Da), with a mean effective pore size of 0.43 nm.

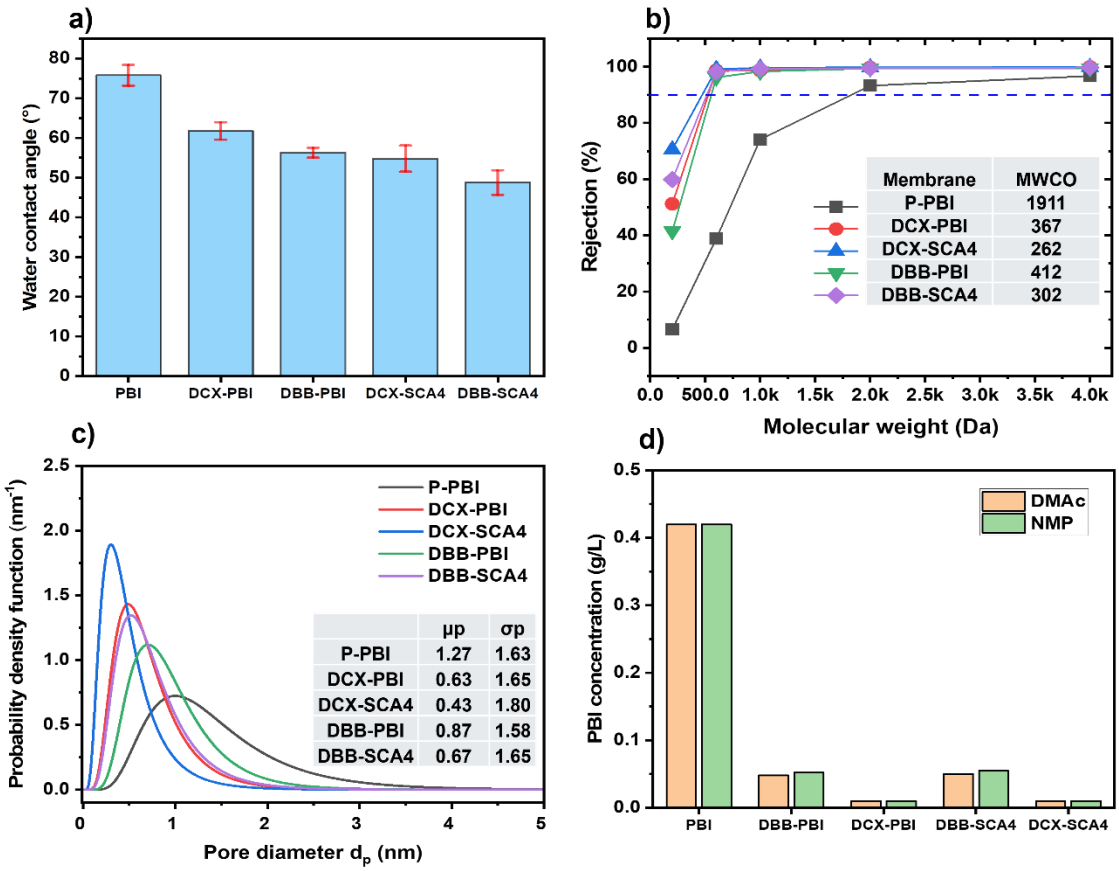


Figure 4.4. (a) The water contact angle of P-PBI, crosslinked, and SCA4-modified membranes (The error bars represent the standard deviation of 5 measurements on different spots). (b) PEG rejection and the MWCO values (inserted table) of the fabricated membranes. (c) Pore size distribution of the pristine and modified membranes. (d) The quantity of PBI dissolved in NMP and DMAc (the membrane samples were kept in the solvents for 60 h at a room temperature of 22 ºC, and the concentration of PBI in the solvent was quantified using a UV-Vis spectrophotometer).

4.2.3. Chemical stability evaluation

Unlike the traditional NF membranes for water treatment, the chemical stability of OSN membranes is particularly important because of the harsh operating conditions. Indicators such as the degree of swelling of the membrane in the solvent can be used to measure the membrane

stability against the solvent [184-186]. Thus, the swelling ratio of the pristine and modified membranes in polar protic, polar aprotic, and non-polar solvents was evaluated (Table 4.4). All the membranes were stable and showed little swelling. It can be seen in Figure 4.5 that all the soaking solvents remained clear after 20 days, except for NMP, which was capable of dissolving pristine PBI completely. Note that NMP was not used for swelling evaluation due to the dissolution of the P-PBI membrane. The DBB crosslinked membrane was dissolved by NMP to a certain level, but did not disintegrate. The DCX crosslinked membrane was stable in NMP, even after 20 days of soaking, as shown in Figure 4.5.

Table 4.4. Solvent swelling degree of the pristine and modified PBI membranes after 20 days of immersion in the solvents.

Solvents	Swelling degree (%)				
	PBI	DCX-PBI	DBB-PBI	DCX-SCA4	DBB-SCA4
IPA	0.73	0.86	0.87	0.94	0.99
Acetone	0.29	0.36	0.46	0.41	0.62
THF	0.65	0.82	0.86	0.85	0.93
Toluene	0.63	0.83	0.88	0.87	0.96
Hexane	0.54	0.64	0.71	0.68	0.73

The solvent stability of the pristine and modified PBI membranes in harsh organic solvents (e.g., DMAc and NMP) was further investigated. The membrane samples were soaked in DMAc and NMP for 60 h, and the dissolved PBI in the solvents was quantified using a UV-Vis spectrophotometer. Figure 4.4(d) shows the concentration of PBI dissolved in DMAc and NMP. Again, pristine PBI was completely disintegrated in NMP and DMAc, whereas the DBB crosslinked membranes showed a little dissolution in the solvents, but did not result in complete membrane disintegration. This was probably due to unreacted groups of DBB that were hydrolyzed and became unstable in harsh organic solvents. In contrast, the DCX crosslinked and DCX-SCA4 membranes showed remarkable stability against both DMAc and NMP (Fig. 4.4d). The good stability of the DCX membrane may be attributed to the aromatic structure of DCX.

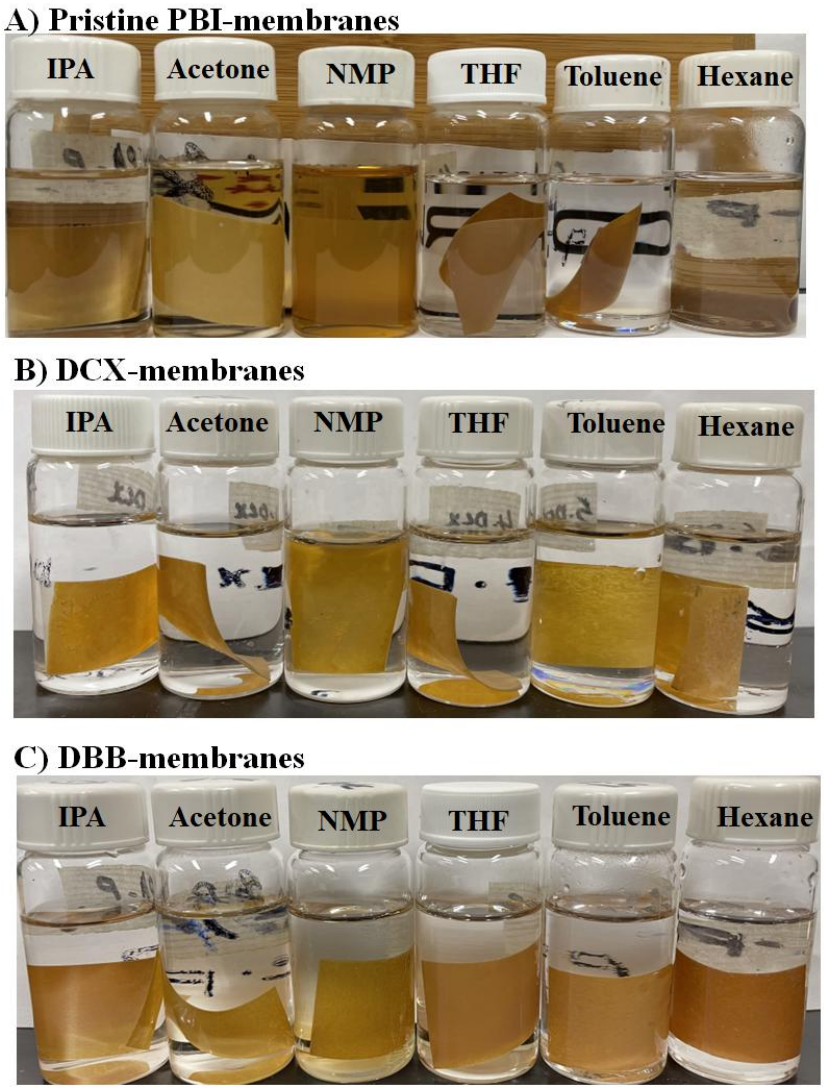


Figure 4.5. Photographs of the membrane's pieces immersed in different solvents for 20 days. The pristine PBI membrane completely disintegrated in NMP (a). The DCX crosslinked membrane showed resistance to all solvents (b), while the DBB crosslinked membrane dissolved to a certain level in NMP (slightly turbid at the bottom) (c).

4.3. OSN performance of membranes

4.3.1. Pure solvent permeance

Pure-solvent permeation experiments were carried out using solvents with different viscosities, molar volumes, and solubility parameters in order to examine how solvent properties and membrane structure affected transport behavior. The properties of the solvents used are given in

Table 4.1. The solvent transport in all membranes was found to be dependent on the properties of the solvents (Fig. 4.6), which was consistent with other OSN membranes reported in the literature [1, 117, 187]. The solvent properties that can influence the permeance of the membrane include solubility parameters (cohesive energy density), viscosity (resistance to flow), and molar volume (molecular size). Figure 4.6(a) shows a trend between the reciprocal solvent viscosity and permeance, demonstrating that the transport of solvent increased with a decrease in solvent viscosity. Since the membrane permeance to the solvent is a volume-based quantity, there have been semiempirical correlations between solvent permeance and the molar volume to viscosity ratio of the solvent [188-190], though the solvent of bigger molecules tends to have a higher viscosity. Figure 4.6(b) shows the membrane permeance vs the molar volume/viscosity ratios of the solvents, and the solvent viscosity appeared to be a more influential factor than the molar volume of solvents as far as the volume-based permeance is concerned. Overall, the permeance of the studied solvents in the membranes followed the order of acetone > n-hexane > toluene > THF > ethanol > IPA.

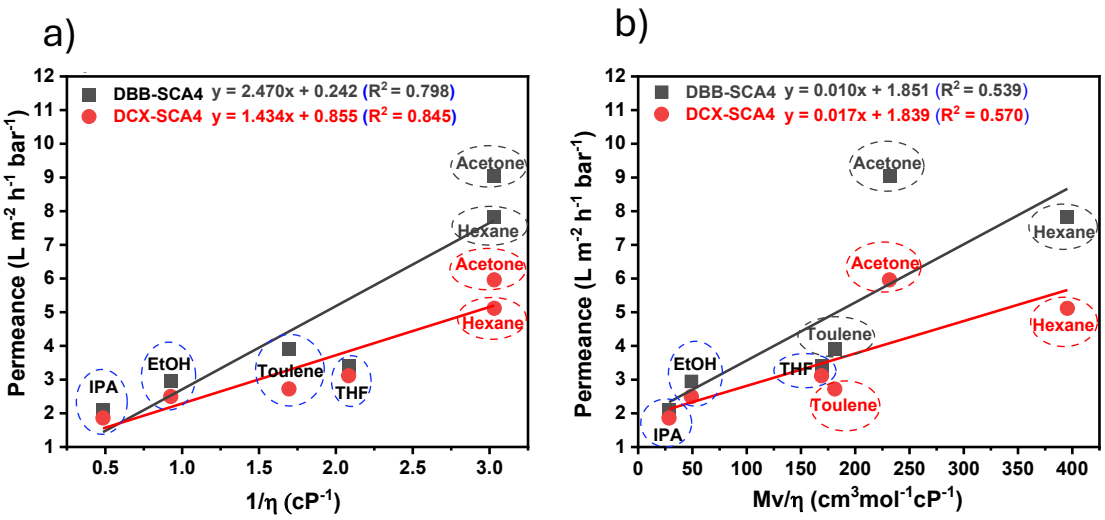


Figure 4.6. (a) Solvent permeance vs 1/η and (b) solvent permeance vs Mv/η for DBB-SCA4 and DCX-SCA4 membranes.

Note that the pristine PBI membrane showed a higher permeance than the modified membranes due to its loose membrane structure (Fig. 4.7). A decrease in the membrane permeance was observed after crosslinking of the PBI membrane with DCX and DBB because of reduced chain

flexibility and tightened microstructure of the PBI membrane, while enhancing chemical stability of the membrane. The reduction in the permeance of DCX and DBB-modified membranes agrees well with their reduced interchain spaces after crosslinking. Note that the DBB crosslinked membrane showed higher permeance than the DCX crosslinked membrane, which was understandable from the standpoint that the degree of crosslinking is affected by the size/shape of the crosslinked molecules. The SCA4-modified membranes showed lower permeance (Fig. 4.7) among all membranes prepared, which may be attributed to the cup-like structure of SCA4, which sharpened and narrowed down the pore size distribution of the membranes [115, 180].

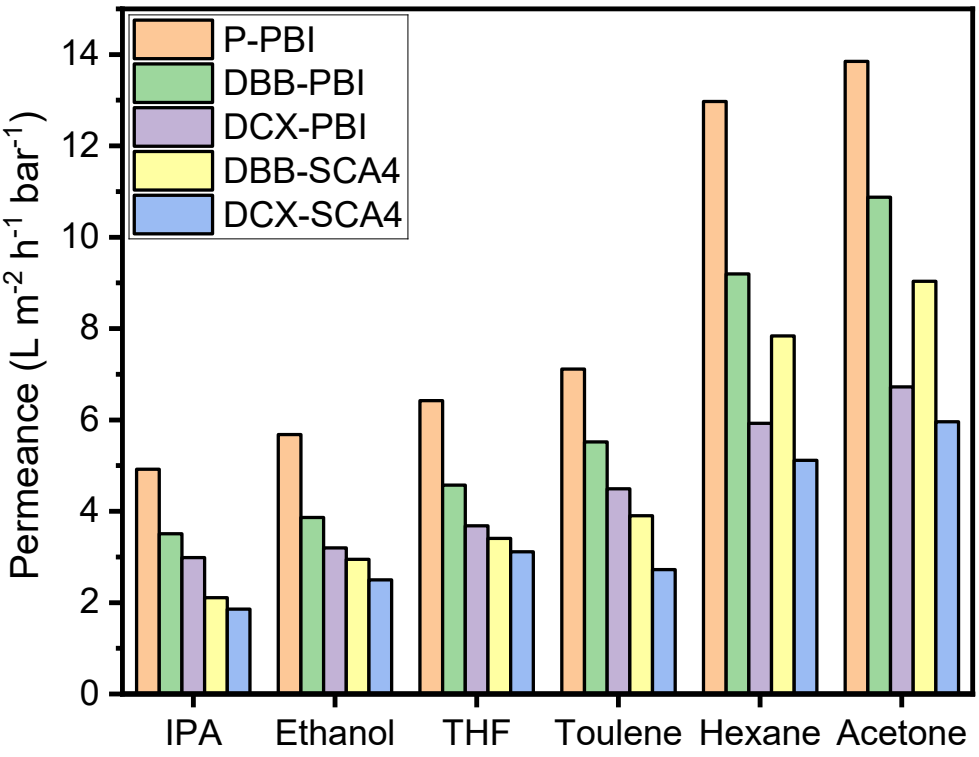


Figure 4.7. Pure solvent permeance of pristine and modified membranes.

4.3.2. Membrane separation performance

The solute rejection performance of the membranes was evaluated in ethanol using dye molecules of different molecular weights. Ethanol was selected as the representative solvent for the rejection tests due to its wide range of industrial applications. Table 4.2 shows the model organic dyes with different molecular weights and configurations used in rejection tests. Figure 4.8(a) shows the rejection profile of RB (MW 1020 g/mol). The pristine PBI membrane showed RB rejection of 80% with an ethanol permeance of 3.3 L/(m^2.h.bar), whereas the DCX and DBB crosslinked membranes displayed RB rejection of 97% and 95%, respectively, with an ethanol permeance of about 2.4 L/(m^2.h.bar). On the other hand, after modification with SCA4, the RB rejection of the membrane reached almost 99%, with an ethanol permeance of 1.8 L/(m^2.h.bar). Similar trends were observed for other dye solutes (e.g., RBB (MW 626.54 g/mol) and MO (MW 327.33 g/mol)) (Figs. 4.8b & 6c). The DCX-SCA4 membrane exhibited a higher RBB rejection (97%) with ethanol permeance of 1.9 L/(m^2.h.bar), while DBB-SCA4 showed 93% rejection with 2.0 L/(m^2.h.bar) of ethanol permeance. DCX and DBB crosslinked membranes rejected 91% and 88% of RBB, with ethanol permeance at 2.7 and 3.0 L/(m^2.h.bar), respectively. The pristine membrane had the lowest RBB rejection (66%) but the highest ethanol permeance (3.8 L/(m^2.h.bar)). When the dye molecular weight was reduced (e.g., MO), rejection declined significantly for P-PBI and crosslinked membranes, except for SCA4-modified membranes, which demonstrated higher rejection of MO in ethanol nanofiltration solvent. Among all the studied membranes, the SCA4-modified membranes showed the highest rejection with a decent ethanol permeance. The good rejection of the SCA4 membranes is derived from the bowl-like shape and small cavity opening of SCA4, which directly provides a size-sieving effect in rejecting molecules greater than their intrinsic cavity [78, 115].

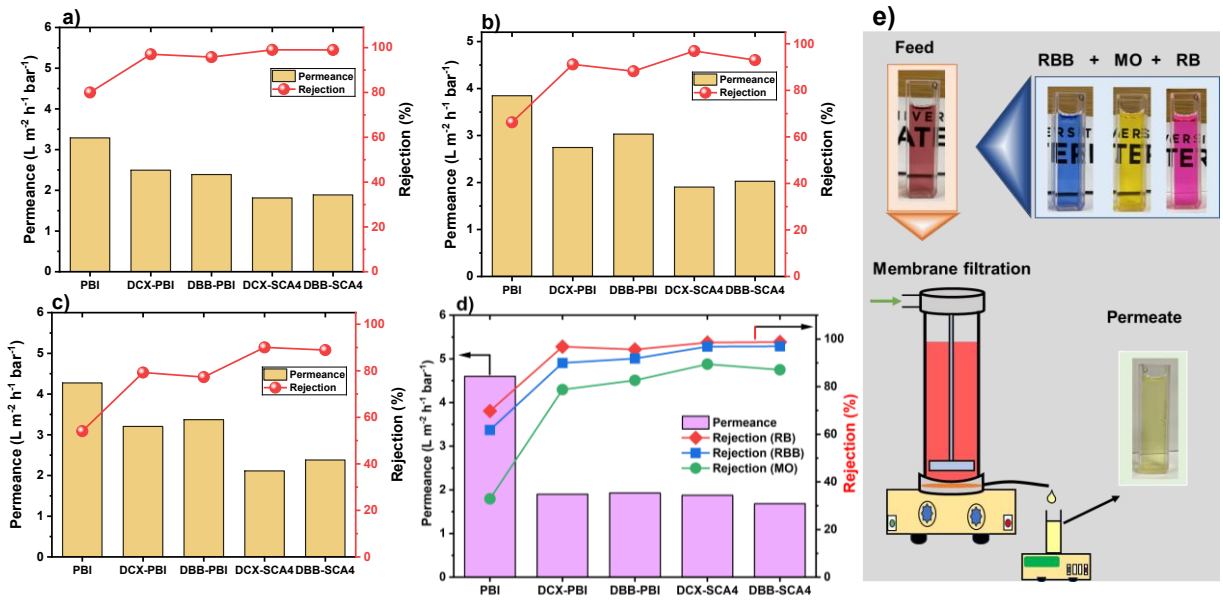


Figure 4.8. (a) Rejection of Rose Bengal, (b) Remazol brilliant blue, (c) Methyl orange in ethanol (Feed solution = 50 ppm). (d) Mixed dye solution filtered through pristine, crosslinked, and SCA4-modified membranes (Feed solution each dye = 20 ppm, temperature = 22 ± 1 ºC, pressure = 8 bar). (e) Pictures of the mixed feed and permeate solution.

4.3.3. Mixed solutes separation

Mixed dye nanofiltration tests were conducted to evaluate the molecular sieving capability of the crosslinked and SCA4-modified membranes. The three dyes were mixed in ethanol at a concentration of 20 ppm each. The feed solution was dark red. After filtration, the permeate was light yellow, matching the colour of MO (Fig. 4.8e). As shown in Figure 4.8(d), the DCX-SCA4 membrane showed a dye rejection of 99% (RB), 97% (RBB) and 90% (MO) with ethanol permeance of 1.8 L/(m^2.h.bar), whereas the DCX crosslinked membrane without SCA4 modification displayed a lower rejection (i.e., 97% (RB), 89% (RBB) and 78% (MO)). The DBB crosslinked membrane exhibited a lower rejection in the mixed solute test, whereas a significantly higher rejection was achieved after modification with SCA4 (Fig. 4.8d). The pristine PBI membrane rejected only 69% (RB), 61% (RBB), and 32% (MO) from the mixed dye solutions. It appears that the SCA4-modified membrane can selectively separate small solute molecules greater than the open cavity of SCA4 (~3 Å) from organic solvents.

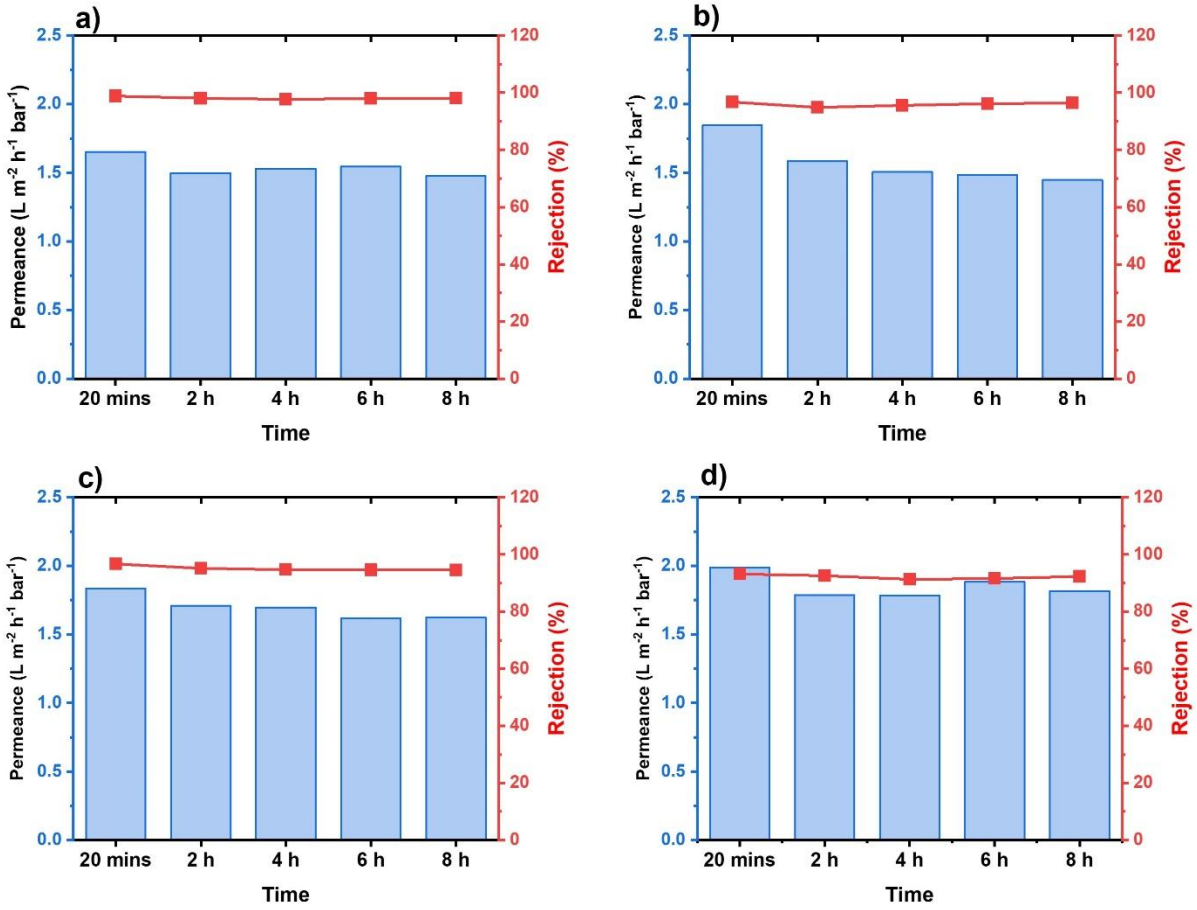


Figure 4.9. The separation performance for dye rejection from ethanol. DCX-SCA4 membrane: (a) Rose Bengal and (b) Remazol brilliant blue. DBB-SCA4 membrane: (c) Rose Bengal and (d) Remazol brilliant blue. Feed solution 50 ppm, temperature 22 ºC, pressure 8 bar.

4.3.4. Membrane durability

The ability of OSN membranes to withstand harsh organic solvents is crucial for their long-term performance and durability. Therefore, OSN was conducted continuously with the SCA4-modified membranes using 50 ppm of RB or RBB in ethanol as a model feed at an operating pressure of 8 bar (Fig. 4.9). Before each experiment, the membranes were compacted with deionized water at 8 bars for 1 h, and then the solvent solution was charged to the filtration unit. The permeate samples collected were intermittently sent back to the feed, and the feed concentration was largely constant throughout the experiment. Figure 4.9 shows that no considerable decrease in membrane permeance or rejection was observed, confirming that the SCA4-modified membranes maintained

consistent performance during an extended period of operation. Both SCA4-modified membranes showed higher rejection to low molecular weight solute (MO, MW = 327 g/mol) and similar permeance to ethanol compared to other OSN membranes reported in the literature (Fig. 4.10)

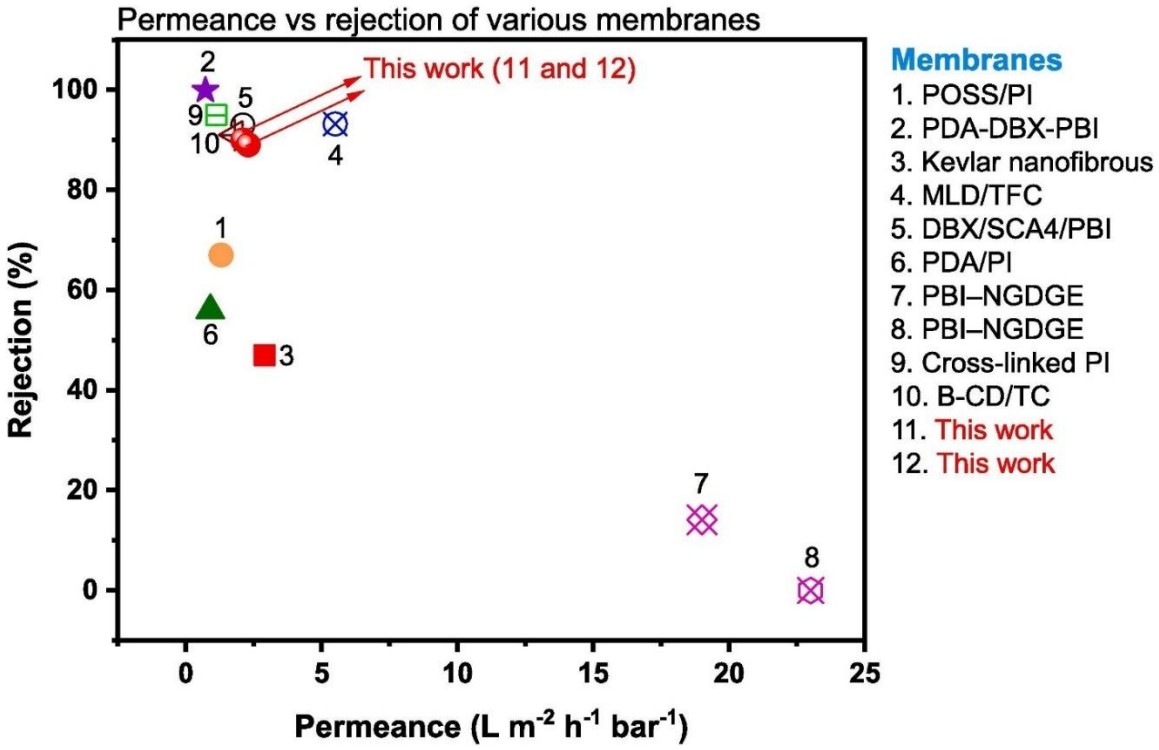


Figure 4.10. Comparison of permeance (solvent ethanol) and rejection (MO, MW 327.33 g/mol) of this work with other membranes reported in the literature. 1. POSS/PI [171]; 2. PDA-DBX-PBI [191]; 3. Kevlar nanofibrous [172]; 4. MLD/TFC [173]; 5. DBX/SCA4/PBI [1]; 6.PDA/PI [154]; 7. PBI–NGDGE [117]; 8. PBI–NGDGE [117]; 9. Crosslinked PI [192]; 10. B-CD/TC [193].

4.4. Conclusions

In this chapter, solvent-resistant PBI membranes with different separation characteristics were prepared using two crosslinkers with distinct molecular structures, namely aromatic DCX and aliphatic DBB. The results showed that crosslinker structure strongly influenced chain packing density, pore size, and chemical stability. While pristine PBI membranes disintegrated in harsh solvents such as NMP and DMAc, DBB-crosslinked membranes showed only slight dissolution, whereas DCX-crosslinked membranes remained stable in all tested solvents. Modification of the crosslinked membranes with SCA4 further reduced the effective pore size and improved rejection

of lower-molecular-weight solutes. Among the fabricated membranes, DCX-SCA4 exhibited the smallest mean pore size and the highest rejection toward low-molecular-weight dyes while maintaining stable OSN performance over extended operation. Overall, this chapter demonstrates that combining crosslinker-structure control with supramolecular modification is an effective strategy for tailoring the pore structure, chemical resistance, and separation performance of PBI-based OSN membranes.

This chapter demonstrated improved pore-size control, chemical resistance, and enhanced separation performance by tuning the membrane structure. Since the crosslinker influences membrane performance, Chapter 5 investigates TGIC as a multifunctional crosslinker for constructing a more chemically stable three-dimensional PBI network.

Chapter 5

Triglycidyl isocyanurate crosslinked PBI membranes for solvent-resistant and extreme pH nanofiltration

**** This chapter is based on the results of a published paper as outlined in the statement of contributions**.*

The results of Chapters 3 and 4 demonstrated that crosslinking plays a critical role in improving the stability and separation performance of PBI membranes. Since it is clear that crosslinker size and structure play a crucial role in designing membranes with distinct separation performance and chemical resistance, this chapter uses a multifunctional crosslinker capable of bridging multiple PBI chains and investigates its influence on membrane performance. Therefore, we report a novel chemically stable PBI membrane produced by covalent crosslinking with triglycidyl isocyanurate (TGIC) for use in OSN and extremely acidic and alkaline conditions. TGIC, a trifunctional epoxy resin, acted as a post-crosslinker by reacting with the N-H groups in the imidazole ring of PBI and forming covalent bonds. The chemical and physical changes in the membrane due to TGIC crosslinking were systematically characterized, confirming the successful crosslinking. The resulting membranes showed excellent OSN performance, achieving near-complete rejection of high molecular weight dyes (e.g., RB and RBB) with permeance comparable to or exceeding previously reported membranes. Importantly, the X-PBI membranes also retained their structural integrity under extremely acidic and alkaline conditions. These results demonstrate that TGIC is an effective crosslinker for fabricating chemically stable PBI membranes suitable for OSN and extreme pH nanofiltration.

5.1. Experimental Methods

5.1.1. Materials

Polybenzimidazole (Celazole S26, 26 wt% in DMAc, stabilize with 1.5 wt% lithium chloride) was provided by PBI Performance Products Inc. Polypropylene (PP) nonwoven backing (Novatexx 2471) was generously supplied by Freudenberg Filtration Technologies Inc. HPLC grade ethanol (EtOH), acetonitrile (methyl cyanide, MeCN), acetone, methanol (MeOH), isopropanol (IPA), n-

hexane, N,N-dimethylacetamide (DMAc), N-methyl-2-pyrrolidone (NMP), N,N-dimethylformamide (DMF), dimethyl sulfoxide (DMSO), hydrochloric acid (HCl, 37 wt%), sulfuric acid (H_2SO_4, 98%), acetic acid (99%) and sodium hydroxide (NaOH) were all purchased from Sigma Aldrich. Rose Bengal (RB, MW 1019.64 g/mol), Brillant Blue R (MW, 858.97 g/mol), Remazol Brilliant Blue (RBB, MW 626.53 g/mol), Allura Red AC (MW, 496.42 g/mol), Methyl Orange (MO, MW 327.33 g/mol), N,N-dimethyl-4-nitroaniline (DMNA, MW 166.18 g/mol), and TGIC were obtained from Thermo Scientific Chemicals. The dyes were used as model solutes to determine the membrane rejection capability.

5.1.2. Membrane fabrication

Asymmetric PBI membranes were prepared by the phase inversion method described in Chapter 3. After phase inversion, the resulting pristine PBI (denoted as P-PBI) membranes were rinsed and stored in a 50:50 acetonitrile/water solution for further experiments. Crosslinking of the membranes was performed following the procedure described by Valtcheva et al. [161] except that a 2 wt% TGIC solution in acetonitrile was used to crosslink PBI. The pristine PBI (P-PBI) membranes were immersed in the TGIC solution at 80 ºC for 24 h under reflux and continuous stirring for crosslinking. The crosslinked PBI membrane (denoted as X-PBI) was thoroughly rinsed and stored in a 50:50 acetonitrile/water solution for further use (see Appendix).

5.1.3. Characterization

Fourier transform infrared (FTIR) spectroscopy of pristine and crosslinked membranes was performed with a Thermo Nicolet 6700 ATR-FTIR spectrometer in ATR mode in the wavelength range of 500 to 4000 cm^{-1} to investigate the chemical changes in the membranes. For the IR analysis, the top layer of PBI was peeled off from the substrate and air dried in a fume hood for 12 h to remove moisture and avoid interference from the PP substrate. X-ray Photoelectron Spectroscopy (XPS) analysis of P-PBI and X-PBI membranes was performed with a Thermo Scientific Aluminum Kα XPS spectrometer (Nexsa G2 Surface Analysis System). The samples were air-dried for 24 hours before analysis. X-ray diffraction (XRD) patterns were obtained in the scanning range of 5-45° using a Rigaku Miniflex II X-ray diffractometer to study the structural changes of the membrane induced by the crosslinker. For XRD analysis, the PBI layer peeled off from the PP substrate was ground into powder to observe PBI crosslinking, thereby eliminating

substrate interference. Scanning electron microscopy (SEM) using a Tescan VEGA TS-5130 was employed to study the surface and cross-sectional morphologies of both pristine and crosslinked membranes. For the SEM analysis, the samples were freeze-fractured in liquid nitrogen and then sputter-coated with gold using a Polaron SEM coater. Atomic force microscopy (AFM) was performed using a Nanoscope MultiMode AFM (Veeco) with NP-STT10 silicon tips (Bruker, USA) under ambient conditions. Topography images were acquired in tapping mode and analyzed with Gwyddion software. The hydrophilicity of both pristine and crosslinked membranes was assessed by measuring the water contact angles (WCA) with a contact angle goniometer from Tantec Inc. A total of six different measurements of each membrane were taken, and the values were averaged. Thermogravimetric analysis (TGA) (TA instrument Q600) was used to study the thermal stability and degree of crosslinking of the membrane. TGA was performed at a heating rate of 10 °C/min under a nitrogen environment. The degree of PBI crosslinking (α) was estimated from the weight losses of the pristine and crosslinked membranes when heated from 200 to 500 °C using equation (1) [183]:

$$\alpha = \frac{W_1/M_{TGIC}}{W_0/M_{PBI}} \quad (1)$$

where W_1 and W_0 are the weight loss of TGIC and the weight of pristine PBI, respectively, and M_{PBI} and M_{TGIC} are the molecular weights of the PBI repeating unit (308 g/mol) and TGIC (297 g/mol). The chemical stability of the membranes was evaluated by immersing membrane samples in harsh solvents, and concentrated acids, including DMAc, NMP, DMSO, DMF, HCl (37%), acetic acid (99%), and sulfuric acid (H_2SO_4, 98%). For the weight of membranes dissolved in these solvents, a separate experiment was performed by peeling off the top PBI layer from the support membrane.

5.1.4. Nanofiltration Performance

The performance of the pristine and crosslinked membranes was evaluated using the dead-end filtration setup described in Chapter 3 (Fig. 3.1), with an effective membrane area of 12.5 cm². Membrane permeance was measured using a series of organic solvents, including IPA, EtOH, MeOH, MeCN, acetone, DMF, and hexane, and membrane rejection was evaluated using dye solutes of different molecular weights. Additional tests were performed under extreme pH

conditions (pH 1 ± 0.2 and 14 ± 0.2) to assess membrane stability and separation performance in highly acidic and alkaline environments. The properties of the organic solvents can be found in Table 3.4 and Table 4.1, Chapter 3&4. The dyes with different molecular weights and properties (including RB, RBB, MO, and DMNA (Table 3.3, Chapter 3) were used as model solutes for the nanofiltration tests. To calculate the MWCO of the membrane, additional tests with two dyes, Allura Red AC and Brilliant Blue R, were conducted in ethanol. For both OSN and extreme pH nanofiltration, a dye concentration of 50 ppm was used. To prepare solutions at pH 14 and pH 1, NaOH pellets were dissolved in deionized water (DI), and concentrated HCl was diluted in DI water. The pH was adjusted using a 0.1 M solution of HCl or NaOH and was measured with a digital pH meter. After dissolving the dyes, the pH was measured again with a pH meter and adjusted as necessary. All experiments were performed at room temperature (22 °C) and at an operating pressure of 6 bar gauge, unless stated otherwise. Before each test, the membrane was preconditioned with deionized water at the same operating pressure. The solvent permeance and solute rejection reported were the average measurements with at least two membrane samples (see Appendix). They were calculated using equations (2) and (3), respectively:

$$P = \frac{V}{A \times t \times \Delta P} \tag{2}$$

$$R = \left(1 - \frac{C_p}{C_f}\right) \times 100\% \tag{3}$$

where P is permeance [L/(m².h.bar)], V is the volume of solvent permeate through the membrane over time t (h) at an applied transmembrane pressure ΔP (bar), and A is the effective membrane area for permeation (m²). C_p and C_f are the dye concentrations in the permeate and feed solution, respectively, and they were measured using a UV–Vis spectrophotometer (Shimadzu UV-1900i). The permeate samples were recycled back to the filtration cell to maintain a constant concentration throughout the experiment (Fig. 3.1, Chapter 3).

5.2. Results and Discussion

5.2.1. Membrane characterization

The TGIC-crosslinked PBI membranes were fabricated through a covalent reaction between the epoxide groups of TGIC and the –NH groups of PBI. The chemical structure of the membrane after crosslinking is shown in Figure 5.1(a). TGIC contains three reactive epoxide groups that can undergo nucleophilic ring-opening reactions with the secondary amine groups of PBI. The reaction involves the opening of the epoxide rings in TGIC, which simultaneously reacts with the -NH groups of the imidazole rings, forming a covalent bond between the opened epoxy sites of TGIC and the -NH groups of PBI chains, as shown in Figure 5.1(a). TGIC serves as a tri-functional crosslinker, forming a rigid three-dimensional network that endows the PBI membrane with improved chemical resistance. The chemical stability of the X-PBI membranes was confirmed by exposure to strong organic solvents (DMAc, DMSO, NMP, and DMF) and acids, as illustrated in Figure 5.1(b-c). The un-crosslinked pristine PBI membrane (P-PBI) was almost completely dissolved in all these organic solvents and concentrated H_2SO_4 after 24 h (Fig. 5.1b). In contrast, the crosslinked membrane (X-PBI) retained its integrity in all the strong solvents and acids, maintaining clear solvents (Fig. 5.1c). The dissolution test revealed that the crosslinked membrane retained about 99% of its mass in these solvents and acids, while the P-PBI membrane was completely dissolved, except in HCl and acetic acid (Table 5.1). The long-term chemical stability of the X-PBI membrane was further tested by soaking the membrane pieces in DMAc and NMP (Fig. 5.1d); after one month, the solvents remained clear, and the X-PBI membrane still retained its structural integrity. This confirms the excellent chemical stability of the X-PBI membrane compared to the pristine membrane.

Table 5.1. Dissolution of P-PBI and X-PBI membranes in harsh solvents.

Solvents	P-PBI (%) [a]	X-PBI (%)
DMAc	0	97 ± 2
NMP	0	98 ± 1
DMSO	0	99 ± 1
DMF	0	99 ± 1
H_2SO_4 (98%)	0	99 ± 1

HCl (37%)	98 ± 1	99 ± 1
Acetic Acid (99%)	98 ± 1	99 ± 1

[a] (%) is the membrane left after 24 h. The top PBI layer was peeled off the support polypropylene, dried, and the weight was recorded. It was then immersed in solvents for 24 hours, dried again, and weighed once more. The mass percentage was subsequently calculated.

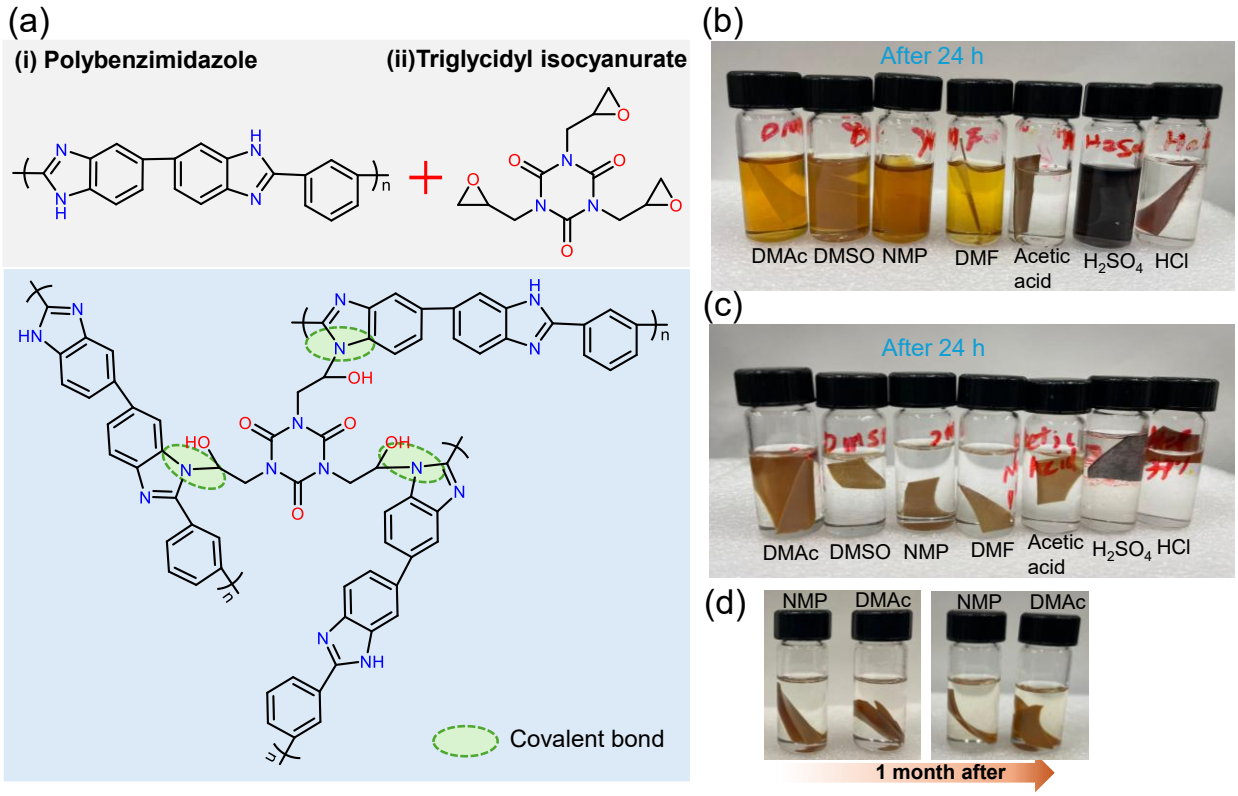


Figure 5.1. (a) Illustration of PBI crosslinking with TGIC. (b) Images of P-PBI membrane (the leftover membrane is the polypropylene substrate, and the PBI top layer is completely dissolved except for acetic acid and HCl, which did not dissolve the P-PBI) and (c) X-PBI membrane after 24 h of soaking in strong organic solvents and acids. (d) Images of the X-PBI membrane immersed in NMP and DMAc on day 1 (left) and after 1 month (right).

The chemical changes induced by the TGIC crosslinker were examined using ATR-FTIR. Figure 5.2 presents the IR spectra of P-PBI and X-PBI membranes. The broad characteristic peaks from 3600 to 3000 cm^{-1} correspond to the N-H stretching of the imidazole ring [10, 161]. The P-PBI showed a prominent broad peak in this region, which was attributed to the N-H stretching

vibrations of secondary amines. The intensity of this peak is reduced in X-PBI, indicating fewer free N-H groups due to chemical crosslinking with TGIC [117]. The X-PBI membranes showed a weak peak in the range of 3000 to 2800 cm^{-1} that was assigned to aliphatic or aromatic C-H stretching vibrations. This further suggests the chemical crosslinking of PBI with TGIC [115, 117, 161]. A significant peak at 1689 cm^{-1} attributed to the C=O groups in TGIC appeared in the spectra of X-PBI, proving a successful crosslinking reaction between TGIC and imidazole rings of PBI [194, 195]. The peak at 1539 cm^{-1} became sharper in X-PBI, suggesting increased C-N interactions or newly formed imide linkages due to crosslinking. The characteristic peak at 763 cm^{-1} in the spectra of both P-PBI and X-PBI was associated with the aromatic C-H bending [161].

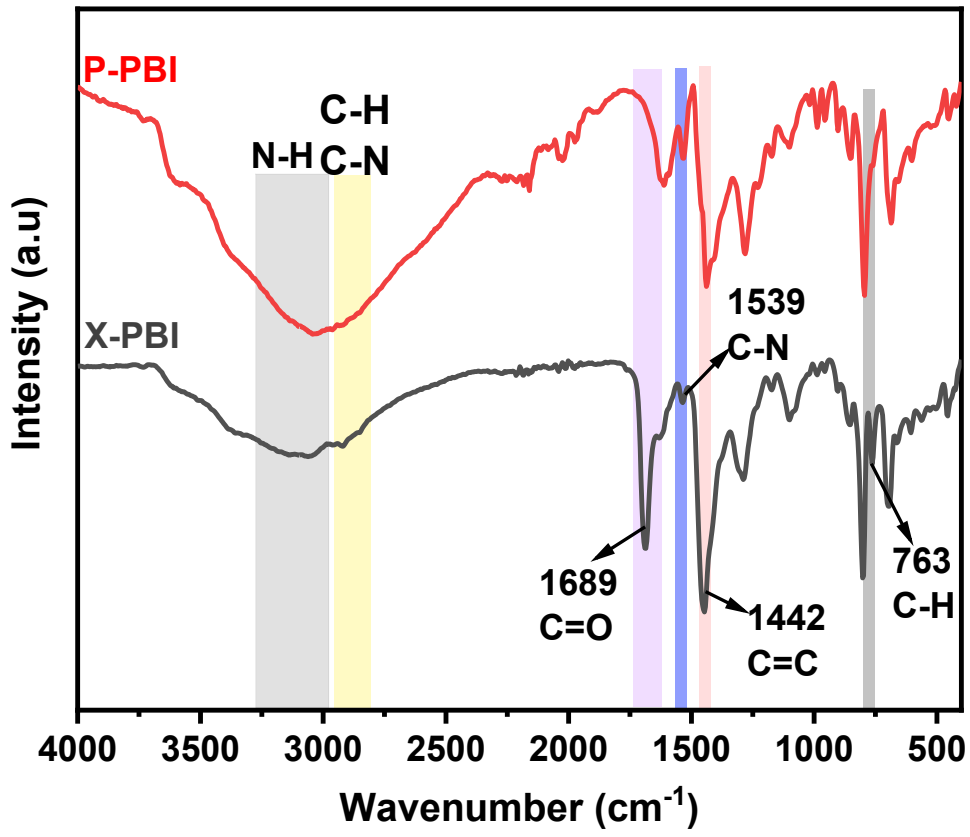


Figure 5.2. FTIR spectra of P-PBI and X-PBI, showing characteristic absorption peaks corresponding to functional groups.

Table 5.2. XPS atomic composition (At%) carbon (C1s), nitrogen (N1s), and oxygen (O1s) of the pristine and crosslinked membranes.

Elements (At%)	P-PBI	X-PBI
C1s	80.53	68.98
N1s	10.80	13.18
O1s	8.67	17.84

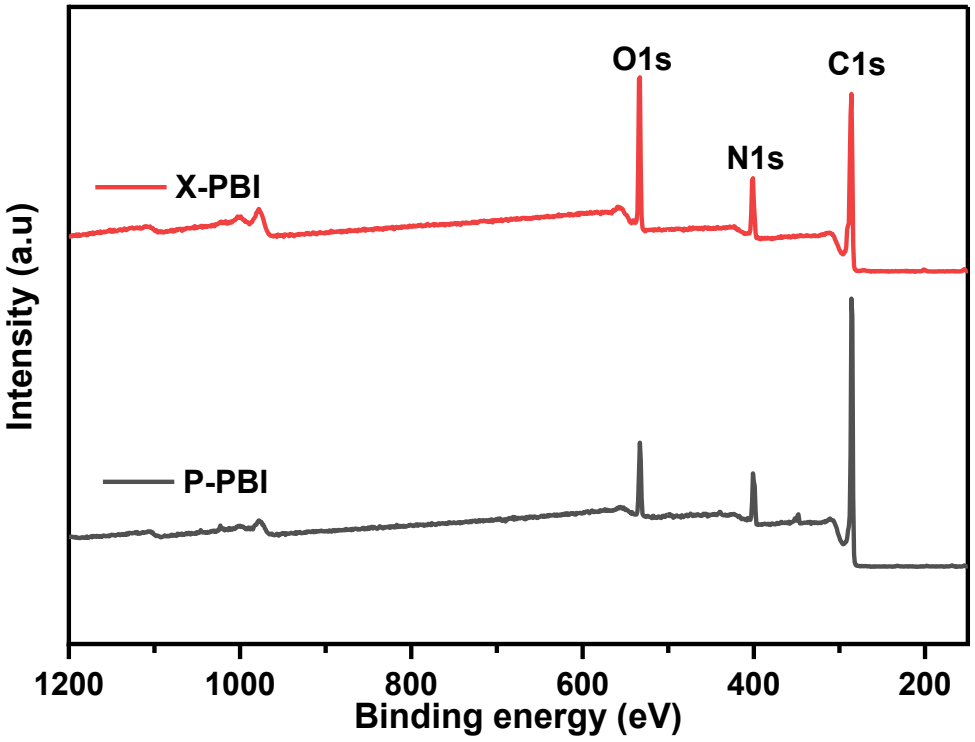


Figure 5.3. XPS spectra of P-PBI and X-PBI membranes.

Similarly, the surface chemistry changes after TGIC crosslinking were also measured by XPS. Figure 5.3 shows the survey spectra of P-PBI and X-PBI membranes, confirming the presence of carbon (C), nitrogen (N), and oxygen (O) as the major elements. Pristine PBI has no O in the structure; the O contents are likely from environmental moisture or surface air contamination. However, as shown in Table 5.2, the oxygen content (O1s) after crosslinking increased from 8.67% (P-PBI) to 17.84% (X-PBI), as expected due to the introduction of oxygen-rich TGIC crosslinker.

While the N1s content slightly increased from 10.80% to 13.18% after crosslinking with TGIC. This increase in O and N contents and decrease in C are consistent with successful crosslinking through the epoxy groups of TGIC reacting with the nucleophilic imidazole –NH– groups of PBI. Figure 5.4(a&b) illustrates the N1s narrow scan spectra of the membranes. In the P-PBI membrane, two main peaks, the –NH– group (secondary amine) and the =N– group (Pyridine type N), were observed at ~399.8 eV and ~398.5 eV, similar to other reported studies [183, 196]. After crosslinking with TGIC, an additional peak at ~400.8 eV was observed, which can be the newly formed N–C/O linkages. The intensity of –NH– peaks was also decreased, suggesting that the imidazole –NH– groups participated in the nucleophilic ring-opening of TGIC epoxides. The narrow C1s spectra scan showed similar changes (Fig. 5.4c&d). The P-PBI showed two main characteristic peaks of C-C and C-N at ~284.6 eV and ~285.7 eV [10]. In X-PBI, a new C-O peak at ~287.8 eV appeared, and the relative intensity of C-N increased. This increase is attributed to both the formation of covalent C–N bonds between TGIC epoxides and PBI amines and the incorporation of the rigid triazine core of TGIC, which is rich in aromatic C-N linkages. These chemical shifts and compositional changes further confirmed the successful crosslinking and the formation of covalent bonds between the TGIC epoxy and PBI imidazole functional groups.

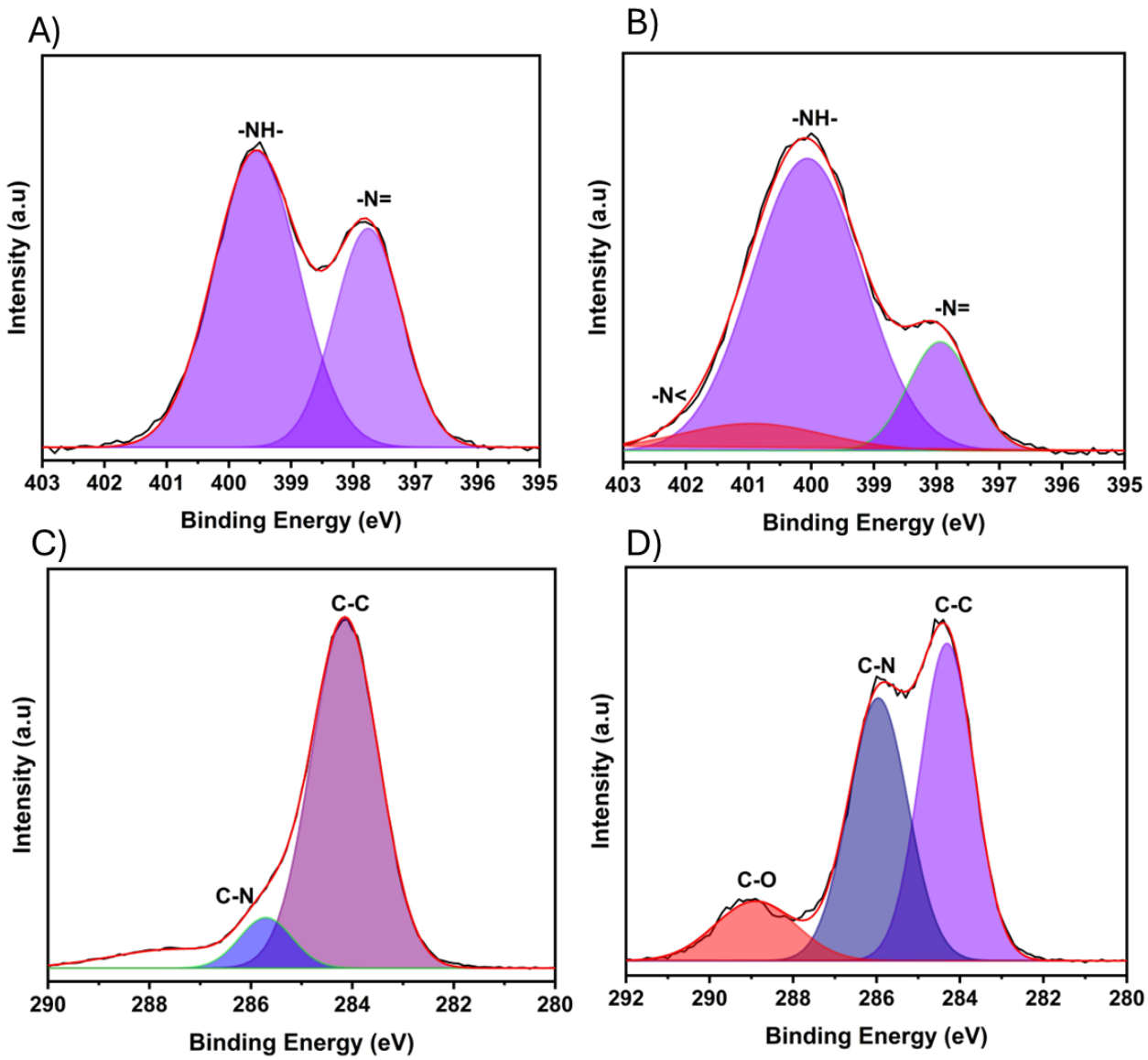


Figure 5.4. N1s XPS narrow scans of P-PBI (a) and X-PBI (b) membranes. C1s XPS narrow scans of P-PBI (c) and X-PBI (d) membranes.

The XRD patterns of the membranes are shown in Figure 5.5. The primary diffraction peaks of both membranes are centered around 19° and 25°, corresponding to the π-π stacking of aromatic polymer chains [10, 194]. However, the intensity and broadness of the peak in P-PBI were more significant than those observed with X-PBI, which indicated that X-PBI had a more amorphous structure. This is probably due to the crosslinker, which disrupted the ordered arrangement of the polymer chains, resulting in a more amorphous structure. The successful crosslinking was further confirmed by analyzing the thermomechanical properties of the pristine and crosslinked

membranes (Fig. 5.6). Both membranes showed a minor weight loss between 100 to 200 °C because of the evaporation of residual moisture and other volatile compounds [10, 194]. However, from 200 °C onward, P-PBI showed minimal weight loss, while X-PBI displayed a significant weight loss starting at around 250 °C. This indicated that X-PBI underwent thermal degradation, likely due to the crosslinker. After 400 °C, a pronounced weight loss was observed in X-PBI, which appeared to suggest that the structural modification of X-PBI due to TGIC began to decompose significantly. These results further proved the successful crosslinking of PBI with TGIC. The degree of crosslinking in X-PBI was estimated from the TGA data from 200 to 500 °C. There was a weight loss of 15.08% in X-PBI between 200 and 500 °C, which was primarily attributed to the TGIC crosslinker. The degree of crosslinking was calculated to be 0.17, a level of crosslinking that is typically enough to render the membrane chemically stable.

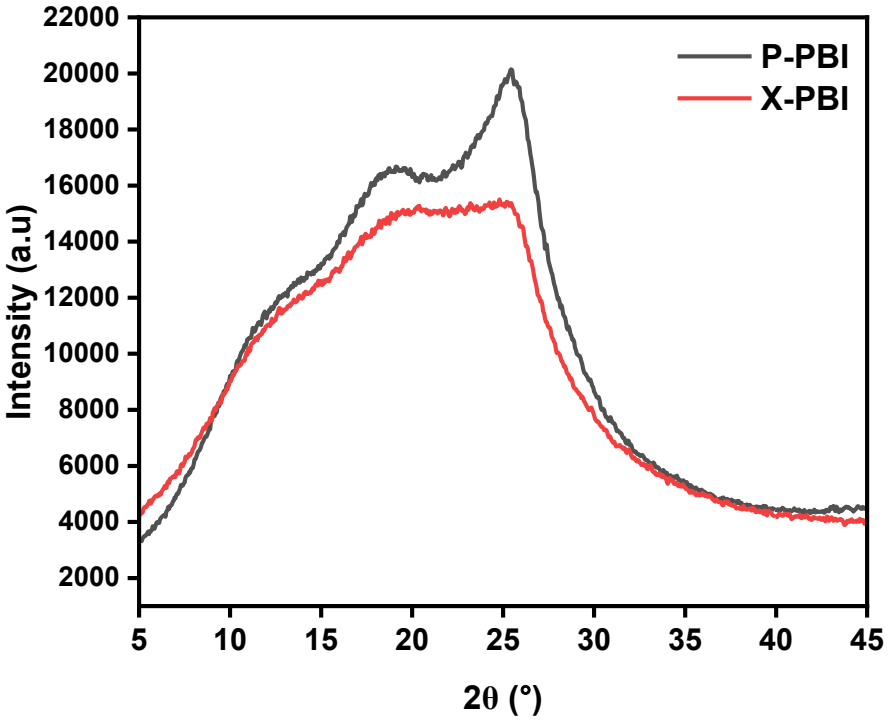


Figure 5.5. X-ray diffraction (XRD) patterns of P-PBI and X-PBI membranes.

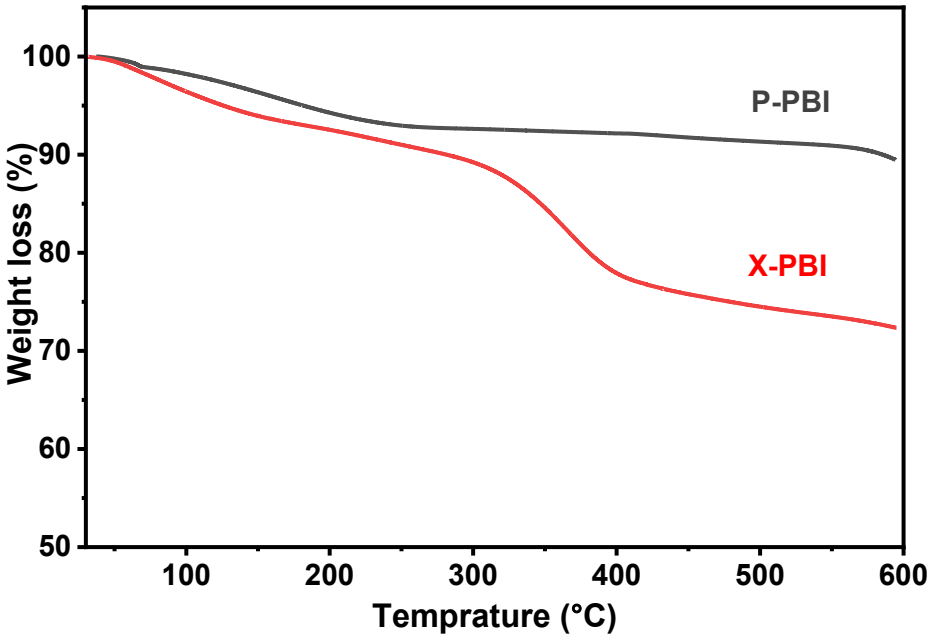


Figure 5.6. Thermogravimetric analysis (TGA) of P-PBI and X-PBI membranes, showing weight loss as a function of temperature.

Figure 5.7 presents the hydrophilicity of P-PBI and X-PBI membranes. The water contact angle (WCA) of P-PBI is approximately 61.2°. Upon crosslinking with TGIC, the WCA of the membrane decreased to around 53.8°. The decrease in WCA after crosslinking suggests enhanced surface hydrophilicity. This change is likely due to the introduction of -OH groups because of the epoxy ring opening during the reaction between TGIC and the PBI, as shown in Figure 5.1(a). Crosslinking can also alter the surface energy of the membrane by introducing hydrophilic groups, thus reducing the water contact angle.

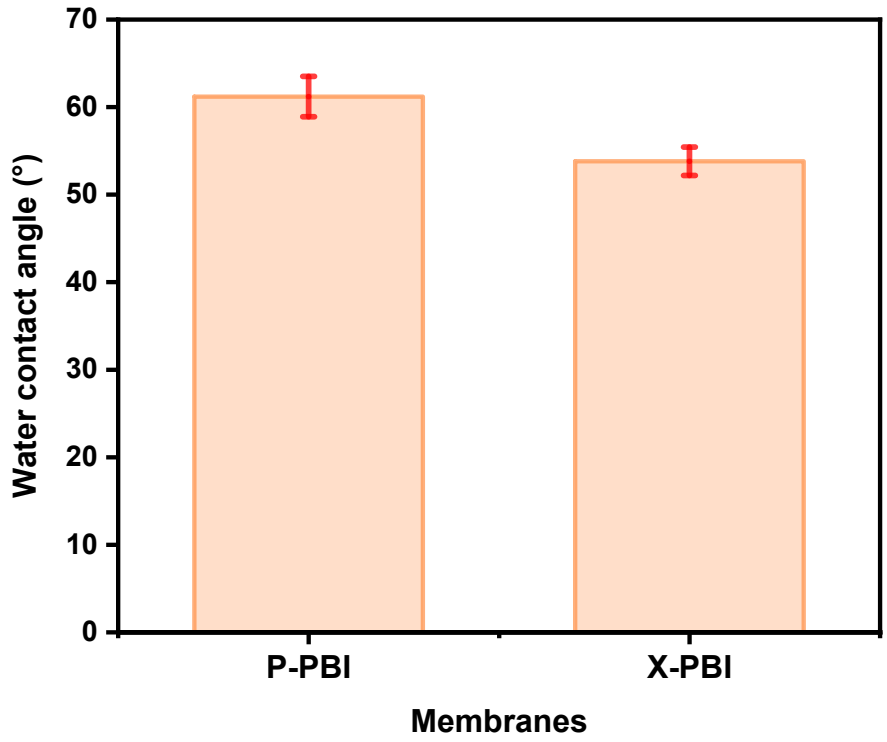


Figure 5.7. Water contact angle of P-PBI and X-PBI membranes, showing surface hydrophilicity.

Additionally, the morphologies of the P-PBI and X-PBI membranes were characterized with SEM and AFM (Fig. 5.8 & 5.9). The cross-sectional images of the membranes displayed a thin, dense skin layer and a porous substructure with interconnected macrovoids and finger-like pores, and there was irregularity in the macrovoid distribution, which is typical of a phase-separated structure (Fig. 5.8a-d) [163, 191]. In general, the X-PBI membrane had a denser, more compact structure than P-PBI, and the finger-like voids in X-PBI were less prominent. In addition, the top selective layer of X-PBI was thicker than P-PBI (Fig. 5.8c&d), which may be a result of expansion during the PBI crosslinking process. The tighter surface layer in X-PBI was due to the rearrangement of the polymer chains during the crosslinking reaction [183]. The top surface images of both pristine and crosslinked membranes are similar and homogeneous, with no visible defects on the membrane surface (Fig. 5.8e&f), which was desired for the nanofiltration applications. The 3D AFM images revealed that the X-PBI membrane has a smoother surface, with a root-mean-square (RMS) roughness (Rq) of 23.34 nm, compared to 31.97 nm for the pristine P-

PBI membrane (Fig. 5.9a&b). This reduction in surface roughness is consistent with the lower WCA observed for the crosslinked membrane, indicating enhanced surface uniformity and improved hydrophilicity.

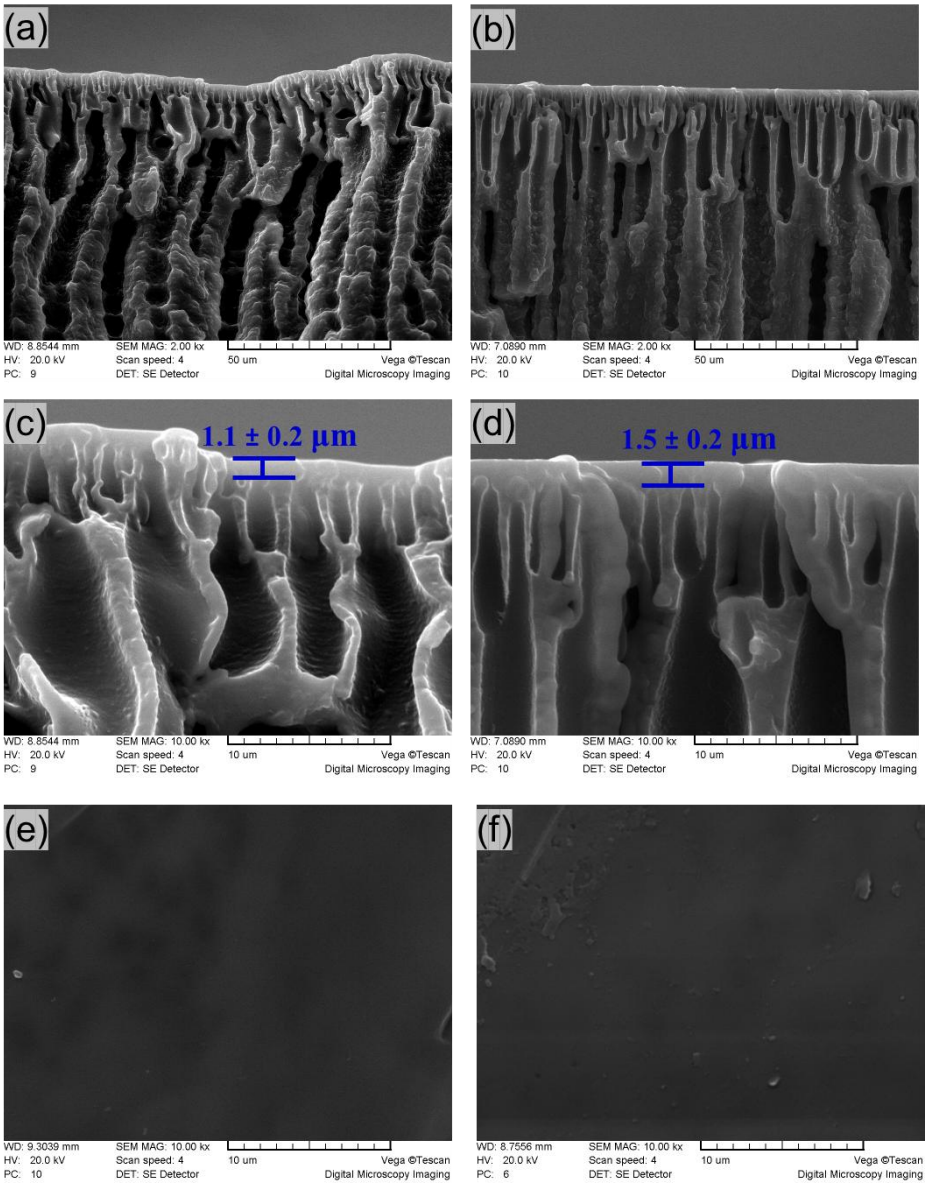


Figure 5.8. SEM images of the cross-sectional and surface morphologies of the P-PBI membrane (a,c & e) and X-PBI membrane (b, d & f).

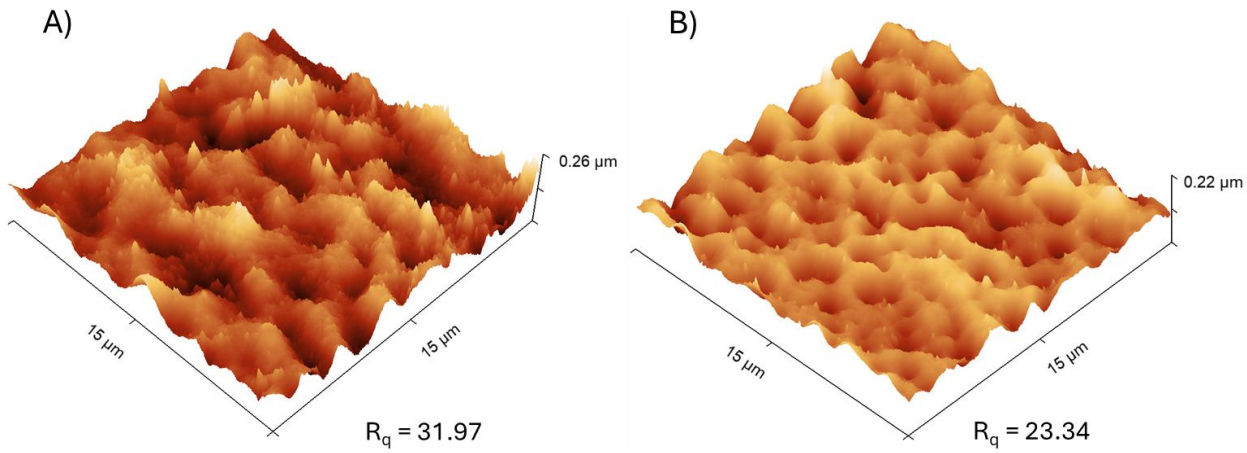


Figure 5.9. AFM 3D images of P-PBI (a) and X-PBI (b) with root-mean-square (RMS) roughness (Rq).

5.2.2. Membrane Performance

5.2.2.1. Organic solvent nanofiltration

The OSN performance of the membranes was evaluated in terms of solvent permeance and solute rejection. Organic solvents with different physicochemical properties were used to examine solvent transport behavior, and dye molecules of different molecular weights were used as model solutes to evaluate membrane selectivity. Mixed-solute experiments were also conducted to assess the fractionation capability of the X-PBI membrane.

Figure 5.10 shows the pure solvent permeance of the P-PBI and X-PBI membranes. The P-PBI membrane showed higher permeance to all the tested solvents than X-PBI, with the highest permeance of 53.4 L/(m^2.h.bar)) to MeCN and the lowest permeance of 6.1 L/(m^2.h.bar) to IPA. This trend was consistent with that reported for other OSN membranes [10, 161, 163]. After crosslinking with TGIC, the membrane (i.e., X-PBI) permeance to the organic solvents decreased. This was not unexpected, as crosslinking would result in a tighter and more rigid membrane structure. The X-PBI membrane displayed the highest permeance to MeCN at 11.5 L/(m^2.h.bar), followed by acetone 5.0 L/(m^2.h.bar), DMF 4.6 L/(m^2.h.bar), MeOH 4.4 L/(m^2.h.bar), hexane 3.5 L/(m^2.h.bar), EtOH 3.1 L/(m^2.h.bar), and IPA 1.1 L/(m^2.h.bar) (Fig. 5.10). The solvent properties had played a significant role in solvent permeation across the membrane. Generally, solvents with lower viscosities tend to permeate more easily through the membrane, leading to higher

permeance. Among the solvents tested, IPA had high viscosity and showed lower permeance, which was consistent with other OSN membranes reported in the literature [1, 115, 191, 197].

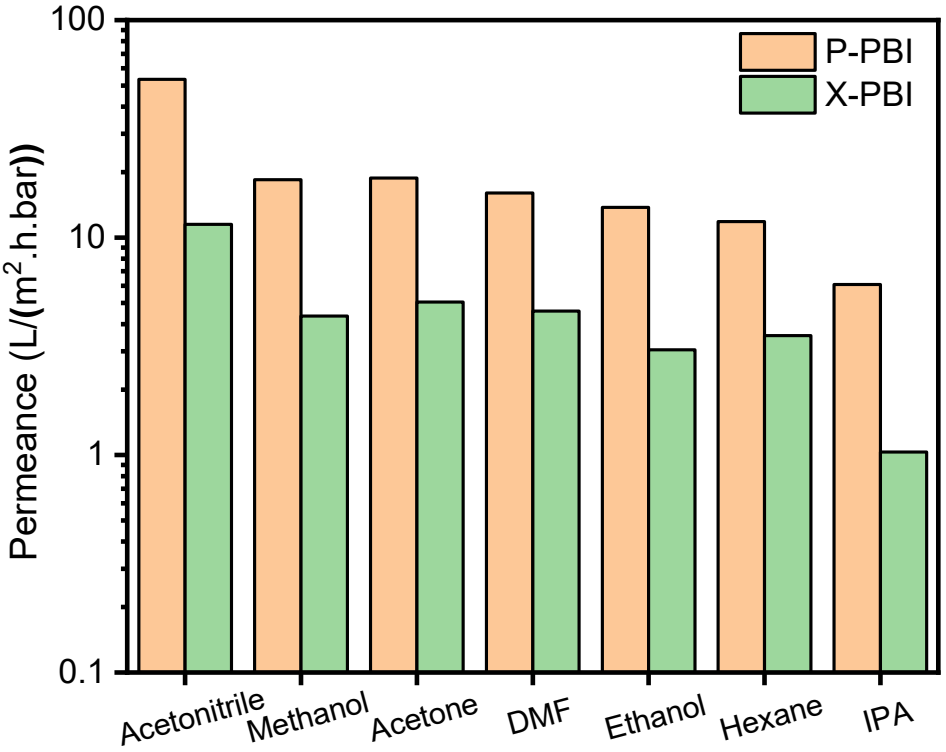


Figure 5.10. Pure solvents permeance of P-PBI and X-PBI membranes at 6 bars.

However, solvent viscosity was not the only factor affecting the permeance; the molecular size of the solvent and the solvent-membrane affinity were also important [198-200]. As shown in Figure 5.11(a), the solvent permeance of X-PBI membrane appeared to be well correlated to a lumped parameter of the solvent properties ($\delta_p/\eta d_m$), where δ_p, η and d_m are the solubility parameter for polarity, viscosity, and molar diameter. The relationship between pressure and permeance of the membrane was also investigated. It can be seen in Figure 5.11(b) that the permeance of the X-PBI membrane to pure ethanol increased linearly with applied pressure, up to a maximum of 8 bars. This strong linear relationship ($R^2 = 0.936$) suggests that the transport of solvent is mainly driven by pressure, which aligns with Darcy's law.

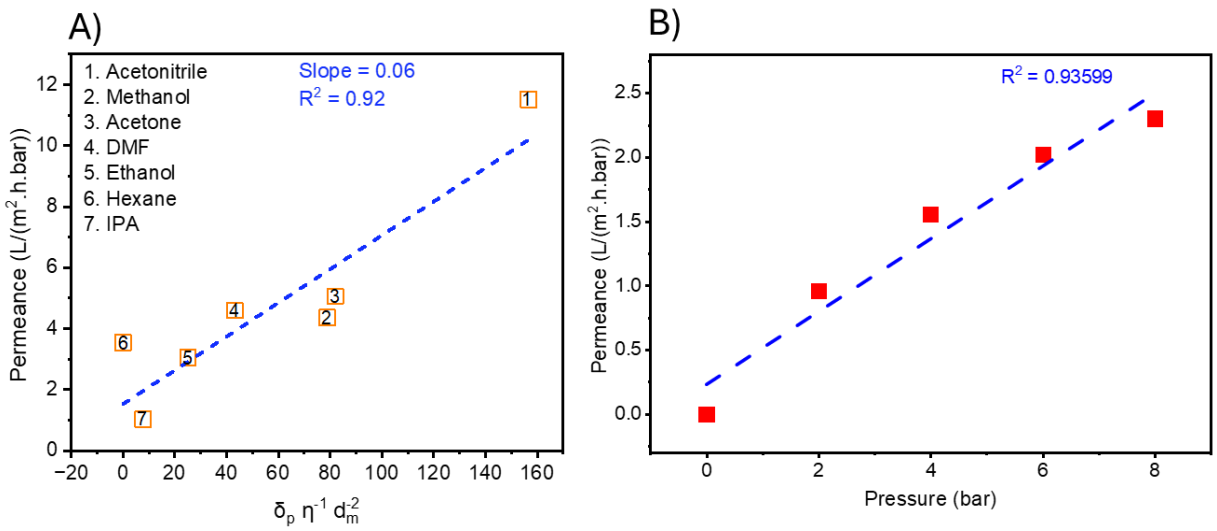


Figure 5.11. Solvent permeance through X-PBI membrane vs a lumped parameter for solvent properties (a). Solvent permeance as a function of the applied pressure (b).

The separation performance of the membrane was tested using ethanol solutions containing RB (MW = 1019.6 g/mol), RBB (MW = 626.5 g/mol), MO (MW = 327.3 g/mol), and DMNA (MW = 166.3 g/mol) as model solutes. The P-PBI membrane rejected 55% of RB, 67% of RBB, 42% MO, and almost no rejection of DMNA (Fig. 5.12a). Despite its relatively high permeability, the pristine P-PBI membrane lacked sufficient selectivity due to its relatively loose structure. On the other hand, the X-PBI membrane yielded near complete rejection (>98%) to the high molecular weight dyes (e.g., RB and RBB) and about 86% rejection to MO (Fig. 5.12b). The UV-vis absorption spectra of dye solutions before and after nanofiltration through the X-PBI membrane are shown in Figure 5.13. For the low-molecular-weight DMNA, to which the P-PBI membrane exhibited no rejection, a 13% rejection was achieved with the X-PBI membrane.

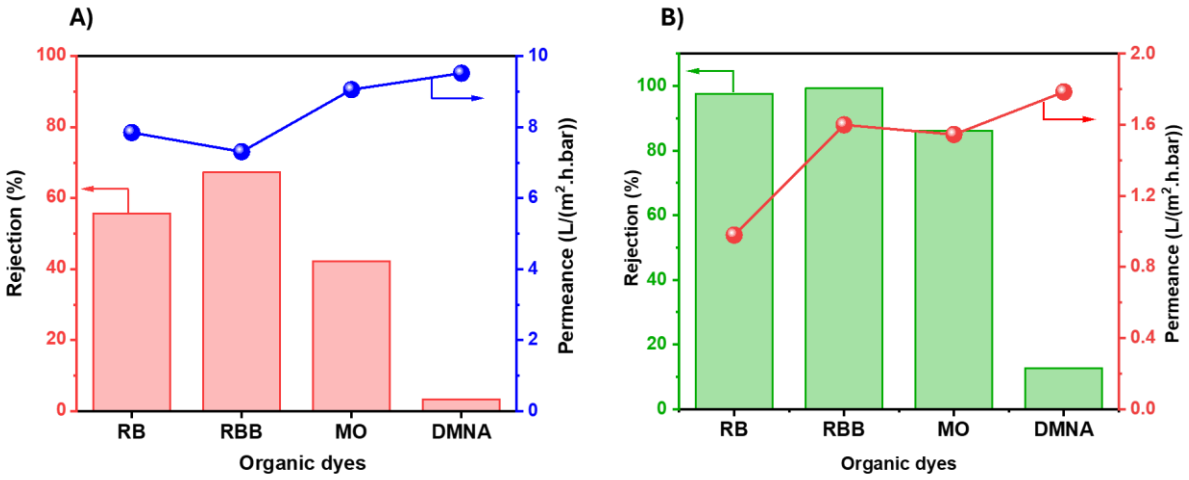


Figure 5.12. Dye rejection of the P-PBI membrane (a) and the X-PBI membrane (b) from ethanol solvent.

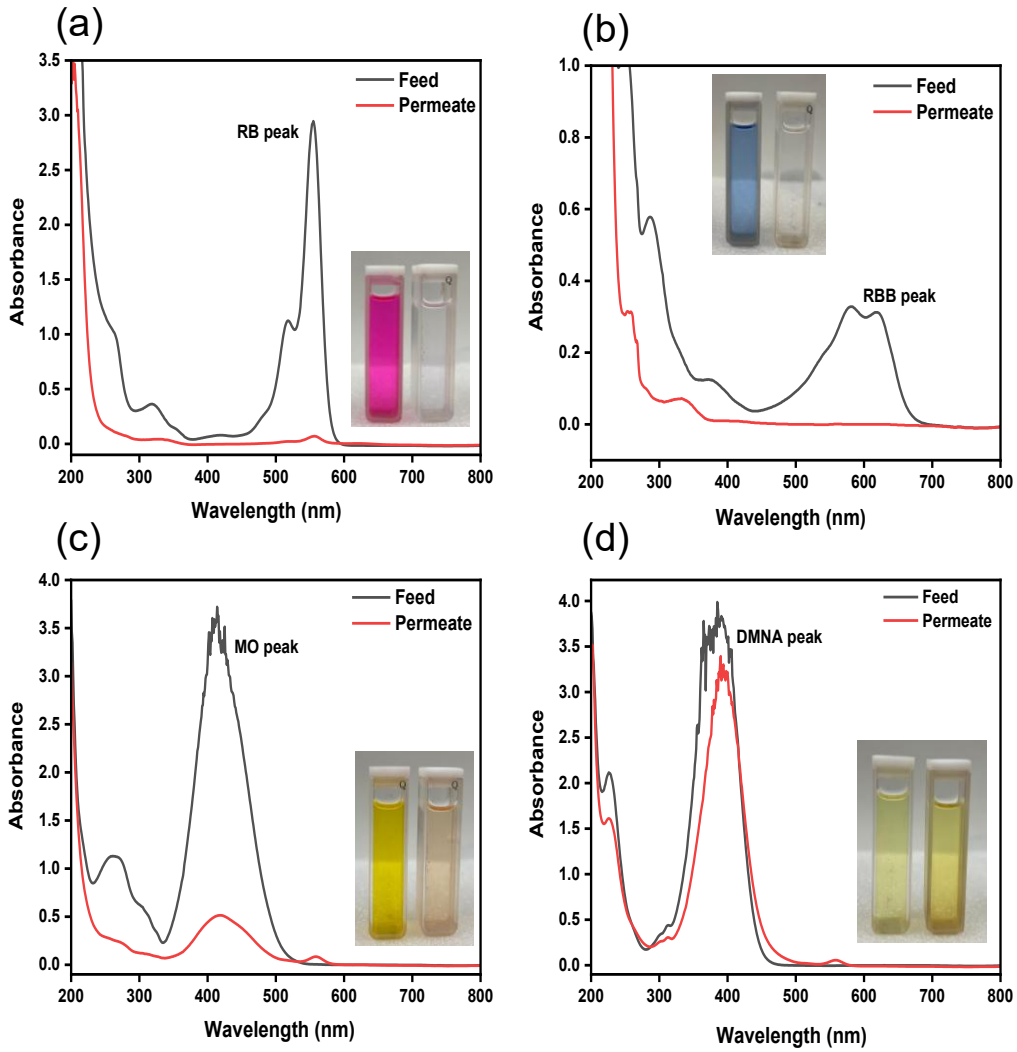


Figure 5.13. UV-vis absorption spectra of dye solutions before and after nanofiltration through the X-PBI membrane: (a) RB, (b) RBB, (c) MO, and (d) DMNA. Insets show the visual appearance of dye solutions before (left) and after (right) nanofiltration.

The rejection performance of the X-PBI membrane was also tested in DMF (Fig. 5.14). The membrane achieved about 94% of RB, 98% of RBB, 72% of MO, and nearly ~4% rejection of DMNA. When compared with ethanol, particularly for RB, the rejection in DMF was slightly lower (94% vs 98% in ethanol). This reduction can be attributed to the differences in solute-solvent-membrane interactions between DMF and ethanol. However, the difference was not pronounced, and the membrane was still able to reject about 94% of RB and 98% of RBB. The lower rejection of the X-PBI membrane to DMNA in both ethanol and DMF was not surprising in view of its much smaller molecular size (MW = 166 g/mol) than the other dyes. Based on the solute rejections, the molecular weight cut-off of the X-PBI membrane was estimated to be ca. 401 Da (Fig. 5.15). Solute dyes with molecular weights above this threshold (e.g., RB and RBB) demonstrated higher rejection due to size exclusion effects. In addition, electrostatic interactions may also have contributed slightly to the solute rejection, especially for charged dyes like RB and RBB, as the crosslinking introduced polar hydroxyl and ether groups from the TGIC ring-opening, which would influence the solute-membrane affinity in polar solvents such as ethanol. However, size exclusion appeared to remain the dominant mechanism for the rejection of high molecular weight dyes. The ethanol permeance of the X-PBI membrane was about 1 L/(m^2.h.bar) during retention of RB and over 1.6 L/(m²·h·bar) for retaining RBB, MO, and DMNA, while DMF permeance was about 2.5 L/(m²·h·bar) during RB, RBB, and MO filtration, and 3.6 L/(m²·h·bar) during DMNA. The higher permeance of DMF is consistent with its lower viscosity relative to ethanol. These results show the good nanofiltration performance of the X-PBI membrane, which effectively filtered ethanol and DMF while rejecting solutes with molecular weights above 401 Da.

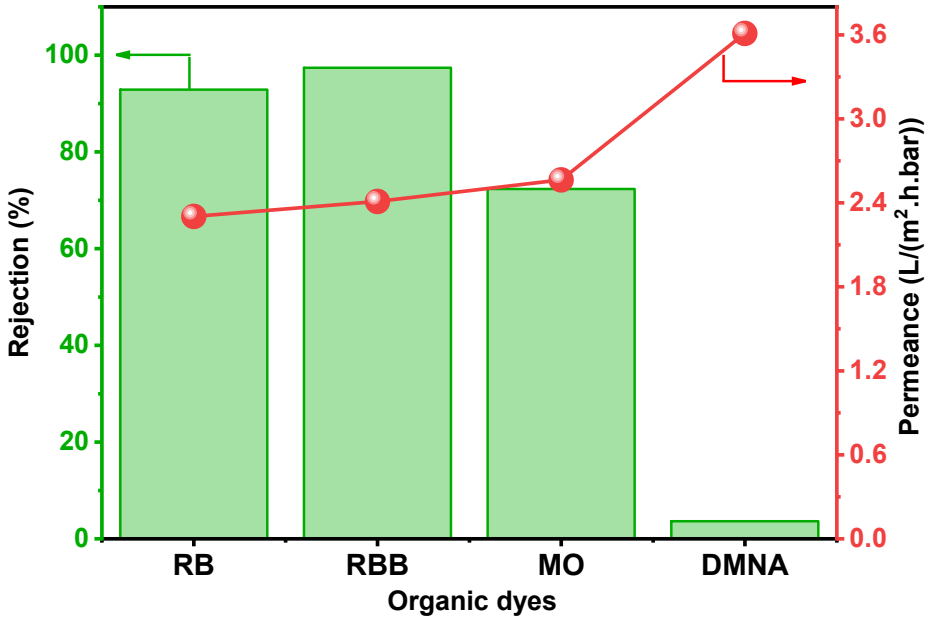


Figure 5.14. Dyes rejection of the X-PBI membrane from DMF solvent.

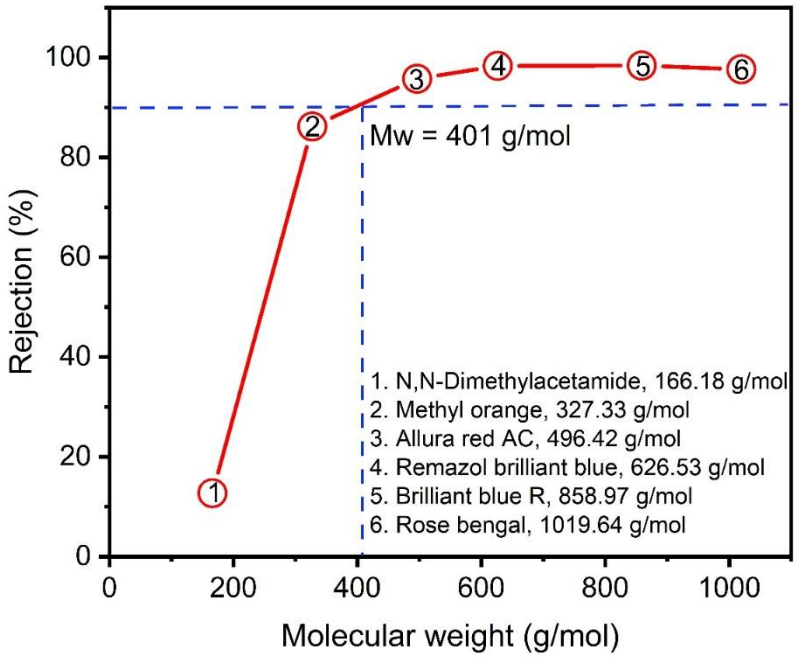


Figure 5.15. Dye rejection in ethanol as a function of molecular weight by the X-PBI membrane.

The performance of the X-PBI membrane was further tested for fractionation and separation of mixed dyes (RB and DMNA) in ethanol (Fig. 5.16a). RB and DMNA were selected for this test because of their distinct molecular weights, colors, and characteristic UV-Vis absorbance peaks at different wavelengths. It is shown that the X-PBI membrane was able to segregate the two dyes from each other in ethanol based on their molecular weights. The membrane effectively retained almost 98% of RB due to its high molecular weight (MW = 1019 g/mol) and rejected less than 5% of low molecular weight solute DMNA (MW = 166 g/mol), allowing most of DMNA to pass through the membrane. The UV-Vis absorption spectra showed no presence of RB peak in the permeate after filtration (Fig. 5.16b), while a large amount of DMNA remained in the filtered ethanol solvent. This was also evident in Figure 5.16(c), where the color of the permeate corresponded to the color of DMNA, which further showed that DMNA had successfully passed through the membrane. The capability of the X-PBI membrane to fractionate mixed solutes in organic solvents makes it a promising candidate for nanofiltration applications in industries. It could be used for enrichments of solutes above the membrane MWCO while recovering solvents, or fractionation of high-value product compounds with different molecular weights/sizes.

The X-PBI membrane performance for the rejection of RB was further evaluated over a filtration period of 10 h (Fig. 5.16d). The RB rejection remained consistently high at 95% throughout the experiment, with a modest permeance to ethanol. This demonstrates the stability of the membrane for prolonged nanofiltration applications. Table 5.3 presents a comparison of the OSN performance of the X-PBI membrane with other crosslinked polymeric membranes reported in the literature. Most crosslinkers reported in the literature have improved the chemical stability of PBI membranes, but they often result in lower permeance or reduced rejection. In contrast, the TGIC X-PBI membranes showed a sharp MWCO of 401 Da and demonstrated higher rejection of high molecular weight dyes, with ethanol permeance comparable or superior to previously reported membranes (Table 5.3). This underscores its potential for challenging industrial applications under harsh chemical conditions.

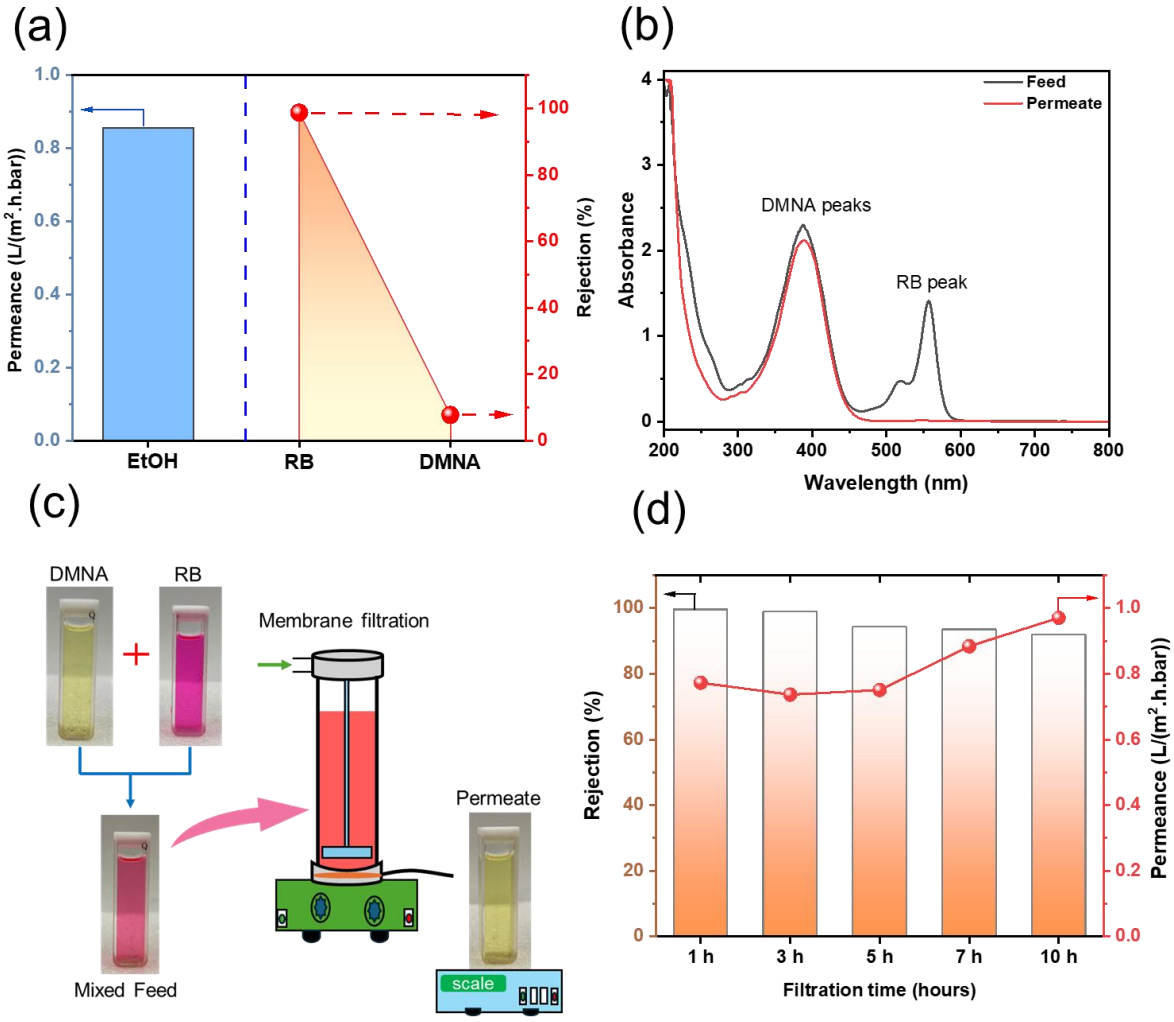


Figure 5.16. Performance of X-PBI membrane for mixed dye separation in ethanol (a). UV-vis absorbance spectra of the RB and DMNA in mixed feed and permeate (b). Protocol and appearance of the mixed feed and permeate after filtration (c). X-PBI rejection of RB from ethanol over a filtration period of 10 h (d).

Table 5.3. Comparison of the OSN performance of TGIC X-PBI membrane with other polymeric membranes reported in the literature.

Membranes	Solvents	Permeance L/(m^2.h.bar)	Solutes [a]	Solute Rejection	References
Trimesoyl chloride X-PBI	Isopropanol	1.36	Tetracycline	92.6 (%)	[196]
Braid-reinforced-PBI	Methanol	3.6	Rose Bengal	>90 (%)	[9]
$KMnO_4$ X-PBI	Ethanol	3.32	Polypropylene Glycol	91.2 (%)	[201]
Crosslinked PVDF	Toluene	0.94	Rose Bengal	98 (%)	[202]
POSS/PI	Ethanol	1.26	Rose Bengal	99 (%)	[171]
Ionically crosslinked sPPSU-HPEI,	Ethanol	1.47	Rose Bengal	99.9 (%)	[203]
50sPPSU-DBX-HPEI25k	Ethanol	4.24	Tetracycline	83 (%)	[176]
PBI–H_2SO_4 Hollow fiber	Methanol	3.5	Tetracycline	98 (%)	[204]
Kevlar nanofibrous	Ethanol	2.9	Methyl Orange	47 (%)	[172]
PDA/PI	Ethanol	0.91	Rose Bengal	99 (%)	[154]
PBI–NGDGE	Ethanol	19	Orange G	84.3 (%)	[117]
PR/PVA/GA	Ethanol	0.38	Rose Bengal	98.3 (%)	[205]
DVS X-PBI	Ethanol	5.88	Polypropylene Glycol	48.3 (%)	[183]
PBI–$K_2S_2O_8$ Hollow fiber	Isopropanol	1.1	Sudan IV	96 (%)	[17]
PBI-DEO	Ethanol	1.02	Sudan IV	55 (%)	[206]

PBI–GA	Ethanol	3.69	Sudan IV	51 (%)	[206]
TGIC X-PBI	Ethanol	1.6	Rose Bengal	~98 (%)	This work
	Ethanol	1.6	Remazol Brilliant Blue	>99 (%)	This work
	Ethanol	1.6	Methyl Orange	86 (%)	This work

[a] Molar weight of solutes (g/mol): Tetracycline = 444; Rose Bengal = 1017; Polypropylene glycol = 950; Methyl Orange = 327; Orange G = 452; Sudan IV = 380; Remazol Brilliant Blue = 626.

5.2.2.2. Extreme pH nanofiltration

Due to the limited stability of commercial NF membranes to extreme pH conditions, chemically stable NF membranes hold great potential for applications involving streams with highly acidic or alkaline pH [207]. Conventional NF membranes are often unable to withstand such harsh conditions due to chemical degradation. Therefore, the TGIC X-PBI membranes were further tested under acidic and basic conditions (Fig. 5.17). Figure 5.17(a) shows the permeance of the X-PBI membrane to water, DMF, and DMF/water mixture (30:70). The membrane showed a water permeance of 8.5 L/(m^2.h.bar) at neutral pH, presumably due to the low viscosity and small molecular size of water molecules, which facilitated water permeation. The permeance of the membrane to DMF and a DMF/water mixture (30:70) was also investigated and compared to pure water permeance, as industrial wastewater is often a mixture of water and organic solvents with varying pH. The membrane showed lower permeance to pure DMF 4.6 L/(m^2.h.bar) than water, which could be attributed to the higher viscosity of DMF than water and its stronger interaction with the membrane. Interestingly, the membrane showed a lower permeance of 2.9 L/(m^2·h·bar) to DMF/water mixture. This could be due to the combined effects of solvent mixing, where the interactions between DMF and water molecules increased the effective viscosity of the solution and surface tension [208, 209] as the two components tended to form hydrates because of their strong interactions [210]. Another reason could be the non-ideal behavior of the DMF/water solution, where the activity coefficients of the components and the osmotic pressure of the solution affected the overall solvent permeance [161].

To investigate the solute rejection of the membrane in acidic and alkaline environments, solute rejection experiments were conducted at pH 14±0.2 and pH 1±0.2 (Fig. 5.17b-f). The X-PBI membrane achieved a high rejection of RBB and RB (over 93%) in all tested conditions, as shown in Figure 5.17(b&c) (Note: the rejection of RB was not evaluated at pH 1 due to the low solubility of RB at this low pH). The permanence of water at pH 14 is higher (6.7 L/(m^2.h.bar)) compared to the other tested conditions. This could be attributed to the hydrolysis of PBI at a higher pH, however, the impact was not significant enough to compromise the solute rejection capability of the membrane, as evidenced by the higher solute rejection at pH 14. The water permeance was significantly lower in an acidic environment compared to alkaline conditions. This instant drop in membrane permeance at pH 1 could be due to a combination of reasons, such as a change in the solution viscosity and molar volume, or the interaction of acids with the crosslinked polymer backbone [161]. However, no change in the retention of RBB at pH 1 was observed, which indicates that the X-PBI membrane retained its separation capability under both extremely acidic and alkaline conditions. This demonstrates that the X-PBI membrane is applicable in both alkaline and acidic conditions for nanofiltration applications.

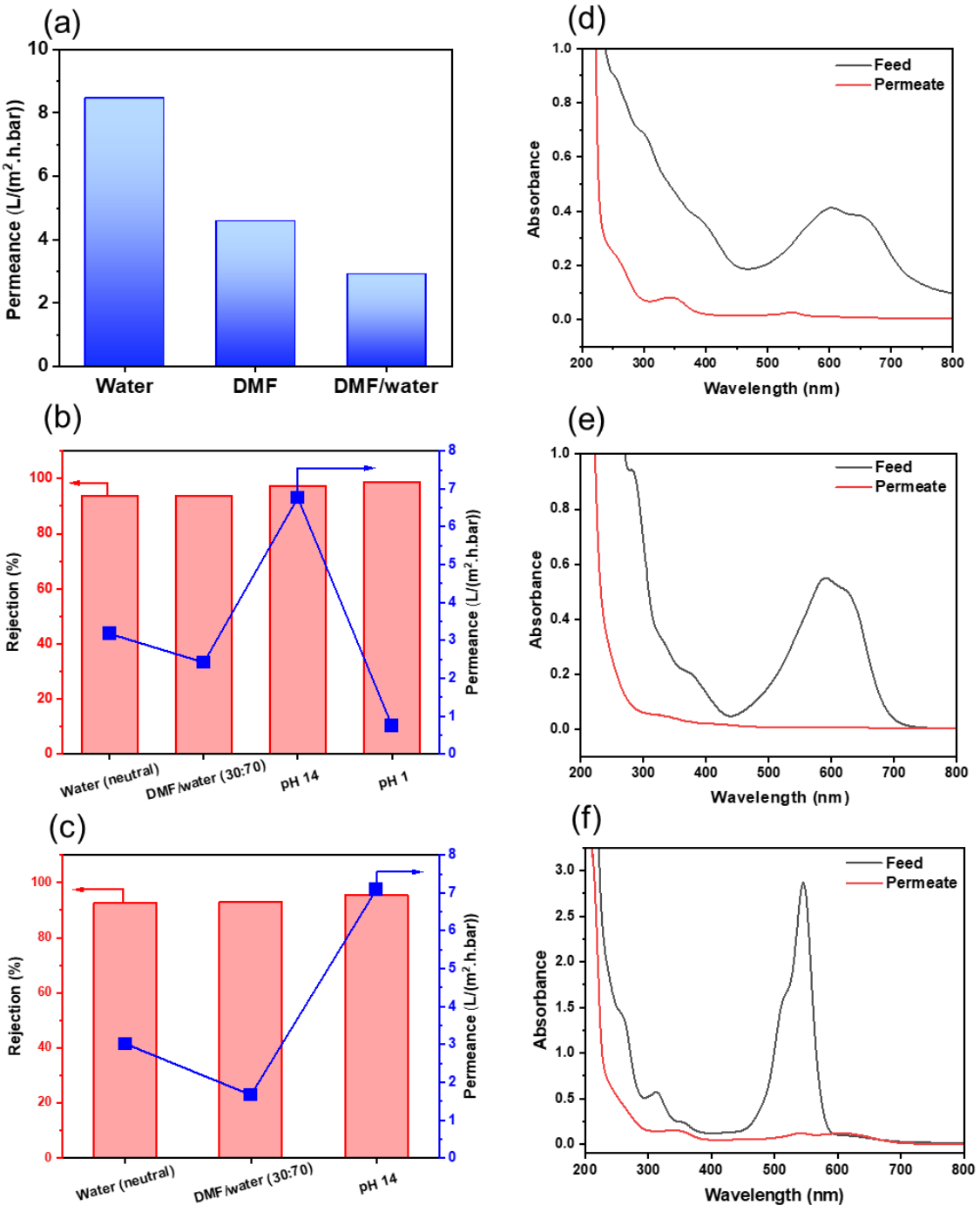


Figure 5.17 (a) The pure permeance of the X-PBI membrane to water, DMF, and a DMF/water mixture (30:70 by wt). (b) Rejection of X-PBI membrane to RBB in different solutions. (c) Rejection of X-PBI membrane to RB in different solutions (the rejection of RB was not evaluated due to its low solubility at pH 1). UV-vis absorption spectra of RBB at pH 14 (d), RBB at pH 1 (e), and RB at pH 14 (f).

5.3. Conclusions

In this chapter, we successfully fabricated PBI nanofiltration membranes covalently crosslinked with TGIC for solvent-resistant and extreme pH nanofiltration applications. The X–PBI membrane showed high chemical stability and OSN performance, enabling the membrane to withstand harsh organic solvents (including DMAc, DMSO, NMP, and DMF) and extreme pH conditions. Characterization with FTIR, XPS, XRD, and TGA confirmed successful crosslinking and structural modifications of the X–PBI membranes. The membranes exhibited excellent performance in separating solutes, achieving near-complete retention of dyes with molecular weight above 401 Da while maintaining favorable permeance to ethanol and DMF. The X–PBI membranes also showed excellent ability to fractionate small molecular weight dyes (e.g., DMNA) from larger solutes (e.g., RB) in ethanol. In addition, the membrane showed higher rejection to RBB at strong alkaline and acidic conditions (pH 1 and 14). The exceptional stability of the X–PBI membrane in harsh chemical environments makes it an ideal candidate for organic solvent nanofiltration or treating waste streams with acidic or alkaline conditions.

Chapter 6 Conclusions and future work

6.1 Conclusions

The work presented in this thesis focused on the development of PBI-based membranes for OSN, with the goal of achieving high chemical resistance, selectivity, and durability under harsh operating conditions. As discussed in Chapter 1, conventional thermal separation processes such as distillation are energy-intensive and environmentally burdensome. Membrane-based OSN, therefore, offers a promising alternative for solvent recovery and solute separation. Thus, this work was designed to fabricate and develop PBI-based membranes with improved chemical and structural stability, while also maintaining high permeance and solute rejection performance. This was achieved through interfacial engineering, chemical crosslinking, and supramolecular functionalization of PBI membranes.

As demonstrated in Chapter 3, an interfacially crosslinked polydopamine/polybenzimidazole (PDA/PBI) composite membrane was successfully fabricated via oxidative polymerization of dopamine and subsequent crosslinking with α,α′-dibromo-p-xylene (DBX). PDA deposition alone was insufficient to produce composite membranes that were chemically stable in harsh polar aprotic solvents. Therefore, the composite membrane was chemically crosslinked with DBX to improve its chemical stability. The PDA coating allowed for finely tuning the MWCO of the membrane. The modified membrane exhibited high rejection of 99% to MO (MW=327 g/mol) and maintained an ethanol permeance of 2.4 L/(m^2.h.bar). In addition, it was demonstrated that the membrane was capable of effectively fractionating mixed solutes during OSN for solutes having molecular weights above and below the MWCO of the membrane. Chapter 3 confirmed that interfacial crosslinking is an effective strategy to produce defect-free, solvent-stable, and high-performing OSN membranes.

In Chapter 4, the effect of crosslinker chemistry on membrane performance was investigated. The membranes were prepared using crosslinkers with aromatic (DCX) and aliphatic (DBB) structures and were selected to illustrate the effect of crosslinker structure on the chain packing density and chemical resistance of the membrane. The pristine PBI membrane disintegrated completely in such harsh solvents as NMP and DMAc, the DBB crosslinked membranes showed

little dissolution, and the DCX crosslinked membrane remained stable in all tested organic solvents. Between the two types of crosslinked membranes, the DCX membranes displayed a smaller mean pore size (0.63 nm) than the DBB membrane (0.87 nm). The effective mean pore size of the membranes was significantly reduced after impregnation with SCA4, and the DCX-SCA4 membrane showed the highest rejection to low-MW dyes. This chapter established the importance of crosslinker structure and supramolecular functionalization in achieving tunable selectivity and chemical robustness of PBI membranes.

As discussed in Chapter 5, we successfully fabricated PBI nanofiltration membranes covalently crosslinked with triglycidyl isocyanurate (TGIC) for solvent-resistant and extreme pH nanofiltration applications. The X-PBI membrane showed high chemical stability and OSN performance, enabling the membrane to withstand harsh organic solvents (including DMAc, DMSO, NMP, and DMF) and extreme pH conditions. The membranes exhibited excellent performance in separating solutes, achieving near-complete retention of dyes with molecular weight above 401 Da while maintaining favorable permeance to ethanol and DMF. The X-PBI membranes also showed excellent ability to fractionate small molecular weight dyes (e.g., DMNA) from larger solutes (e.g., RB) in ethanol. In addition, the membrane showed higher rejection to RBB in strong alkaline and acidic conditions (pH 14 and pH 1). The exceptional stability of the X-PBI membrane in harsh chemical environments makes it an ideal candidate for organic solvent nanofiltration or treating waste streams with acidic or alkaline conditions.

Overall, this thesis establishes a clear structure-property-performance relationship for PBI-based OSN membranes. The results demonstrate that different molecular engineering strategies can be used to systematically improve membrane performance. Collectively, these results highlight how rational control of polymer chemistry, crosslinking architecture, and molecular interactions can mitigate the traditional permeability-selectivity trade-off in polymeric membranes. The findings provide a framework for designing next-generation solvent-resistant membranes and position PBI as a promising platform for sustainable organic solvent separations.

6.2. Future Work

Based on the findings presented in the thesis, several future research directions are proposed to advance the large-scale applications of PBI-based membranes for OSN. This work has

demonstrated progress in improving the chemical resistance, selectivity, and durability of PBI membranes for OSN. However, additional efforts are required to translate these membranes for large-scale industrial applications. Therefore, the following research areas may be prioritized for further development of PBI membranes:

A. Chemical resistance and sustainable crosslinking strategies:

The chemical resistance of the membrane is particularly important when dealing with harsh organic solvents. Pristine PBI was found to dissolve in polar aprotic solvents during chemical stability tests and therefore could not be employed to nanofiltrate polar aprotic solvents. Hence, the PBI membrane must undergo a post-treatment (e.g., chemical crosslinking) to be sufficiently resistant for use in a wide range of organic solvents. Therefore, one important direction for further research is the development of new crosslinking molecules and strategies. However, the crosslinking techniques used at present often involve the use of harsh chemicals that pose environmental risks. Therefore, it is essential to seek green chemistry approaches to crosslink PBI membranes that involve no or minimal use of hazardous substances. This strategy will alleviate their use for industrial applications.

B. Understanding solvent-membrane interactions and swelling behavior:

The swelling of PBI membranes in different organic solvents remains insufficiently understood and often overlooked. A deeper investigation of solvent-polymer interactions, including molecular-level swelling dynamics and free-volume changes, is essential to predict long-term performance. Advanced spectroscopic techniques and molecular simulation tools can help understand how solvent polarity, size, and hydrogen-bonding characteristics affect membrane morphology and transport. Employing artificial intelligence, modelling, and machine learning tools could also help better understand these interactions.

C. Realistic permeation studies using complex solvent mixtures and industrial conditions:

Future research should focus beyond single-solvent permeation tests and extend to realistic multicomponent solvent systems that will better represent industrial environments. To ensure operational reliability, it is highly recommended to assess the separation efficiency, chemical

integrity, and structural stability of PBI membranes before, during, and after prolonged exposure to aggressive industrial solvents, elevated pressures, and temperature fluctuations. These studies will provide essential data on aging behavior and allow for the refinement of crosslinking and stabilization processes while providing a more accurate understanding of selectivity, fouling resistance, and potential degradation mechanisms under practical conditions.

D. Scale-up and module development:

To scale up PBI-based membranes, future research must transition from laboratory-scale flat-sheet configurations to hollow-fiber or spiral-wound modules. Extended continuous-operation testing should also be performed to evaluate long-term mechanical and chemical durability under cyclic solvent exposure and pressure fluctuations.

E. Techno-economic and life-cycle evaluation:

Evaluating the long-term performance, economic feasibility, and environmental impact of PBI-based membranes is essential to determine their suitability for commercial use. Therefore, life-cycle assessment and cost-benefit analyses should be incorporated to guide process optimization and ensure that membrane production aligns with sustainability and circular economy principles.

F. Other application area:

PBI-based membranes have potential applications in the petroleum industry, where heat-driven separation, such as distillation, is a common practice for separating molecules at high temperatures up to 400ºC, but little research has been conducted. The increasing demand for critical minerals (e.g., lithium ions for batteries) and resource recovery from wastewater (e.g., nitrogen and phosphorus for fertilizers) is currently a hot research topic. One can use PBI as a stimuli-responsive membrane material for the recovery/separation of lithium ions from geothermal brine and seawater due to its amphoteric nature. PBI membranes may also be explored for nitrogen and phosphorus recovery from wastewater under harsh conditions. These membranes can also be used for the removal of radioactive compounds where extreme acidity and temperature exist. However, little research has been done.

References

[1] S.S. Beshahwored, Y.-H. Huang, Z.G. Abdi, C.-C. Hu, T.-S. Chung, Polybenzimidazole (PBI) membranes cross-linked with various cross-linkers and impregnated with 4-sulfocalix [4]arene (SCA4) for organic solvent nanofiltration (OSN), Journal of Membrane Science 663 (2022). https://doi.org/10.1016/j.memsci.2022.121039.

[2] Y. Cheng, S.J. Datta, S. Zhou, J. Jia, O. Shekhah, M. Eddaoudi, Advances in metal-organic framework-based membranes, Chem Soc Rev (2022). https://doi.org/10.1039/d2cs00031h.

[3] S.H. Kim, M.A. Khan, K.S. Im, P. Kang, S.Y. Nam, Enhanced Organic Solvent Nanofiltration Membranes with Double Permeance via Laser-Induced Graphitization of Polybenzimidazole, Advanced Materials Interfaces (2024). https://doi.org/10.1002/admi.202400490.

[4] H. Dou, M. Xu, B. Wang, Z. Zhang, G. Wen, Y. Zheng, D. Luo, L. Zhao, A. Yu, L. Zhang, Z. Jiang, Z. Chen, Microporous framework membranes for precise molecule/ion separations, Chem Soc Rev 50(2) (2021) 986-1029. https://doi.org/10.1039/d0cs00552e.

[5] D.S. Sholl, R.P. Lively, Seven chemical separations to change the world, Nature 532(7600) (2016) 435-437. https://doi.org/DOI 10.1038/532435a.

[6] M.S. Denny, J.C. Moreton, L. Benz, S.M. Cohen, Metal-organic frameworks for membrane-based separations, Nat Rev Mater 1(12) (2016). https://doi.org/ARTN 1607810.1038/natrevmats.2016.78.

[7] Y.N. Liu, M.O. Coppens, Z.Y. Jiang, Mixed-dimensional membranes: chemistry and structure-property relationships, Chemical Society Reviews 50(21) (2021) 11747-11765. https://doi.org/10.1039/d1cs00737h.

[8] R.W. Baker, Overview of Membrane Science and Technology, Membrane Technology and Applications2004, pp. 1-14. https://doi.org/https://doi.org/10.1002/0470020393.ch1.

[9] B. Zhao, G.M. Shi, J.-Y. Lai, T.-S. Chung, Braid-reinforced polybenzimidazole (PBI) hollow fiber membranes for organic solvent nanofiltration (OSN), Separation and Purification Technology 290 (2022) 120811. https://doi.org/10.1016/j.seppur.2022.120811.

[10] J. Hu, R. Hardian, M. Gede, T. Holtzl, G. Szekely, Reversible crosslinking of polybenzimidazole-based organic solvent nanofiltration membranes using difunctional

organic acids: Toward sustainable crosslinking approaches, Journal of Membrane Science 648 (2022) 120383. https://doi.org/10.1016/j.memsci.2022.120383.

[11] H. Zhou, A. Akram, A.J.C. Semiao, R. Malpass-Evans, C.H. Lau, N.B. McKeown, W. Zhang, Enhancement of performance and stability of thin-film nanocomposite membranes for organic solvent nanofiltration using hypercrosslinked polymer additives, Journal of Membrane Science 644 (2022) 120172. https://doi.org/10.1016/j.memsci.2021.120172.

[12] C. Wang, M.J. Park, D.H. Seo, E. Drioli, H. Matsuyama, H. Shon, Recent advances in nanomaterial-incorporated nanocomposite membranes for organic solvent nanofiltration, Separation and Purification Technology 268 (2021) 118657. https://doi.org/10.1016/j.seppur.2021.118657.

[13] G.M. Shi, Y. Feng, B. Li, H.M. Tham, J.-Y. Lai, T.-S. Chung, Recent progress of organic solvent nanofiltration membranes, Progress in Polymer Science 123 (2021) 101470. https://doi.org/10.1016/j.progpolymsci.2021.101470.

[14] M.A. Abdulhamid, G. Szekely, Organic solvent nanofiltration membranes based on polymers of intrinsic microporosity, Current Opinion in Chemical Engineering 36 (2022) 100804. https://doi.org/10.1016/j.coche.2022.100804.

[15] Z.J. Santanu Karan, Andrew G. Livingston, Sub–10 nm polyamide nanofilms with ultrafast solvent transport for molecular separation, Science 348(6241) (2015) 1347-1351.

[16] C. Li, S. Li, L. Lv, B. Su, M.Z. Hu, High solvent-resistant and integrally crosslinked polyimide-based composite membranes for organic solvent nanofiltration, Journal of Membrane Science 564 (2018) 10-21. https://doi.org/10.1016/j.memsci.2018.06.048.

[17] B. Zhao, G.M. Shi, K.Y. Wang, J.-Y. Lai, T.-S. Chung, Employing a green cross-linking method to fabricate polybenzimidazole (PBI) hollow fiber membranes for organic solvent nanofiltration (OSN), Separation and Purification Technology 255 (2021) 117702. https://doi.org/10.1016/j.seppur.2020.117702.

[18] A.V. Volkov, V.V. Parashchuk, D.F. Stamatialis, V.S. Khotimsky, V.V. Volkov, M. Wessling, High permeable PTMSP/PAN composite membranes for solvent nanofiltration, Journal of Membrane Science 333(1-2) (2009) 88-93. https://doi.org/10.1016/j.memsci.2009.01.050.

[19] A.K. Hołda, B. Aernouts, W. Saeys, I.F.J. Vankelecom, Study of polymer concentration and evaporation time as phase inversion parameters for polysulfone-based SRNF membranes,

Journal of Membrane Science 442 (2013) 196-205. https://doi.org/10.1016/j.memsci.2013.04.017.

[20] J. Li, M. Zhang, W. Feng, L. Zhu, L. Zhang, PIM-1 pore-filled thin film composite membranes for tunable organic solvent nanofiltration, Journal of Membrane Science 601 (2020) 117951. https://doi.org/10.1016/j.memsci.2020.117951.

[21] D. Zedel, A. Drews, M. Kraume, Retention of surfactants by organic solvent nanofiltration and influences on organic solvent flux, Separation and Purification Technology 158 (2016) 396-408. https://doi.org/10.1016/j.seppur.2015.12.040.

[22] X.Q. Cheng, Y.L. Zhang, Z.X. Wang, Z.H. Guo, Y.P. Bai, L. Shao, Recent Advances in Polymeric Solvent-Resistant Nanofiltration Membranes, Advances in Polymer Technology 33(S1) (2014) n/a-n/a. https://doi.org/10.1002/adv.21455.

[23] P. Marchetti, M.F. Jimenez Solomon, G. Szekely, A.G. Livingston, Molecular separation with organic solvent nanofiltration: a critical review, Chem Rev 114(21) (2014) 10735-806. https://doi.org/10.1021/cr500006j.

[24] Q. Liu, S.J.D. Smith, K. Konstas, D. Ng, K. Zhang, M.R. Hill, Z. Xie, Construction of ultrathin PTMSP/Porous nanoadditives membranes for highly efficient organic solvent nanofiltration (OSN), Journal of Membrane Science 620 (2021) 118911. https://doi.org/10.1016/j.memsci.2020.118911.

[25] E.J. Kappert, M.J.T. Raaijmakers, K. Tempelman, F.P. Cuperus, W. Ogieglo, N.E. Benes, Swelling of 9 polymers commonly employed for solvent-resistant nanofiltration membranes: A comprehensive dataset, Journal of Membrane Science 569 (2019) 177-199. https://doi.org/10.1016/j.memsci.2018.09.059.

[26] J. Chau, K.K. Sirkar, Organic solvent mixture separation during reverse osmosis and nanofiltration by a perfluorodioxole copolymer membrane, Journal of Membrane Science 618 (2021) 118663. https://doi.org/10.1016/j.memsci.2020.118663.

[27] C. Liu, G. Dong, T. Tsuru, H. Matsuyama, Organic solvent reverse osmosis membranes for organic liquid mixture separation: A review, Journal of Membrane Science 620 (2021) 118882. https://doi.org/10.1016/j.memsci.2020.118882.

[28] Y. Chen, Y. Bai, L. Meng, W. Zhang, J. Xia, Z. Xu, R. Sun, Y. Lv, T. Liu, Engineering nanocomposite metal-phenolic network membranes with hollow MOFs via in-situ etching

for High-efficiency organic solvent nanofiltration, Chemical Engineering Journal 437 (2022) 135289. https://doi.org/10.1016/j.cej.2022.135289.

[29] L. Nie, C.Y. Chuah, T.H. Bae, J.M. Lee, Graphene-Based Advanced Membrane Applications in Organic Solvent Nanofiltration, Advanced Functional Materials 31(6) (2020) 2006949. https://doi.org/10.1002/adfm.202006949.

[30] S.K. Lim, K. Goh, T.-H. Bae, R. Wang, Polymer-based membranes for solvent-resistant nanofiltration: A review, Chinese Journal of Chemical Engineering 25(11) (2017) 1653-1675. https://doi.org/10.1016/j.cjche.2017.05.009.

[31] M. Priske, M. Lazar, C. Schnitzer, G. Baumgarten, Recent Applications of Organic Solvent Nanofiltration, Chemie Ingenieur Technik 88(1-2) (2016) 39-49. https://doi.org/10.1002/cite.201500084.

[32] Y.H. See Toh, F.W. Lim, A.G. Livingston, Polymeric membranes for nanofiltration in polar aprotic solvents, Journal of Membrane Science 301(1-2) (2007) 3-10. https://doi.org/10.1016/j.memsci.2007.06.034.

[33] B.-H. Jeong, E.M.V. Hoek, Y. Yan, A. Subramani, X. Huang, G. Hurwitz, A.K. Ghosh, A. Jawor, Interfacial polymerization of thin film nanocomposites: A new concept for reverse osmosis membranes, Journal of Membrane Science 294(1-2) (2007) 1-7. https://doi.org/10.1016/j.memsci.2007.02.025.

[34] D. Aili, J. Yang, K. Jankova, D. Henkensmeier, Q. Li, From polybenzimidazoles to polybenzimidazoliums and polybenzimidazolides, Journal of Materials Chemistry A 8(26) (2020) 12854-12886. https://doi.org/10.1039/d0ta01788d.

[35] H. Vogel, C.S. Marvel, Polybenzimidazoles, new thermally stable polymers, Journal of Polymer Science 50(154) (1961) 511-539. https://doi.org/10.1002/pol.1961.1205015419.

[36] J.A. Asensio, E.M. Sanchez, P. Gomez-Romero, Proton-conducting membranes based on benzimidazole polymers for high-temperature PEM fuel cells. A chemical quest, Chem Soc Rev 39(8) (2010) 3210-39. https://doi.org/10.1039/b922650h.

[37] J. Sanchez-Lainez, M. Etxeberria-Benavides, O. David, C. Tellez, J. Coronas, Green Preparation of Thin Films of Polybenzimidazole on Flat and Hollow Fiber Supports: Application to Hydrogen Separation, ChemSusChem 14(3) (2021) 952-960. https://doi.org/10.1002/cssc.202002700.

[38] D.A. Chatfield, Stepwise Thermal-Degradation of a Polybenzimidazole Foam, J Polym Sci Pol Chem 19(3) (1981) 601-618. https://doi.org/DOI 10.1002/pol.1981.170190301.

[39] K.Y. Wang, M. Weber, T.-S. Chung, Polybenzimidazoles (PBIs) and state-of-the-art PBI hollow fiber membranes for water, organic solvent and gas separations: a review, Journal of Materials Chemistry A 10(16) (2022) 8687-8718. https://doi.org/10.1039/d2ta00422d.

[40] J. Olvera-Mancilla, C. Aguilar-Lugo, C.A. Fernández-Gijón, J. Palacios-Alquisira, M. Zolotukhin, L. Alexandrova, Processable N-Substituted Polybenzimidazole; Direct Synthesis, ChemistrySelect 5(17) (2020) 5082-5091. https://doi.org/10.1002/slct.202000434.

[41] Y. Iwakura, Y. Imai, K. Uno, Polyphenylenebenzimidazoles, J Polym Sci Part A 2(6pa) (1964) 2605-&. https://doi.org/DOI 10.1002/pol.1964.100020611.

[42] H. Vogel, C.S. Marvel, Polybenzimidazoles .2., J Polym Sci Part A 1(5) (1963) 1531-&. https://doi.org/DOI 10.1002/pol.1963.100010507.

[43] T.-S. Chung, A Critical Review of Polybenzimidazoles, Polymer Reviews 37(2) (1997) 277-301. https://doi.org/10.1080/15321799708018367.

[44] E.W. Choe, Catalysts for the Preparation of Polybenzimidazoles, Journal of Applied Polymer Science 53(5) (1994) 497-506. https://doi.org/DOI 10.1002/app.1994.070530504.

[45] B. Huang, X.Y. Wang, H. Fang, S.H. Jiang, H.Q. Hou, Mechanically strong sulfonated polybenzimidazole PEMs with enhanced proton conductivity, Mater Lett 234 (2019) 354-356. https://doi.org/10.1016/j.matlet.2018.09.131.

[46] S. Singha, T. Jana, J.A. Modestra, A.N. Kumar, S.V. Mohan, Highly efficient sulfonated polybenzimidazole as a proton exchange membrane for microbial fuel cells, Journal of Power Sources 317 (2016) 143-152. https://doi.org/10.1016/j.jpowsour.2016.03.103.

[47] J. Lobato, P. Cañizares, M.A. Rodrigo, J.J. Linares, J.A. Aguilar, Improved polybenzimidazole films for HPO-doped PBI-based high temperature PEMFC, Journal of Membrane Science 306(1-2) (2007) 47-55. https://doi.org/10.1016/j.memsci.2007.08.028.

[48] J.S. Yang, L.N. Cleemann, T. Steenberg, C. Terkelsen, Q.F. Li, J.O. Jensen, H.A. Hjuler, N.J. Bjerrum, R.H. He, High Molecular Weight Polybenzimidazole Membranes for High Temperature PEMFC, Fuel Cells 14(1) (2014) 7-15. https://doi.org/10.1002/fuce.201300070.

[49] S.C. Kumbharkar, M.N. Islam, R.A. Potrekar, U.K. Kharul, Variation in acid moiety of polybenzimidazoles: Investigation of physico-chemical properties towards their applicability as proton exchange and gas separation membrane materials, Polymer 50(6) (2009) 1403-1413. https://doi.org/10.1016/j.polymer.2009.01.043.

[50] K. Geng, Y. Li, Y. Xing, L.H. Wang, N.W. Li, A novel polybenzimidazole membrane containing bulky naphthalene group for vanadium flow battery, Journal of Membrane Science 586 (2019) 231-239. https://doi.org/10.1016/j.memsci.2019.05.062.

[51] A. Carollo, E. Quartarone, C. Tomasi, P. Mustarelli, F. Belotti, A. Magistris, F. Maestroni, M. Parachini, L. Garlaschelli, P.P. Righetti, Developments of new proton conducting membranes based on different polybenzimidazole structures for fuel cells applications, Journal of Power Sources 160(1) (2006) 175-180. https://doi.org/10.1016/j.jpowsour.2006.01.081.

[52] D. Aili, A.G. Wright, M.R. Kraglund, K. Jankova, S. Holdcroft, J.O. Jensen, Towards a stable ion-solvating polymer electrolyte for advanced alkaline water electrolysis, Journal of Materials Chemistry A 5(10) (2017) 5055-5066. https://doi.org/10.1039/c6ta10680c.

[53] S.C. Kumbharkar, P.B. Karadkar, U.K. Kharul, Enhancement of gas permeation properties of polybenzimidazoles by systematic structure architecture, Journal of Membrane Science 286(1-2) (2006) 161-169. https://doi.org/10.1016/j.memsci.2006.09.030.

[54] A.G. Wright, J.T. Fan, B. Britton, T. Weissbach, H.F. Lee, E.A. Kitching, T.J. Peckham, S. Holdcroft, Hexamethyl-terphenyl poly(benzimidazolium): a universal hydroxide-conducting polymer for energy conversion devices, Energy & Environmental Science 9(6) (2016) 2130-2142. https://doi.org/10.1039/c6ee00656f.

[55] X. Li, R.P. Singh, K.W. Dudeck, K.A. Berchtold, B.C. Benicewicz, Influence of polybenzimidazole main chain structure on H2/CO2 separation at elevated temperatures, Journal of Membrane Science 461 (2014) 59-68. https://doi.org/10.1016/j.memsci.2014.03.008.

[56] H. Borjigin, K.A. Stevens, R. Liu, J.D. Moon, A.T. Shaver, S. Swinnea, B.D. Freeman, J.S. Riffle, J.E. McGrath, Synthesis and characterization of polybenzimidazoles derived from tetraaminodiphenylsulfone for high temperature gas separation membranes, Polymer 71 (2015) 135-142. https://doi.org/10.1016/j.polymer.2015.06.021.

[57] Q.F. Li, H.C. Rudbeck, A. Chromik, J.O. Jensen, C. Pan, T. Steenberg, M. Calverley, N.J. Bjerrum, J. Kerres, Properties, degradation and high temperature fuel cell test of different types of PBI and PBI blend membranes, Journal of Membrane Science 347(1-2) (2010) 260-270. https://doi.org/10.1016/j.memsci.2009.10.032.

[58] J.S. Yang, Y.X. Xu, L. Zhou, Q.T. Che, R.H. He, Q.F. Li, Hydroxyl pyridine containing polybenzimidazole membranes for proton exchange membrane fuel cells, Journal of Membrane Science 446 (2013) 318-325. https://doi.org/10.1016/j.memsci.2013.07.004.

[59] H.T. Pu, L. Wang, H.Y. Pan, D.C. Wan, Synthesis and Characterization of Fluorine-Containing Polybenzimidazole for Proton Conducting Membranes in Fuel Cells, J Polym Sci Pol Chem 48(10) (2010) 2115-2122. https://doi.org/10.1002/pola.23979.

[60] N.N. Krishnan, H.J. Lee, H.J. Kim, J.Y. Kim, I. Hwang, J.H. Jang, E.A. Cho, S.K. Kim, D. Henkensmeier, S.A. Hong, T.H. Lim, Sulfonated poly(ether sulfone)/sulfonated polybenzimidazole blend membrane for fuel cell applications, European Polymer Journal 46(7) (2010) 1633-1641. https://doi.org/10.1016/j.eurpolymj.2010.03.005.

[61] J.K. Jang, T.H. Kim, S.J. Yoon, J.Y. Lee, J.C. Lee, Y.T. Hong, Highly proton conductive, dense polybenzimidazole membranes with low permeability to vanadium and enhanced H2SO4 absorption capability for use in vanadium redox flow batteries, Journal of Materials Chemistry A 4(37) (2016) 14342-14355. https://doi.org/10.1039/c6ta05080h.

[62] A.L. Gulledge, B. Gu, B.C. Benicewicz, A New Sequence Isomer of AB-Polybenzimidazole for High-Temperature PEM Fuel Cells, J Polym Sci Pol Chem 50(2) (2012) 306-313. https://doi.org/10.1002/pola.25034.

[63] S. Ali, I.A. Shah, I. Ihsanullah, X. Feng, Nanocomposite membranes for organic solvent nanofiltration: Recent advances, challenges, and prospects, Chemosphere (2022) 136329. https://doi.org/10.1016/j.chemosphere.2022.136329.

[64] G.R. Guillen, Y.J. Pan, M.H. Li, E.M.V. Hoek, Preparation and Characterization of Membranes Formed by Nonsolvent Induced Phase Separation: A Review, Industrial & Engineering Chemistry Research 50(7) (2011) 3798-3817. https://doi.org/10.1021/ie101928r.

[65] W. Lu, Z. Yuan, Y. Zhao, H. Zhang, H. Zhang, X. Li, Porous membranes in secondary battery technologies, Chem Soc Rev 46(8) (2017) 2199-2236. https://doi.org/10.1039/c6cs00823b.

[66] S. Ali, X. Feng, Interfacially Cross-Linked Polydopamine/Polybenzimidazole Composite Membranes for Organic Solvent Nanofiltration, ACS Appl Mater Interfaces 16(47) (2024) 65517-65528. https://doi.org/10.1021/acsami.4c14283.

[67] S. Yousef, A. Tonkonogovas, S.I. Lukosiute, A. Mohamed, Gas permeation and selectivity characteristics of sponge-like and finger-like structures of polysulfone membranes, Fuel 347 (2023). https://doi.org/ARTN 12847610.1016/j.fuel.2023.128476.

[68] R.P. Singh, G.J. Dahe, K.W. Dudeck, K.A. Berchtold, Macrovoid-free high performance polybenzimidazole hollow fiber membranes for elevated temperature H2/CO2 separations, International Journal of Hydrogen Energy 45(51) (2020) 27331-27345. https://doi.org/10.1016/j.ijhydene.2020.07.091.

[69] X.Y. Guo, Z.H. Qiao, D.H. Liu, C.L. Zhong, Mixed-matrix membranes for CO separation: role of the third component, Journal of Materials Chemistry A 7(43) (2019) 24738-24759. https://doi.org/10.1039/c9ta09012f.

[70] S. Zhang, L. Shen, H. Deng, Q. Liu, X. You, J. Yuan, Z. Jiang, S. Zhang, Ultrathin Membranes for Separations: A New Era Driven by Advanced Nanotechnology, Adv Mater 34(21) (2022) e2108457. https://doi.org/10.1002/adma.202108457.

[71] J.D. Moon, A.T. Bridge, C. D'Ambra, B.D. Freeman, D.R. Paul, Gas separation properties of polybenzimidazole/thermally-rearranged polymer blends, Journal of Membrane Science 582 (2019) 182-193. https://doi.org/10.1016/j.memsci.2019.03.067.

[72] X.R. Wang, M.X. Shan, X.L. Liu, M. Wang, C.M. Doherty, D. Osadchii, F. Kapteijn, High-Performance Polybenzimidazole Membranes for Helium Extraction from Natural Gas, ACS Appl. Mater. Interfaces 11(22) (2019) 20098-20103. https://doi.org/10.1021/acsami.9b05548.

[73] A. Naderi, A.A. Tashvigh, T.S. Chung, H/CO separation enhancement via chemical modification of polybenzimidazole nanostructure, Journal of Membrane Science 572 (2019) 343-349. https://doi.org/10.1016/j.memsci.2018.11.020.

[74] J.M. Pérez-Francisco, J.L. Santiago-García, M.I. Loría-Bastarrachea, D.R. Paul, B.D. Freeman, M. Aguilar-Vega, CMS membranes from PBI/PI blends: Temperature effect on gas transport and separation performance, Journal of Membrane Science 597 (2020). https://doi.org/ARTN 11770310.1016/j.memsci.2019.117703.

[75] M.A. Abdulhamid, R. Hardian, P.M. Bhatt, S.J. Datta, A. Ramirez, J. Gascon, M. Eddaoudi, G. Szekely, Molecular engineering of intrinsically microporous polybenzimidazole for energy-efficient gas separation, Applied Materials Today 26 (2022). https://doi.org/10.1016/j.apmt.2021.101271.

[76] J. Olvera-Mancilla, C. Aguilar-Lugo, L. Fomina, F.M. Sanchez-Arevalo, M.O. González-Díaz, R. Sulub-Sulub, M. Aguilar-Vega, L. Alexandrova, Fluorinated Polybenzimidazole as a Novel Precursor for Carbon Molecular Sieve Membranes with Enhanced Gas Separation Properties, Industrial & Engineering Chemistry Research 61(19) (2022) 6587-6599. https://doi.org/10.1021/acs.iecr.2c00020.

[77] M.D. Liu, J. Emery, R.L. Guo, Microporous pentiptycene-based polybenzimidazole membranes for high temperature H2/CO separation, Journal of Membrane Science 718 (2025). https://doi.org/ARTN 12367310.1016/j.memsci.2024.123673.

[78] J. Wu, C.Z. Liang, A. Naderi, T.S. Chung, Tunable Supramolecular Cavities Molecularly Homogenized in Polymer Membranes for Ultraefficient Precombustion CO(2) Capture, Adv Mater 34(3) (2022) e2105156. https://doi.org/10.1002/adma.202105156.

[79] L. Zhu, M.T. Swihart, H. Lin, Unprecedented size-sieving ability in polybenzimidazole doped with polyprotic acids for membrane H2/CO2 separation, Energy & Environmental Science 11(1) (2018) 94-100. https://doi.org/10.1039/c7ee02865b.

[80] L. Hu, V.T. Bui, L. Huang, R.P. Singh, H. Lin, Facilely Cross-Linking Polybenzimidazole with Polycarboxylic Acids to Improve H(2)/CO(2) Separation Performance, ACS Appl Mater Interfaces 13(10) (2021) 12521-12530. https://doi.org/10.1021/acsami.0c23098.

[81] M. Etxeberria-Benavides, T. Johnson, S. Cao, B. Zornoza, J. Coronas, J. Sanchez-Lainez, A. Sabetghadam, X.L. Liu, E. Andres-Garcia, F. Kapteijn, J. Gascon, O. David, PBI mixed matrix hollow fiber membrane: Influence of ZIF-8 filler over H2/CO separation performance at high temperature and pressure, Separation and Purification Technology 237 (2020). https://doi.org/ARTN 11634710.1016/j.seppur.2019.116347.

[82] L. Zhu, M.T. Swihart, H. Lin, Tightening polybenzimidazole (PBI) nanostructure via chemical cross-linking for membrane H2/CO2separation, Journal of Materials Chemistry A 5(37) (2017) 19914-19923. https://doi.org/10.1039/c7ta03874g.

[83] A. Naderi, A. Asadi Tashvigh, T.-S. Chung, M. Weber, C. Maletzko, Molecular design of double crosslinked sulfonated polyphenylsulfone /polybenzimidazole blend membranes for an efficient hydrogen purification, Journal of Membrane Science 563 (2018) 726-733. https://doi.org/10.1016/j.memsci.2018.06.033.

[84] R.P. Singh, X. Li, K.W. Dudeck, B.C. Benicewicz, K.A. Berchtold, Polybenzimidazole based random copolymers containing hexafluoroisopropylidene functional groups for gas separations at elevated temperatures, Polymer 119 (2017) 134-141. https://doi.org/10.1016/j.polymer.2017.04.075.

[85] J. Sánchez-Laínez, B. Zornoza, M. Carta, R. Malpass-Evans, N.B. McKeown, C. Téllez, J. Coronas, Hydrogen Separation at High Temperature with Dense and Asymmetric Membranes Based on PIM-EA(H)-TB/PBI Blends, Industrial & Engineering Chemistry Research 57(49) (2018) 16909-16916. https://doi.org/10.1021/acs.iecr.8b04209.

[86] L. Zhu, D. Yin, Y. Qin, S. Konda, S. Zhang, A. Zhu, S. Liu, T. Xu, M.T. Swihart, H. Lin, Sorption-Enhanced Mixed Matrix Membranes with Facilitated Hydrogen Transport for Hydrogen Purification and CO2 Capture, Advanced Functional Materials 29(36) (2019). https://doi.org/10.1002/adfm.201904357.

[87] W.H. Zhang, M.J. Yin, Q. Zhao, C.G. Jin, N.X. Wang, S.L. Ji, C.L. Ritt, M. Elimelech, Q.F. An, Graphene oxide membranes with stable porous structure for ultrafast water transport, Nature Nanotechnology 16(3) (2021) 337-+. https://doi.org/10.1038/s41565-020-00833-9.

[88] M.A. Shannon, P.W. Bohn, M. Elimelech, J.G. Georgiadis, B.J. Mariñas, A.M. Mayes, Science and technology for water purification in the coming decades, Nature 452(7185) (2008) 301-310. https://doi.org/10.1038/nature06599.

[89] S. Daer, N. Akther, Q. Wei, H.K. Shon, S.W. Hasan, Influence of silica nanoparticles on the desalination performance of forward osmosis polybenzimidazole membranes, Desalination 491 (2020) 8. https://doi.org/10.1016/j.desal.2020.114441.

[90] N. Akther, S. Daer, Q. Wei, I. Janajreh, S.W. Hasan, Synthesis of polybenzimidazole (PBI) forward osmosis (FO) membrane and computational fluid dynamics (CFD) modeling of concentration gradient across membrane surface, Desalination 452 (2019) 17-28. https://doi.org/10.1016/j.desal.2018.11.003.

[91] M.F. Flanagan, I.C. Escobar, Novel charged and hydrophilized polybenzimidazole (PBI) membranes for forward osmosis, Journal of Membrane Science 434 (2013) 85-92. https://doi.org/10.1016/j.memsci.2013.01.039.

[92] K.Y. Wang, Q. Yang, T.-S. Chung, R. Rajagopalan, Enhanced forward osmosis from chemically modified polybenzimidazole (PBI) nanofiltration hollow fiber membranes with a thin wall, Chemical Engineering Science 64(7) (2009) 1577-1584. https://doi.org/10.1016/j.ces.2008.12.032.

[93] K.Y. Wang, T.-S. Chung, Polybenzimidazole nanofiltration hollow fiber for cephalexin separation, AIChE Journal 52(4) (2006) 1363-1377. https://doi.org/10.1002/aic.10741.

[94] K.Y. Wang, Y. Xiao, T.-S. Chung, Chemically modified polybenzimidazole nanofiltration membrane for the separation of electrolytes and cephalexin, Chemical Engineering Science 61(17) (2006) 5807-5817. https://doi.org/10.1016/j.ces.2006.04.031.

[95] X. Wang, P. Jayaweera, R.A. Alrasheed, S.A. Aljlil, Y.M. Alyousef, M. Alsubaei, H. AlRomaih, I. Jayaweera, Preparation of Polybenzimidazole Hollow-Fiber Membranes for Reverse Osmosis and Nanofiltration by Changing the Spinning Air Gap, Membranes 8(4) (2018) 13. https://doi.org/10.3390/membranes8040113.

[96] L. Hu, M. You, J. Meng, Chlorination as a simple but effective method to improve the water/salt selectivity of polybenzimidazole for desalination membrane applications, Journal of Membrane Science 638 (2021). https://doi.org/10.1016/j.memsci.2021.119745.

[97] P. Staiti, F. Lufrano, A.S. Aricò, E. Passalacqua, V. Antonucci, Sulfonated polybenzimidazole membranes - preparation and physico-chemical characterization, Journal of Membrane Science 188(1) (2001) 71-78. https://doi.org/Doi 10.1016/S0376-7388(01)00359-3.

[98] S. Cong, J. Wang, Z. Wang, X. Liu, Polybenzimidazole (PBI) and benzimidazole-linked polymer (BILP) membranes, Green Chemical Engineering 2(1) (2021) 44-56. https://doi.org/10.1016/j.gce.2020.11.007.

[99] Z. Zhou, O. Zholobko, X.-F. Wu, T. Aulich, J. Thakare, J. Hurley, Polybenzimidazole-Based Polymer Electrolyte Membranes for High-Temperature Fuel Cells: Current Status and Prospects, Energies 14(1) (2020). https://doi.org/10.3390/en14010135.

[100] K.D. Kreuer, A. Fuchs, M. Ise, M. Spaeth, J. Maier, Imidazole and pyrazole-based proton conducting polymers and liquids, Electrochimica Acta 43(10-11) (1998) 1281-1288. https://doi.org/Doi 10.1016/S0013-4686(97)10031-7.

[101] M. Wales, E. Gebremichael, X. Wang, E. Perea, P. Jayaweera, I. Jayaweera, Flue Gas Desulfurization (FGD) Wastewater Treatment Using Polybenzimidazole (PBI) Hollow Fiber (HF) Membranes, Membranes 11(6) (2021) 13. https://doi.org/10.3390/membranes11060430.

[102] K.Y. Wang, T.-S. Chung, J.-J. Qin, Polybenzimidazole (PBI) nanofiltration hollow fiber membranes applied in forward osmosis process, Journal of Membrane Science 300(1-2) (2007) 6-12. https://doi.org/10.1016/j.memsci.2007.05.035.

[103] W.F. Yong, H. Zhang, Recent advances in polymer blend membranes for gas separation and pervaporation, Progress in Materials Science 116 (2021). https://doi.org/10.1016/j.pmatsci.2020.100713.

[104] G.P. Liu, W.Q. Jin, Pervaporation membrane materials: Recent trends and perspectives, Journal of Membrane Science 636 (2021). https://doi.org/ARTN 11955710.1016/j.memsci.2021.119557.

[105] Y.K. Ong, G.M. Shi, N.L. Le, Y.P. Tang, J. Zuo, S.P. Nunes, T.S. Chung, Recent membrane development for pervaporation processes, Progress in Polymer Science 57 (2016) 1-31. https://doi.org/10.1016/j.progpolymsci.2016.02.003.

[106] K.Y. Wang, T.S. Chung, R. Rajagopalan, Dehydration of tetrafluoropropanol (TFP) by pervaporation via novel PBI/BTDA-TDI/MDI co-polyimide (P84) dual-layer hollow fiber membranes, Journal of Membrane Science 287(1) (2007) 60-66. https://doi.org/10.1016/j.memsci.2006.10.009.

[107] Y. Wang, M. Gruender, T.S. Chung, Pervaporation dehydration of ethylene glycol through polybenzimidazole (PBI)-based membranes. 1. Membrane fabrication, Journal of Membrane Science 363(1-2) (2010) 149-159. https://doi.org/10.1016/j.memsci.2010.07.024.

[108] G.M. Shi, Y. Wang, T.S. Chung, Dual-layer PBI/P84 hollow fibers for pervaporation dehydration of acetone, Aiche Journal 58(4) (2012) 1133-1145. https://doi.org/10.1002/aic.12625.

[109] T.-S. Chung, W.F. Guo, Y. Liu, Enhanced Matrimid membranes for pervaporation by homogenous blends with polybenzimidazole (PBI), Journal of Membrane Science 271(1-2) (2006) 221-231. https://doi.org/10.1016/j.memsci.2005.07.042.

[110] C.B. Shogbon, J.L. Brousseau, H.F. Zhang, B.C. Benicewicz, Y.A. Akpalu, Determination of the molecular parameters and studies of the chain conformation of polybenzimidazole in DMAc/LiCl, Macromolecules 39(26) (2006) 9409-9418. https://doi.org/10.1021/ma0609836.

[111] Y. Wang, S.H. Goh, T.S. Chung, Miscibility study of Torlon® polyamide-imide with Matrimid® 5218 polyimide and polybenzimidazole, Polymer 48(10) (2007) 2901-2909. https://doi.org/10.1016/j.polymer.2007.03.040.

[112] Y. Wang, T.S. Chung, B.W. Neo, M. Gruender, Processing and engineering of pervaporation dehydration of ethylene glycol via dual-layer polybenzimidazole (PBI)/polyetherimide (PEI) membranes, Journal of Membrane Science 378(1-2) (2011) 339-350. https://doi.org/10.1016/j.memsci.2011.05.020.

[113] Y. Wang, T.S. Chung, M. Gruender, Sulfonated polybenzimidazole membranes for pervaporation dehydration of acetic acid, Journal of Membrane Science 415 (2012) 486-495. https://doi.org/10.1016/j.memsci.2012.05.035.

[114] Y. Wang, Pervaporation Dehydration of Ethyl Acetate via PBI/PEI Hollow Fiber Membranes, Industrial & Engineering Chemistry Research 54(11) (2015) 3082-3089. https://doi.org/10.1021/ie504681v.

[115] K.Y. Wang, B. Li, T.-S. Chung, 3D-macrocycles impregnated polybenzimidazole hollow fiber membranes with excellent organic solvent resistance for industrial solvent recovery, Journal of Membrane Science 638 (2021). https://doi.org/10.1016/j.memsci.2021.119678.

[116] Q.S. Yao, S.X. Li, R.R. Zhang, L.H. Han, B.W. Su, High-throughput thin-film composite membrane via interfacial polymerization using monomers of ultra-low concentration on tannic acid - Copper interlayer for organic solvent nanofiltration, Separation and Purification Technology 258 (2021) 13. https://doi.org/10.1016/j.seppur.2020.118027.

[117] J. Lee, H. Yang, G. Park, T.H. Bae, Highly stable epoxy-crosslinked polybenzimidazole membranes for organic solvent nanofiltration under strongly basic conditions, Journal of Membrane Science 661 (2022) 8. https://doi.org/10.1016/j.memsci.2022.120951.

[118] A.A. Tashvigh, T.S. Chung, Robust polybenzimidazole (PBI) hollow fiber membranes for organic solvent nanofiltration, Journal of Membrane Science 572 (2019) 580-587. https://doi.org/10.1016/j.memsci.2018.11.048.

[119] L.A. Murdock, B.C. Benicewicz, Teaching an Old Dog New Tricks: Synthesis, Processing, and Application of Polybenzimidazole (PBI) Membranes, ACS Applied Energy Materials 7(1) (2023) 239-249. https://doi.org/10.1021/acsaem.3c02560.

[120] Z. Zhou, Z. Zhao, X. Yang, H. Zhai, L. Ai, J. Chen, S. Holmes, Improving the performance and long-term durability of high-temperature PEMFCs: A polyvinylpyrrolidone grafting modification strategy of polybenzimidazole membrane, Journal of Membrane Science 710 (2024). https://doi.org/10.1016/j.memsci.2024.123135.

[121] S. Kumar B, B. Sana, G. Unnikrishnan, T. Jana, S. Kumar K. S, Polybenzimidazole co-polymers: their synthesis, morphology and high temperature fuel cell membrane properties, Polymer Chemistry 11(5) (2020) 1043-1054. https://doi.org/10.1039/c9py01403a.

[122] G. Pourcelly, Membranes for Low and Medium Temperature Fuel Cells. State-of-the-Art and New Trends, Petrol Chem+ 51(7) (2011) 480-491. https://doi.org/10.1134/S0965544111070103.

[123] A.C. Dupuis, Proton exchange membranes for fuel cells operated at medium temperatures: Materials and experimental techniques, Progress in Materials Science 56(3) (2011) 289-327. https://doi.org/10.1016/j.pmatsci.2010.11.001.

[124] J. Escorihuela, J. Olvera-Mancilla, L. Alexandrova, L.F. del Castillo, V. Compañ, Recent Progress in the Development of Composite Membranes Based on Polybenzimidazole for High Temperature Proton Exchange Membrane (PEM) Fuel Cell Applications, Polymers 12(9) (2020). https://doi.org/ARTN 186110.3390/polym12091861.

[125] J. Wang, G. Liu, A. Wang, W. Ji, L. Zhang, T. Zhang, J. Li, H. Pan, H. Tang, H. Zhang, Novel N-alkylation synthetic strategy of imidazolium cations grafted polybenzimidazole for high temperature proton exchange membrane fuel cells, Journal of Membrane Science 669 (2023). https://doi.org/10.1016/j.memsci.2022.121332.

[126] M.A. Imran, T. Li, X. Wu, X. Yan, A.-S. Khan, G. He, Sulfonated polybenzimidazole/amine functionalized titanium dioxide (sPBI/AFT) composite electrolyte membranes for high temperature proton exchange membrane fuel cells usage,

Chinese Journal of Chemical Engineering 28(9) (2020) 2425-2437. https://doi.org/10.1016/j.cjche.2020.05.016.

[127] W. Wu, X. Guan, S. Zhang, G. Ma, C. Li, X. Zhou, D. Yu, Y. Luo, S. Wang, High-density quaternized polymer ionic liquid/polybenzimidazole cross-linked membrane achieves excellent acid stability, Journal of Membrane Science 713 (2025). https://doi.org/10.1016/j.memsci.2024.123383.

[128] Y. Zhang, F. Ji, J. Li, M. Zhang, C. Deng, H. Cheng, Z. Cui, W. Cai, Inorganic Lewis Base-Modified Polybenzimidazole for High-Temperature Proton-Exchange Membrane Fuel Cell Applications, ACS Applied Energy Materials 7(12) (2024) 5275-5284. https://doi.org/10.1021/acsaem.4c00891.

[129] S. Kang, C. Zhang, G. Xiao, D. Yan, G. Sun, Synthesis and properties of soluble sulfonated polybenzimidazoles from 3,3′-disulfonate-4,4′-dicarboxylbiphenyl as proton exchange membranes, Journal of Membrane Science 334(1-2) (2009) 91-100. https://doi.org/10.1016/j.memsci.2009.02.021.

[130] B. Zhang, X. Li, S. Lv, X. Sun, H. Zhang, P. Zhou, Y. Chen, J. Zheng, S. Li, S. Zhang, High-performance polybenzimidazole composite membranes doped with nitrogen-rich porous nanosheets for high-temperature fuel cells, Journal of Membrane Science 709 (2024). https://doi.org/10.1016/j.memsci.2024.123119.

[131] X.F. Guan, W.Z. Wu, S.Y. Zhang, G.P. Ma, X.P. Zhou, C.C. Li, D. Yu, Y. Luo, S. Wang, High hydrogen-bond density polymeric ionic liquid composited high temperature proton exchange membrane with exceptional long-term fuel cell performance, Journal of Membrane Science 717 (2025). https://doi.org/ARTN 12352310.1016/j.memsci.2024.123523.

[132] B. Xing, O. Savadogo, Hydrogen/oxygen polymer electrolyte membrane fuel cells (PEMFCs) based on alkaline-doped polybenzimidazole (PBI), Electrochem Commun 2(10) (2000) 697-702. https://doi.org/Doi 10.1016/S1388-2481(00)00107-7.

[133] M. Kawahara, J. Morita, M. Rikukawa, K. Sanui, N. Ogata, Synthesis and proton conductivity of thermally stable polymer electrolyte: poly(benzimidazole) complexes with strong acid molecules, Electrochimica Acta 45(8-9) (2000) 1395-1398. https://doi.org/Doi 10.1016/S0013-4686(99)00349-7.

[134] Z. Guo, J. Chen, J.J. Byun, M. Perez–Page, Z. Ji, Z. Zhao, S.M. Holmes, Insights into the performance and degradation of polybenzimidazole/muscovite composite membranes in high–temperature proton exchange membrane fuel cells, Journal of Membrane Science 641 (2022). https://doi.org/10.1016/j.memsci.2021.119868.

[135] J. Peng, X. Fu, J. Luo, L. Wang, X. Peng, Fabrication of high performance high-temperature proton exchange membranes through constructing stable cation-rich domain in polybenzimidazole membrane, Chemical Engineering Journal 453 (2023). https://doi.org/10.1016/j.cej.2022.139609.

[136] R. Haider, Y. Wen, Z.F. Ma, D.P. Wilkinson, L. Zhang, X. Yuan, S. Song, J. Zhang, High temperature proton exchange membrane fuel cells: progress in advanced materials and key technologies, Chem Soc Rev 50(2) (2021) 1138-1187. https://doi.org/10.1039/d0cs00296h.

[137] C. Liu, S.B. Khan, M. Lee, K.I. Kim, K. Akhtar, H. Han, A.M. Asiri, Fuel cell based on novel hyper-branched polybenzimidazole membrane, Macromol Res 21(1) (2013) 35-41. https://doi.org/10.1007/s13233-012-0191-2.

[138] D.Y. Nikumbe, C.M. Pawar, D.D. Khairnar, P. Madiyan, R.K. Nagarale, Redox Flow Batteries with an Amphoteric Sulfonated Poly(styrene-co-2-vinyl benzimidazole) Membrane, ACS Applied Energy Materials 8(9) (2025) 6056-6070. https://doi.org/10.1021/acsaem.5c00465.

[139] J. Wang, W. Xu, F. Xu, L. Dai, Y. Wu, Y. Wang, S. Li, Z. Xu, A polybenzimidazole-covalent organic framework hybrid membrane with highly efficient proton-selective transport channels for vanadium redox flow battery, Journal of Membrane Science 695 (2024). https://doi.org/10.1016/j.memsci.2024.122470.

[140] S. Kunz, T.T. Bui, D. Emmel, J. Janek, D. Henkensmeier, D. Schroder, Aqueous Redox Flow Cells Utilizing Verdazyl Cations enabled by Polybenzimidazole Membranes, ChemSusChem 17(21) (2024) e202400550. https://doi.org/10.1002/cssc.202400550.

[141] Y. Su, S. Liu, W. Zhu, K. Huang, G. Mu, P. Jiang, J. Liu, G. Yang, Z. He, J. Wang, Nature of Solvent/Nonsolvent Strategy in Achieving Superior Polybenzimidazole Membrane for Vanadium Redox Flow Battery, ChemSusChem 18(10) (2025) e202402513. https://doi.org/10.1002/cssc.202402513.

[142] T. Gao, C. Li, W. Bai, Y. Luo, D. Yu, S. Wang, High Proton Conductivity Membrane Based on Sulfonated Polybenzimidazole by Doping Ethylenediaminetetraacetic Acid-Modified

MOF-808 for Vanadium Flow Battery, ACS Applied Polymer Materials 6(11) (2024) 6552-6560. https://doi.org/10.1021/acsapm.4c00845.

[143] T.T. Bui, M. Shin, S. Abbas, M.M. Ikhsan, X.H. Do, A. Dayan, M.R. Almind, S. Park, D. Aili, J. Hjelm, J. Hwang, H.Y. Ha, K. Azizi, Y. Kwon, D. Henkensmeier, Sulfonated para-Polybenzimidazole Membranes for Use in Vanadium Redox Flow Batteries, Advanced Energy Materials (2024). https://doi.org/10.1002/aenm.202401375.

[144] B. Pang, X. Wu, Y. guo, M. Yang, R. Du, W. Chen, X. Yan, F. Cui, G. He, Anionic conductive group tunable amphoteric polybenzimidazole ion conductive membrane for vanadium redox flow battery, Journal of Membrane Science (2023). https://doi.org/10.1016/j.memsci.2023.121351.

[145] Y. Wang, K. Geng, Q. Tan, T. Guo, X. Hu, H. Tang, L. Liu, N. Li, Highly Ion Selective Proton Exchange Membrane Based on Sulfonated Polybenzimidazoles for Iron–Chromium Redox Flow Battery, ACS Applied Energy Materials 5(12) (2022) 15918-15927. https://doi.org/10.1021/acsaem.2c03471.

[146] P. Song, Y. Zhang, H. Du, Q. Wang, Q.-F. An, Simply designed sulfonated polybenzimidazole membranes for iron-chromium redox flow battery, Journal of Membrane Science 719 (2025). https://doi.org/10.1016/j.memsci.2025.123745.

[147] C. Wang, M.J. Park, H. Yu, H. Matsuyama, E. Drioli, H.K. Shon, Recent advances of nanocomposite membranes using layer-by-layer assembly, Journal of Membrane Science 661 (2022). https://doi.org/10.1016/j.memsci.2022.120926.

[148] C. Wang, M.J. Park, D.H. Seo, S. Phuntsho, R.R. Gonzales, H. Matsuyama, E. Drioli, H.K. Shon, Inkjet printed polyelectrolyte multilayer membrane using a polyketone support for organic solvent nanofiltration, Journal of Membrane Science 642 (2022) 119943. https://doi.org/10.1016/j.memsci.2021.119943.

[149] G. Falca, V.E. Musteata, S. Chisca, M.N. Hedhili, C. Ong, S.P. Nunes, Naturally Extracted Hydrophobic Solvent and Self-Assembly in Interfacial Polymerization, ACS Appl Mater Interfaces 13(37) (2021) 44824-44832. https://doi.org/10.1021/acsami.1c07584.

[150] M. Cook, P.R.J. Gaffney, L.G. Peeva, A.G. Livingston, Roll-to-roll dip coating of three different PIMs for Organic Solvent Nanofiltration, Journal of Membrane Science 558 (2018) 52-63. https://doi.org/10.1016/j.memsci.2018.04.046.

[151] H.C. Yang, R.Z. Waldman, M.B. Wu, J. Hou, L. Chen, S.B. Darling, Z.K. Xu, Dopamine: Just the Right Medicine for Membranes, Advanced Functional Materials 28(8) (2018). https://doi.org/10.1002/adfm.201705327.

[152] C. Zhang, Y. Lv, W.Z. Qiu, A. He, Z.K. Xu, Polydopamine Coatings with Nanopores for Versatile Molecular Separation, ACS Appl Mater Interfaces 9(16) (2017) 14437-14444. https://doi.org/10.1021/acsami.7b03115.

[153] C. Zhang, Y. Ou, W.X. Lei, L.S. Wan, J. Ji, Z.K. Xu, CuSO4/H2O2-Induced Rapid Deposition of Polydopamine Coatings with High Uniformity and Enhanced Stability, Angew Chem Int Ed Engl 55(9) (2016) 3054-7. https://doi.org/10.1002/anie.201510724.

[154] Y. Xu, F. You, H. Sun, L. Shao, Realizing Mussel-Inspired Polydopamine Selective Layer with Strong Solvent Resistance in Nanofiltration toward Sustainable Reclamation, ACS Sustainable Chemistry & Engineering 5(6) (2017) 5520-5528. https://doi.org/10.1021/acssuschemeng.7b00871.

[155] H. Li, X. Li, G. Ouyang, L. Huang, L. Li, W. Li, W. Huang, D. Li, Ultrathin organic solvent nanofiltration membrane with polydopamine-HKUST-1 interlayer for organic solvent separation, Journal of Environmental Sciences (2023). https://doi.org/10.1016/j.jes.2023.05.027.

[156] D. Zhao, J.F. Kim, G. Ignacz, P. Pogany, Y.M. Lee, G. Szekely, Bio-Inspired Robust Membranes Nanoengineered from Interpenetrating Polymer Networks of Polybenzimidazole/Polydopamine, ACS Nano 13(1) (2019) 125-133. https://doi.org/10.1021/acsnano.8b04123.

[157] J. Wang, J. Zhu, M.T. Tsehaye, J. Li, G. Dong, S. Yuan, X. Li, Y. Zhang, J. Liu, B. Van der Bruggen, High flux electroneutral loose nanofiltration membranes based on rapid deposition of polydopamine/polyethyleneimine, Journal of Materials Chemistry A 5(28) (2017) 14847-14857. https://doi.org/10.1039/c7ta02661g.

[158] J. Lin, C.Y. Tang, C. Huang, Y.P. Tang, W. Ye, J. Li, J. Shen, R. Van den Broeck, J. Van Impe, A. Volodin, C. Van Haesendonck, A. Sotto, P. Luis, B. Van der Bruggen, A comprehensive physico-chemical characterization of superhydrophilic loose nanofiltration membranes, Journal of Membrane Science 501 (2016) 1-14. https://doi.org/10.1016/j.memsci.2015.11.044.

[159] Y. Chung, D. Park, H. Kim, S.E. Nam, S. Kang, Novel method for the facile control of molecular weight cut-off (MWCO) of ceramic membranes, Water Res 215 (2022) 118268. https://doi.org/10.1016/j.watres.2022.118268.

[160] P.S. Zhong, X.Z. Fu, T.S. Chung, M. Weber, C. Maletzko, Development of Thin-Film Composite forward Osmosis Hollow Fiber Membranes Using Direct Sulfonated Polyphenylenesulfone (sPPSU) as Membrane Substrates, Environmental Science & Technology 47(13) (2013) 7430-7436. https://doi.org/10.1021/es4013273.

[161] I.B. Valtcheva, S.C. Kumbharkar, J.F. Kim, Y. Bhole, A.G. Livingston, Beyond polyimide: Crosslinked polybenzimidazole membranes for organic solvent nanofiltration (OSN) in harsh environments, Journal of Membrane Science 457 (2014) 62-72. https://doi.org/10.1016/j.memsci.2013.12.069.

[162] A. Oxley, P.R.J. Gaffney, D. Kim, P.G. Marchetti, A. Livingston, Graft modification of polybenzimidazole membranes for organic solvent ultrafiltration with scale up to spiral wound modules, Journal of Membrane Science 647 (2022). https://doi.org/ARTN 12019910.1016/j.memsci.2021.120199.

[163] A. Oxley, A.G. Livingston, Effect of polymer molecular weight on the long-term process stability of crosslinked polybenzimidazole organic solvent nanofiltration (OSN) membranes, Journal of Membrane Science 689 (2024). https://doi.org/10.1016/j.memsci.2023.122149.

[164] A. Oxley, A.G. Livingston, Anti-fouling membranes for organic solvent nanofiltration (OSN) and organic solvent ultrafiltration (OSU): graft modified polybenzimidazole (PBI), Journal of Membrane Science 662 (2022). https://doi.org/10.1016/j.memsci.2022.120977.

[165] D.J. Chen, S.S. Yu, M. Yang, D.D. Li, X.F. Li, Solvent resistant nanofiltration membranes based on crosslinked polybenzimidazole, Rsc Advances 6(21) (2016) 16925-16932. https://doi.org/10.1039/c5ra27044h.

[166] I.B. Valtcheva, P. Marchetti, A.G. Livingston, Crosslinked polybenzimidazole membranes for organic solvent nanofiltration (OSN): Analysis of crosslinking reaction mechanism and effects of reaction parameters, Journal of Membrane Science 493 (2015) 568-579. https://doi.org/10.1016/j.memsci.2015.06.056.

[167] A. Asadi Tashvigh, T.-S. Chung, Facile fabrication of solvent resistant thin film composite membranes by interfacial crosslinking reaction between polyethylenimine and dibromo-p-

xylene on polybenzimidazole substrates, Journal of Membrane Science 560 (2018) 115-124. https://doi.org/10.1016/j.memsci.2018.05.019.

[168] F. Qiu, Y. Sun, Y. Zhang, H. Liu, L. Shao, Q. Huang, Electrospun PTFE nanofibrous composite membranes featuring a fiber network structure for organic solvent nanofiltration (OSN), Separation and Purification Technology 330 (2024). https://doi.org/10.1016/j.seppur.2023.125416.

[169] Y. Peng, W. Song, E. Wang, Q. Yang, B. Su, COFs interlayer manipulated interfacial polymerization for fabricating high performance OSN membrane with overall covalently crosslinked structure, Journal of Membrane Science 697 (2024). https://doi.org/10.1016/j.memsci.2024.122588.

[170] Z.G. Abdi, J.-C. Chen, T.-S. Chung, Novel amino-beta cyclodextrin-based organic solvent nanofiltration membranes with fast and stable solvent transport, Journal of Membrane Science 689 (2024). https://doi.org/10.1016/j.memsci.2023.122197.

[171] Y.C. Xu, Y.P. Tang, L.F. Liu, Z.H. Guo, L. Shao, Nanocomposite organic solvent nanofiltration membranes by a highly-efficient mussel-inspired co-deposition strategy, Journal of Membrane Science 526 (2017) 32-42. https://doi.org/10.1016/j.memsci.2016.12.026.

[172] S. Yuan, J. Swartenbroekx, Y. Li, J. Zhu, F. Ceyssens, R. Zhang, A. Volodine, J. Li, P. Van Puyvelde, B. Van der Bruggen, Facile synthesis of Kevlar nanofibrous membranes via regeneration of hydrogen bonds for organic solvent nanofiltration, Journal of Membrane Science 573 (2019) 612-620. https://doi.org/10.1016/j.memsci.2018.12.047.

[173] X. Shui, J. Li, M. Zhang, C. Fang, L. Zhu, Tailoring ultrathin microporous polyamide films with rapid solvent transport by molecular layer-by-layer deposition, Journal of Membrane Science 628 (2021). https://doi.org/10.1016/j.memsci.2021.119249.

[174] A. Asadi Tashvigh, Y. Feng, M. Weber, C. Maletzko, T.-S. Chung, 110th Anniversary: Selection of Cross-Linkers and Cross-Linking Procedures for the Fabrication of Solvent-Resistant Nanofiltration Membranes: A Review, Industrial & Engineering Chemistry Research 58(25) (2019) 10678-10691. https://doi.org/10.1021/acs.iecr.9b02408.

[175] M.A. Abdulhamid, R. Hardian, G. Szekely, Waltzing around the stereochemistry of membrane crosslinkers for precise molecular sieving in organic solvents, Journal of Membrane Science 638 (2021) 119724. https://doi.org/10.1016/j.memsci.2021.119724.

[176] A. Asadi Tashvigh, L. Luo, T.-S. Chung, M. Weber, C. Maletzko, Performance enhancement in organic solvent nanofiltration by double crosslinking technique using sulfonated polyphenylsulfone (sPPSU) and polybenzimidazole (PBI), Journal of Membrane Science 551 (2018) 204-213. https://doi.org/10.1016/j.memsci.2018.01.047.

[177] J. Wu, S. Japip, T.-S. Chung, Infiltrating molecular gatekeepers with coexisting molecular solubility and 3D-intrinsic porosity into a microporous polymer scaffold for gas separation, Journal of Materials Chemistry A 8(13) (2020) 6196-6209. https://doi.org/10.1039/c9ta12028a.

[178] Y. Zhang, H. Sun, H. Sadam, Y. Liu, L. Shao, Supramolecular chemistry assisted construction of ultra-stable solvent-resistant membranes for angstrom-sized molecular separation, Chemical Engineering Journal 371 (2019) 535-543. https://doi.org/10.1016/j.cej.2019.04.096.

[179] J. Liu, D. Hua, Y. Zhang, S. Japip, T.S. Chung, Precise Molecular Sieving Architectures with Janus Pathways for Both Polar and Nonpolar Molecules, Adv Mater 30(11) (2018). https://doi.org/10.1002/adma.201705933.

[180] T.-S. Chung, J.-Y. Lai, The potential of calixarenes for membrane separation, Chemical Engineering Research and Design 183 (2022) 538-545. https://doi.org/10.1016/j.cherd.2022.05.031.

[181] Z.G. Abdi, J.-C. Chen, T.-S. Chung, Infiltration of 3D-macrocycles to integrally skinned asymmetric P84 co-polyimide membranes for boron removal, Desalination 540 (2022). https://doi.org/10.1016/j.desal.2022.115988.

[182] B. Li, S. Japip, J.-Y. Lai, T.-S. Chung, Revitalize integrally skinned hollow fiber membranes with spatially impregnated 3D-macrocycles for organic solvent nanofiltration, Chemical Engineering Journal 422 (2021) 130015. https://doi.org/10.1016/j.cej.2021.130015.

[183] S.J. Shin, Y.-I. Park, H. Park, J.B. You, D. Kim, S.H. Bae, S. Kwon, Y. Yoo, Solvent-resistant crosslinked polybenzimidazole membrane for use in enhanced molecular separation, Journal of Membrane Science 695 (2024). https://doi.org/10.1016/j.memsci.2024.122463.

[184] L. Jin, L. Hu, S. Liang, Z. Wang, G. Xu, X. Yang, A novel organic solvent nanofiltration (OSN) membrane fabricated by Poly(m-phenylene isophthalamide) (PMIA) under large-

scale and continuous process, Journal of Membrane Science 647 (2022) 120259. https://doi.org/10.1016/j.memsci.2022.120259.

[185] M.H. Davood Abadi Farahani, D. Hua, T.-S. Chung, Cross-linked mixed matrix membranes (MMMs) consisting of amine-functionalized multi-walled carbon nanotubes and P84 polyimide for organic solvent nanofiltration (OSN) with enhanced flux, Journal of Membrane Science 548 (2018) 319-331. https://doi.org/10.1016/j.memsci.2017.11.037.

[186] M.H. Davood Abadi Farahani, T.-S. Chung, Solvent resistant hollow fiber membranes comprising P84 polyimide and amine-functionalized carbon nanotubes with potential applications in pharmaceutical, food, and petrochemical industries, Chemical Engineering Journal 345 (2018) 174-185. https://doi.org/10.1016/j.cej.2018.03.153.

[187] S. Wang, Z. Wang, S. Zhu, S. Liu, F. Zhang, J. Jin, Highly porous ultrathin polyamide membranes for fast separation of small molecules from organic solvents, Journal of Membrane Science 675 (2023). https://doi.org/10.1016/j.memsci.2023.121540.

[188] A. Volkov, A. Yushkin, A. Grekhov, A. Shutova, S. Bazhenov, S. Tsarkov, V. Khotimsky, T.J.H. Vlugt, V. Volkov, Liquid permeation through PTMSP: One polymer for two different membrane applications, Journal of Membrane Science 440 (2013) 98-107. https://doi.org/10.1016/j.memsci.2013.03.067.

[189] J. Geens, B. Van der Bruggen, C. Vandecasteele, Transport model for solvent permeation through nanofiltration membranes, Separation and Purification Technology 48(3) (2006) 255-263. https://doi.org/10.1016/j.seppur.2005.07.032.

[190] D. Bhanushali, S. Kloos, C. Kurth, D. Bhattacharyya, Performance of solvent-resistant membranes for non-aqueous systems: solvent permeation results and modeling, Journal of Membrane Science 189(1) (2001) 1-21. https://doi.org/Doi 10.1016/S0376-7388(01)00356-8.

[191] S. Ali, X.S. Feng, Interfacially Cross-Linked Polydopamine/Polybenzimidazole Composite Membranes for Organic Solvent Nanofiltration, ACS Appl. Mater. Interfaces 16(47) (2024) 65517-65528. https://doi.org/10.1021/acsami.4c14283.

[192] H. Mariën, I.F.J. Vankelecom, Transformation of cross-linked polyimide UF membranes into highly permeable SRNF membranes via solvent annealing, Journal of Membrane Science 541 (2017) 205-213. https://doi.org/10.1016/j.memsci.2017.06.080.

[193] L.F. Villalobos, T. Huang, K.V. Peinemann, Cyclodextrin Films with Fast Solvent Transport and Shape-Selective Permeability, Adv Mater 29(26) (2017). https://doi.org/10.1002/adma.201606641.

[194] P. Sun, Z. Li, S. Wang, X. Yin, Performance enhancement of polybenzimidazole based high temperature proton exchange membranes with multifunctional crosslinker and highly sulfonated polyaniline, Journal of Membrane Science 549 (2018) 660-669. https://doi.org/10.1016/j.memsci.2017.10.053.

[195] Z. Xu, K. Zhang, Y. Cheng, X. Sun, H. Ren, H. Wei, Q. Wang, L. Wang, Z. Zhang, G. Wang, Locally π-π conjugated polyimide cured triglycidyl isocyanurate epoxy resin with enhanced dielectric polarization and microwave absorption performance for X and Ku bands, Chemical Engineering Journal 483 (2024). https://doi.org/10.1016/j.cej.2024.149186.

[196] M.H. Davood Abadi Farahani, T.-S. Chung, A novel crosslinking technique towards the fabrication of high-flux polybenzimidazole (PBI) membranes for organic solvent nanofiltration (OSN), Separation and Purification Technology 209 (2019) 182-192. https://doi.org/10.1016/j.seppur.2018.07.026.

[197] E. Yang, M. Kim, Y. Liang, J. Byun, H. Kim, K.C. Mamani, I.S. Kim, H. Choi, Facile fabrication of robust and tight PIMs-based TFC hollow fiber membranes with a semi-interpenetrating polymer network via liquid phase cross-linking for organic solvent nanofiltration, Journal of Membrane Science 713 (2025). https://doi.org/10.1016/j.memsci.2024.123338.

[198] R. Verbeke, I. Nulens, M. Thijs, M. Lenaerts, M. Bastin, C. Van Goethem, G. Koeckelberghs, I.F.J. Vankelecom, Solutes in solvent resistant and solvent tolerant nanofiltration: How molecular interactions impact membrane rejection, Journal of Membrane Science 677 (2023). https://doi.org/10.1016/j.memsci.2023.121595.

[199] S. Rezaei Hosseinabadi, L.A.J. Rutgeerts, I.F.J. Vankelecom, Molecular weight resolution of solvent resistant nanofiltration (SRNF) membranes, Journal of Membrane Science 683 (2023). https://doi.org/10.1016/j.memsci.2023.121792.

[200] P. Marchetti, A. Butté, A.G. Livingston, An improved phenomenological model for prediction of solvent permeation through ceramic NF and UF membranes, Journal of Membrane Science 415 (2012) 444-458. https://doi.org/10.1016/j.memsci.2012.05.030.

[201] S.J. Shin, Y.-I. Park, H. Park, Y.H. Cho, G.Y. Won, Y. Yoo, A facile crosslinking method for polybenzimidazole membranes toward enhanced organic solvent nanofiltration performance, Separation and Purification Technology 299 (2022) 121783. https://doi.org/10.1016/j.seppur.2022.121783.

[202] M. Mertens, C. Van Goethem, M. Thijs, G. Koeckelberghs, I.F.J. Vankelecom, Crosslinked PVDF-membranes for solvent resistant nanofiltration, Journal of Membrane Science 566 (2018) 223-230. https://doi.org/10.1016/j.memsci.2018.08.051.

[203] A. Asadi Tashvigh, L. Luo, T.-S. Chung, M. Weber, C. Maletzko, A novel ionically cross-linked sulfonated polyphenylsulfone (sPPSU) membrane for organic solvent nanofiltration (OSN), Journal of Membrane Science 545 (2018) 221-228. https://doi.org/10.1016/j.memsci.2017.09.076.

[204] A. Asadi Tashvigh, T.-S. Chung, Robust polybenzimidazole (PBI) hollow fiber membranes for organic solvent nanofiltration, Journal of Membrane Science 572 (2019) 580-587. https://doi.org/10.1016/j.memsci.2018.11.048.

[205] Z. Zhai, X. Wang, Y. Huang, Y. Zhao, Fabrication of phenolic resin membrane with polyvinyl alcohol fiber skeleton by electrospinning for organic solvent nanofiltration, Separation and Purification Technology 332 (2024). https://doi.org/10.1016/j.seppur.2023.125852.

[206] D.Y. Xing, S.Y. Chan, T.-S. Chung, The ionic liquid [EMIM]OAc as a solvent to fabricate stable polybenzimidazole membranes for organic solvent nanofiltration, Green Chem. 16(3) (2014) 1383-1392. https://doi.org/10.1039/c3gc41634h.

[207] C. Van Goethem, M.M. Magboo, M. Mertens, M. Thijs, G. Koeckelberghs, I.F.J. Vankelecom, A scalable crosslinking method for PVDF-based nanofiltration membranes for use under extreme pH conditions, Journal of Membrane Science 611 (2020). https://doi.org/10.1016/j.memsci.2020.118274.

[208] A. El Fadil, S. Rezaei Hosseinabadi, R. de Oliveira Silva, D. Sakellariou, K. Nijmeijer, I.F.J. Vankelecom, Strong impact of exposure to water/solvent mixtures on permeance of nanofiltration membranes, Journal of Membrane Science 699 (2024). https://doi.org/10.1016/j.memsci.2024.122651.

[209] D.R. Machado, D. Hasson, R. Semiat, Effect of solvent properties on permeate flow through nanofiltration membranes. Part I: investigation of parameters affecting solvent flux,

Journal of Membrane Science 163(1) (1999) 93-102. https://doi.org/Doi 10.1016/S0376-7388(99)00158-1.

[210] J. Bougard, R. Jadot, Solvation in Aqueous N,N-Dimethylformamide, J Chem Thermodyn 7(12) (1975) 1185-1188. https://doi.org/Doi 10.1016/0021-9614(75)90040-3.

Appendices

Appendix A. Membrane Fabrication and Handling Considerations

The following practical observations were made during membrane fabrication and performance evaluation. These points are included to facilitate reproducibility of the experimental procedures and to highlight factors that can significantly influence membrane performance.

1. Membrane Storage

PBI membranes should be stored in an appropriate liquid (e.g., water or an organic solvent (acetonitrile, IPA, etc.)) immediately after fabrication and before performance testing. Drying of the membrane can result in pore collapse, increased brittleness, and the formation of microcracks. Maintaining the membrane in a wet state preserves its porous structure and ensures consistent experimental results. If long-term storage outside a liquid environment is required, a suitable pore-preservation procedure should be employed before drying.

2. Prevention of Membrane Cracking During Performance Testing

Care must be taken during membrane installation in the filtration cell. Excessive tightening of the cell screws or rapid pressurization of the feed solution can induce mechanical stresses that cause membrane cracking. Even microscopic cracks, which may not be immediately visible, can create non-selective flow pathways, resulting in artificially high solvent permeance and reduced solute rejection.

Therefore, each membrane should be carefully inspected for visible defects before filtration experiments. If unexpected changes in permeability or rejection occur during testing, the membrane should be removed and replaced with a new one for further testing. Only membranes free from visible cracks or defects should be used for evaluating membrane separation performance.

Note: Throughout this study, membrane performance data were obtained only from membranes that were visually confirmed to be free of defects before testing.

Appendix B. Representative Permeance Data and Error Analysis

Table A1 presents the solvent permeance of the three initially fabricated membranes (P-PBI, PBI-DCX, and PBI-DBB), reported as the mean ± standard deviation from three independent measurements. These data represent the preliminary membrane screening experiments performed during the early stages of this research. The purpose of including these results is to demonstrate the experimental reproducibility and the variability associated with the permeance measurements through standard deviation (error analysis). The standard deviations shown in Table A1 indicate that the permeance measurements are generally reproducible across different solvents if a good membrane is evaluated. Based on these preliminary results, only two membranes were evaluated for the work presented in Chapters 3, 4, and 5.

Table A1. Solvent permeance (mean ± standard deviation, $n = 3$) for P-PBI, PBI-DCX, and PBI-DBB membranes.

Solvent	P-PBI (LMH bar^{-1})	PBI-DCX (LMH bar^{-1})	PBI-DBB (LMH bar^{-1})
IPA	2.25 ± 0.45	1.66 ± 0.92	1.72 ± 0.78
Acetone	5.19 ± 0.40	4.75 ± 1.08	5.02 ± 0.80
THF	2.98 ± 0.33	2.58 ± 0.78	2.73 ± 0.35
Toluene	3.42 ± 1.12	2.36 ± 0.99	1.94 ± 0.49
Hexane	5.61 ± 0.77	3.80 ± 0.97	4.70 ± 0.34

Values are reported as mean ± standard deviation (n = 3).

Appendix C. Representative Rejection and Permeance Data

The data presented in Table A2 represent the preliminary membrane-screening experiments conducted to evaluate the separation performance of the fabricated PBI-based membranes. Rejection was measured using three model organic dyes: Rose Bengal (RB), Reactive Brilliant Blue (RBB), and Methyl Orange (MO), while ethanol permeance was determined under identical operating conditions. The results are reported as the mean ± standard deviation from three independent experiments using different membranes and are included to provide representative error analysis for both rejection and permeance measurements.

The relatively small standard deviations obtained for both rejection and permeance indicate good experimental reproducibility. Most rejection measurements exhibited standard deviations below 3%, and ethanol permeance generally showed low variability.

Based on these preliminary results, only two membranes were evaluated for the work presented in Chapters 3, 4, and 5.

Table A2. Rejection and ethanol permeance of the initially fabricated PBI, PBI-DCX, and PBI-DBB membranes. Values are reported as the mean ± standard deviation from three independent experiments (n = 3).

Membrane	Dye	Rejection (%)	Ethanol Permeance (LMH bar^{-1})
P-PBI	RB	80.73 ± 2.90	3.05 ± 0.07
	RBB	67.86 ± 5.08	3.77 ± 0.03
	MO	51.21 ± 3.63	3.94 ± 0.21
PBI-DCX	RB	96.69 ± 1.23	2.97 ± 0.07
	RBB	93.16 ± 2.33	3.04 ± 0.40
	MO	82.74 ± 1.65	3.42 ± 0.06
PBI-DBB	RB	95.41 ± 1.12	2.98 ± 0.03

Membrane	Dye	Rejection (%)	Ethanol Permeance (LMH bar^{-1})
	RBB	88.43 ± 1.04	3.31 ± 0.93
	MO	76.06 ± 3.48	3.47 ± 0.47

Values are reported as mean ± standard deviation (n = 3).